Title
Multi-scale Modeling of Arctic Methane Cycling Using the CLM-Microbe Model

Author
Wang, Yihui

Publication Date
2022

Peer reviewed|Thesis/dissertation

Multi-scale Modeling of Arctic Methane Cycling Using the CLM-Microbe Model

By

YIHUI WANG

DISSERTATION

Submitted in partial satisfaction of the requirements for the degree of

DOCTOR OF PHILOSOPHY

in

Ecology

a joint program in the

OFFICES OF GRADUATE STUDIES

of the

UNIVERSITY OF CALIFORNIA DAVIS

and

SAN DIEGO STATE UNIVERSITY

Approved:

Xiaofeng Xu, Chair

Randy A. Dahlgren

Donatella Zona

Daniel M. Ricciuto

Jorge L. Mazza Rodrigues

Committee in Charge

2022

ACKNOWLEDGEMENT

I would like to thank everyone who help and supported my Ph.D study. I want to express my deep and sincere gratitude to my advisor, Dr. Xiaofeng Xu, giving me the opportunity to do research and providing invaluable guidance throughout this research. His motivation, diligence, vision and sincerity have deeply inspired me. I want to thank Dr. Fengming Yuan from ORNL, for providing technical supports for my research. I want to thank my mentor at UC Davis, Dr. Randy Dahlgren, for warmly hosting me and advising me; and thank Dr. Benjamin Houlton for inviting me to his weekly group meetings. I want to thank Drs. Jorge Rodrigues, Donatella Zona, David Lipson, Daniel Ricciuto, for being on my QE committee and/or dissertation committee. Their invaluable comments on my research are substantially helpful in completing this research and finalizing my dissertation. I also want to thank Kyle Arndt, for providing me research data.

I give thanks to members of Xu's and Houlton's labs for their academic and emotional supports. I want to give special thanks to Fenghui Yuan, Liyuan He, Jia Jia, Nannan Wang, Ziyu Guo, Jianzhao Liu, Lihua Zhang, Linna Ma, Yunjiang Zuo and Yanqiu Zhou. They always help me and encourage me. I want to thank JDPE and GGE cohorts for happy memories from annual orientation and Odyssey. I give special thanks to Theresa Burnham, Christopher Knight, Molly Clemens, Lais Lima, Roman Nava and Kavita Irene Rajah. I also want to thank Mrs. Patti Swinford, Medora Bratlien, Jamie Rhine, Cecilia Arpallan, and JoAnna Lewis for their help on program paper works.

I am extremely grateful to my parents for their love, caring and supporting. I am very much thankful to my husband for his love, understanding and continuing support me to complete this research. I am deeply grateful to my daughter for bringing me joy and happiness.

ABSTRACT

Methane (CH_4) emissions from Arctic polygonal tundra are spatially heterogeneous due to the complex soil hydrology. This spatial heterogeneity in CH_4 emissions requires a reliable upscaling approach to reach accurate regional CH_4 budgets in the Arctic tundra. Additionally, Arctic regions have been warming two to four times faster than the global average in recent decades. CH_4 emission from the Arctic is increasing under climate warming. However, interactions among temperature, soil water table and vegetation complicate a full understanding of emission rates and their magnitude in a changing climate. In this dissertation, I applied the CLM-Microbe model to examine microtopographic impacts on CH_4 and CO_2 fluxes across seven landscape types in Utqiaġvik, Alaska: trough, low-centered polygon (LCP) center, LCP transition, LCP rim, high-centered polygon (HCP) center, HCP transition, and HCP rim. Low-elevation and thus wetter landscape types (i.e., trough, transitions, and LCP center) had larger CH_4 emissions rates with greater seasonal variations than high-elevation and drier landscape types (rims and HCP center). Substrate availability for methanogenesis was identified as the most important factor determining CH_4 emission. Upscaled CH_4 emissions at the eddy covariance (EC) domain using an area-weighted approach were underestimated by 20% and 25% at daily and hourly time steps. Combined with three footprint algorithms, I upscaled CH_4 fluxes from a plot level to EC domains (200 m × 200 m) for three sites in Utqiaġvik (US-Beo, US-Bes, and US-Brw), one in Atqasuk (US-Atq) and one in Ivotuk (US-Ivo). Three footprint algorithms are the homogenous footprint (HF) that assumes even contribution of all grid cells, the gradient footprint (GF) that assumes gradually declining contribution from center grid cells to edges, and the dynamic footprint (DF) that considers the impacts of wind and heterogeneity of land surface. DF performed better than HF and GF algorithms in capturing the temporal variation in daily CH_4 flux in each month, while the

model accuracy was similar among the three algorithms due to flat landscapes. Temporal variations in CH_4 flux during 2013-2015 were predominately explained by air temperature (67-74%), followed by precipitation (22-36%). Spatial heterogeneities in vegetation and elevation dominated spatial variations in CH_4 flux for all EC domains despite relatively weak differences in simulated CH_4 flux among three footprint algorithms. Finally, I projected CH_4 emissions during 2016-2100 for all these five sites under three Shared Socioeconomic Pathways (SSP) scenarios derived from three climate models. CH_4 emission exhibited a stronger response (630 - 850% increase) under SSP5-8.5 than under SPP1-2.6 and SSP2-4.5, likely supported by a simultaneous enhanced precipitation-induced expansion of anoxic conditions for methanogenesis. All three CH_4 transport pathways (i.e. diffusion, ebullition, and plant-mediated transport) are increasing by 2100, and ebullition contributed most to CH_4 emissions under three SSP scenarios across five sites. Temperature sensitivity for CH_4 emission differed using three climate models (i.e., BCC-CSM2-MR, CESM2, and EC-Earth3) with a Q_{10} range of 2.7-60.9 under SSP1-2.6, 3.8-17.6 under SSP2-4.5, and 5.7-17.2 under SSP5-8.5. This study advanced our understanding of the mechanisms of current and future CH_4 emissions in the highly heterogeneous Arctic landscape. The CLM-Microbe model was testified as a powerful tool that can simulate CH_4 flux at both plot and landscape scales at a high temporal resolution, upscale terrestrial CH_4 flux integrated with an appropriate algorithm, and project future CH_4 emissions in Arctic landscapes under different climate scenarios.

INTRODUCTION

Atmospheric methane (CH_4), a potent greenhouse gas (GHG) with a 100-year global warming potential 28-34 times that of carbon dioxide (CO_2), has increased 250% since the industrial revolution to 1860 ppb in 2018 (National Oceanic and Atmospheric Administration, NOAA/ESRL, www.esrl.noaa.gov/gmd/ccgg/trends_ch4/) (IPCC, 2014; Saunois et al., 2016; Hopcroft et al., 2017). Variations in CH_4 emissions have been explained by soil temperature and water table, oxygen, substrate and nutrient availability, thaw depth, soil pH and redox potential, and vegetation and microbial communities (Yvon-Durocher et al., 2014; Lipson et al., 2013; Miller et al., 2015; Schuur et al., 2015; Ebrahimi et al., 2017; Grant et al. 2017a, 2017b). Arctic soils contain a large pool of terrestrial carbon (C) and are vulnerable to climate warming and permafrost thaw (Kim et al., 2015; Lynch et al., 2018), and some estimates predicted 92 ± 17 Pg C loss as CO_2 and CH_4 fluxes by 2100 (McGuire et al., 2018; Zheng et al., 2018). Previous studies have found that Arctic tundra ecosystems have shifted from net CO_2 sinks to sources (Belshe et al., 2013; Oechel et al., 1993); whether they behave as sinks or sources of atmospheric CH_4 largely depends on local microtopography (Jørgensen et al., 2014; Nauta et al., 2015; Oh et al., 2016; Tan et al., 2015). Minor changes in surface elevation might shift Arctic soils from sinks to sources of atmospheric CH_4 (Olivas et al., 2010; Zona et al., 2011). Arctic tundra landscapes are highly heterogeneous with varying properties of permafrost, topography, hydrology, soil, vegetation and microbes (Davidson et al., 2016; Liljedahl et al., 2016; Deng et al., 2017; Wilkman et al., 2018). Therefore, it is critically important to understand microtopographic impacts on CH_4 emissions and dynamics for modeling and predicting the ecosystem C exchange in Arctic tundra ecosystems.

Spatial heterogeneity in land surface properties has been shown to be a key source of large variabilities and uncertainties in CH_4 fluxes in the Arctic (Bridgham et al., 2013; Davidson et al.,

2016; Sturtevant & Oechel, 2013; Xu et al., 2014; Zona et al., 2011), as the production, consumption, and transport processes of CH_4 are primarily related to hydrology, vegetation, and microbial activities (Vaughn et al., 2016). Modeling and predicting the spatial variability of CH_4 emissions at broader scales depend on the upscaling algorithms that consider heterogeneous landscapes (Davidson et al., 2016; Xu et al., 2016). Numerous empirical and mechanistic modeling studies have attempted to upscale the static chambers measurements (10^{-2} - 1 m^2) to the landscape scale (10^4 - 10^5 m^2) and evaluated against eddy covariance (EC) flux (Baldocchi, 2008; Chen et al., 2012; Davidson et al., 2017; Xu and Tian, 2012). Yet, these estimates ignored the impacts of the spatial variability of CH_4 flux within the source area. Accurate regional estimations of CH_4 flux require an upscaling approach that considers the mechanistic CH_4 processes, including the key factors that control CH_4 flux across time and space (Xu et al., 2016).

Arctic regions have been warming two to four times faster than the global average in recent decades (Hansen et al 2007; Miner et al., 2022). Air temperature in the Arctic has increased at a rate of 0.755 °C/decade during 1998–2012 (Chen et al., 2020) and could continue to increase by more than 10°C by 2100 relative to present-day, corresponding to about 30% more than the best estimate of warming (IPCC, 2021). Field experiments and model simulations for the Arctic found that warming increased CH_4 fluxes by 15 – 550% or had no effect due to changes in soil water table and vegetation (Granberg et al., 2001; Ma et al., 2017; Turetsky et al., 2008; Updegraff et al., 2001; Verville et al., 1998). However, interactions among temperature, soil moisture status, and vegetation complicate a full understanding of CH_4 emission rates and their magnitude in a changing climate.

In my dissertation, I sought to better understand the mechanisms of CH_4 cycling from the plot to landscape scales in Arctic tundra and investigate the responses of future CH_4 emission and

cycling to climate change. The research questions addressed in my three chapters are: 1) Modeling the microtopographic effects on CH_4 dynamics in the northern Arctic tundra using the CLM-Microbe model; 2) Upscaling the plot-level CH_4 fluxes to EC domains using three footprint algorithms in five Arctic tundra ecosystems; and 3) Projecting the CH_4 emission and processes under three SSP scenarios from 2016 to 2100 in Arctic tundra.

Chapter 1

Mechanistic Modeling of Microtopographic Impacts on CO_2 and CH_4 Fluxes in an Alaskan Tundra Ecosystem Using the CLM-Microbe Model

This chapter has already been published by Wiley-Blackwell.

Yihui Wang, Fengming Yuan, Fenghui Yuan, Baohua Gu, Melanie S. Hahn, Margaret S. Torn, Daniel M. Ricciuto, Jitendra Kumar, Liyuan He, Donatella Zona, David A. Lipson, Robert Wagner, Walter C. Oechel, Stan D. Wullschleger, Peter E. Thornton, and Xiaofeng Xu. 2019. Mechanistic modeling of microtopographic impacts on CO2 and CH4 fluxes in an alaskan tundra ecosystem using the CLM-microbe model. Journal of Advances in Modeling Earth Systems, 11(12), 4288-4304. https://doi.org/10.1029/2019MS001771

Abstract

Spatial heterogeneities in soil hydrology have been confirmed as a key control on CO_2 and CH_4 fluxes in the Arctic tundra ecosystem. In this study, we applied a mechanistic ecosystem model, CLM- Microbe, to examine the microtopographic impacts on CO_2 and CH_4 fluxes across seven landscape types in Utqiaġvik, Alaska: trough, low-centered polygon (LCP) center, LCP transition, LCP rim, high-centered polygon (HCP) center, HCP transition, and HCP rim. We first validated the CLM-Microbe model against static-chamber measured CO_2 and CH_4 fluxes in 2013 for three landscape types: trough, LCP center, and LCP rim. Model application showed that low-elevation and thus wetter landscape types (i.e., trough, transitions, and LCP center) had larger CH_4 emissions rates with greater seasonal variations than high- elevation and drier landscape types (rims and HCP center). Sensitivity analysis indicated that substrate availability for methanogenesis (acetate, CO_2 + H_2) is the most important factor determining CH_4 emission, and vegetation physiological properties largely affect the net ecosystem carbon exchange and ecosystem respiration in Arctic tundra ecosystems. Modeled CH_4 emissions for different microtopographic

features were upscaled to the eddy covariance (EC) domain with an area-weighted approach before validation against EC-measured CH_4 fluxes. The model underestimated the EC-measured CH_4 flux by 20% and 25% at daily and hourly time steps, suggesting the importance of the time step in reporting CH_4 flux. The strong microtopographic impacts on CO_2 and CH_4 fluxes call for a model-data integration framework for better understanding and predicting carbon flux in the highly heterogeneous Arctic landscape.

Introduction

Spatial heterogeneity in land surface properties has been shown to be a key source of large variabilities and uncertainties in CO_2 and CH_4 fluxes in the Arctic (Bridgham et al., 2013; Davidson et al., 2016; Sturtevant & Oechel, 2013; Xu et al., 2014; Zona et al., 2011). Polygonal ground patterns create a complex mosaic of micro- topographic features with poorly drained low-centered polygons (LCPs) surrounded by high rims and well- drained high-centered polygons (HCPs) surrounded by low trough as results of the annual freeze–thaw cycles across the northern Alaskan coastal plain (Hinkel et al., 2005; Throckmorton et al., 2015; Zona et al., 2011). Microtopography strongly affects soil water content and active layer depth (Atchley et al., 2016; Grant, Mekonnen, Riley, Arora, & Torn, 2017a; Grant, Mekonnen, Riley, Wainwright, et al., 2017b; Lu & Zhuang, 2012), soil temperature and thermal conductivity (Abolt et al., 2018*;* Kumar et al., 2016), soil pH and O_2 availability (Lipson et al., 2012; Zona et al., 2011), soil chemistry (Lipson et al., 2013; Newman et al., 2015; Semenchuk et al., 2015), vegetation types and canopy height (Davidson et al., 2016; von Fischer et al., 2010), and microbial community structure (Tas et al., 2018; Wagner et al., 2017). Therefore, the large spatial heterogeneities in microtopographic features are critically important for modeling and predicting the ecosystem carbon (C) exchange

in Arctic tundra ecosystems.

Previous studies have found that Arctic tundra ecosystems have shifted from net CO_2 sinks to sources (Belshe et al., 2013; Oechel et al., 1993); whether they behave as sinks or sources of atmospheric CH_4 largely depends on local microtopography (Jørgensen et al., 2014; Nauta et al., 2015; Oh et al., 2016; Tan et al., 2015). Minor changes in surface elevation might shift Arctic soils from sinks to sources of atmospheric CH_4 (Olivas et al., 2010; Zona et al., 2011). CH_4 is produced in the poorly drained low-elevation ground with anoxic conditions, whereas atmospheric CH_4 can be oxidized in well-drained high-elevation ground (Atchley et al., 2016; Grant, Mekonnen, Riley, Arora, & Torn, 2017a; Lipson et al., 2012; von Fischer et al., 2010; Zona et al., 2011). Microtopography also affects the CO_2 flux by altering the soil water content and O_2 concentration (Olivas et al., 2010). In addition, soil hydrological conditions affect vegetation growth and substrate availability, further influencing ecosystem C input and microbial community structure and altering the transport and production of CH_4, root respiration, and microbial respiration (Davidson et al., 2016; von Fischer et al., 2010; Wagner et al., 2017). Thus, accurate quantification of the strength of C sinks or sources requires explicit consideration of the microtopographic effects on C cycling in Arctic tundra ecosystems (Ebrahimi & Or, 2017).

To more accurately capture the fine-scale variations in CH_4 and CO_2 fluxes in Arctic tundra, microtopo- graphic effects need to be considered by ecosystem models as microbial functions such as fermentation, C mineralization, methanogenesis, and methanotrophy dramatically differ between wet and dry polygons (Tas et al., 2018). A number of mechanistic CH_4 models have incorporated the mechanisms of CH_4 production, consumption, and transport pathways (Xu et al., 2016), such as the *ecosys* model (Grant, Mekonnen, Riley, Arora, & Torn, 2017a), CLM-Microbe (Xu et al., 2015), CLM4Me (Riley et al., 2011), LPJ-WHyMe (Wania et al., 2010), and NEST-

DNDC (Zhang et al., 2012). However, few CH_4 models explicitly simulate microtopography and are capable of investigating the microtopographic impacts on CH_4 and CO_2 fluxes in Arctic tundra (Grant, Mekonnen, Riley, Arora, & Torn, 2017a; Kaiser et al., 2017). For example, the *ecosys* model indicates that microtopography determines CH_4 and CO_2 emissions by regulating soil water content, active layer depth, and O_2 availability (Grant, Mekonnen, Riley, Arora, & Torn, 2017a). The CLM-Microbe model simulates fine-scale thermal and hydrological dynamics and microbial mechanisms for CH_4 production and oxidation (Xu et al., 2015), which allows investigation of Arctic CH_4 and CO_2 fluxes across multiple scales from a microbial perspective.

In this study, we used the CLM-Microbe model to simulate the microtopographic effects on CH_4 and CO_2 flux. We aimed to address three questions: (1) How do different microtopographic types affect CH_4 and CO_2 fluxes in Arctic tundra ecosystems? (2) Which processes are more important in controlling CH_4 and CO_2 fluxes among the microtopographic types? (3) How do annual estimates of CH_4 and CO_2 fluxes differ under the microtopographic impacts in the Arctic? The field observational data from the U.S. Department of Energy's Office of Science Next Generation Ecosystem Experiments (NGEE)-Arctic project were integrated with the CLM-Microbe model to understand microtopographic impacts on land surface CH_4 and CO_2 fluxes in an Arctic tundra landscape.

Methodology

Site Description

Our study area is located within the Barrow Environmental Observatory (BEO), ~6 km east of Utqiaġvik (formerly Barrow), Alaska (71.3°N, 156.5°W), operated by the NGEE-Arctic project (https://ngee-arctic. ornl.gov/). It has a polar maritime climate with mean annual air

temperature of −12.0 °C in winter and 3.3 °C in summer (June–August), and with mean annual precipitation of 173 mm and the majority of precipitation falling during summer months (Liljedahl et al., 2011). Snowmelt usually ends in early to mid- June and the wind direction is predominantly from east to west throughout the year (Wainwright et al., 2017). The dominant plants are mosses (*Dicranum elongatum*, *Sphagnum*), lichens, and vascular plants (such as *Carex aquatilis*); plant distribution is governed by surface moisture variability (Zona et al., 2011).

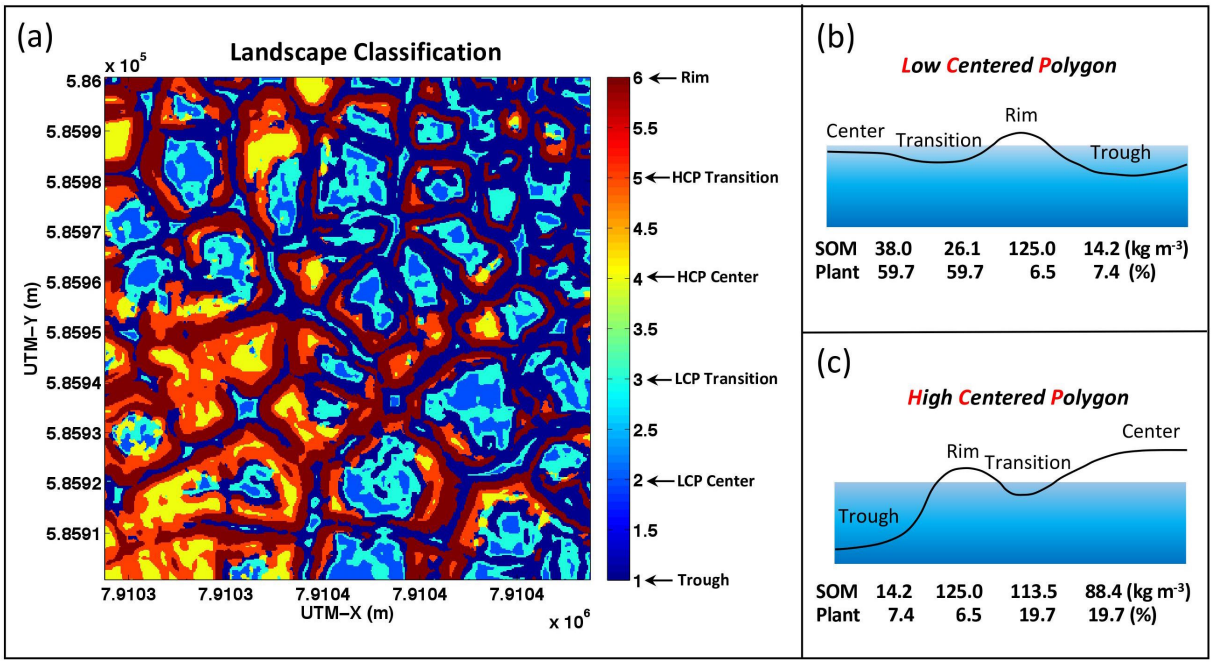

Figure 1. (a) The landscape classification map for area C (100 m × 100 m). Red indicates high surface elevation and blue indicates low surface elevation. Values on the legend are indexes used to identify different landscape types. Diagrams depict the landscape types for (b) low-centered polygon and (c) high-centered polygon with internal polygonal feature: center, rim, transition, and trough (Yuan et al., 2017).

The landscapes are highly heterogeneous with polygonal landscape patterns. The NGEE-Arctic project established four 100 m × 100 m intensively sampled areas within the BEO (Langford et al., 2016). The sampled areas are dominated by the LCPs and HCPs with internal features of center, rim, transition, and trough (Figure 1a). Accordingly, seven landscape types were classified within the study area: trough (35.0% of total area), LCP center (6.9%), LCP rim (12.2%), LCP

transition (14.3%), HCP center (13.2%), HCP rim (12.2%), and HCP transition (6.2%). Soil organic matter density and plant cover used in model simulations for each landscape type are shown in Figure 1.

Data Availability Statement

The CH_4 and CO_2 fluxes were monitored using the static chamber approach on several dates during June– September 2012 and 2013 (Torn, 2016). Transparent and opaque surface chambers were placed within the study area in the trough, LCP center, and LCP rim. The CO_2 fluxes from the transparent chambers were considered to be the net ecosystem exchange of CO_2 (NEE), and those from the opaque chambers were considered the ecosystem respiration (ER). NEE (i.e., ER − GPP) is negative when CO_2 uptake via photosynthesis is greater than CO_2 release from ER. The concentrations of soil dissolved organic carbon (DOC), CH_4 and CO_2 were measured for the trough, LCP center, and LCP rim in 2013–2014 (Herndon et al., 2015a; Herndon et al., 2015). An eddy covariance (EC) tower was installed in the center of the study area to measure CH_4 and CO_2 fluxes in 2012; those data are available from the NGEE Arctic project website (Raz-Yaseef et al., 2013). It is noted that this data set has been updated to 2012–2016 although we used the previous data set for 2012–2013. Daily and hourly fluxes of CH_4 and CO_2 were calculated based on the half-hourly EC data. Detailed information about the measurement protocols is posted in the NGEE Arctic archives (http://ngee-arctic.ornl.gov/).

Model Description and Driving Data

The CLM-Microbe model branches from the framework of default CLM 4.5 by developing a new representation of CH_4 production and consumption (Xu et al., 2015), in association with the decomposition subroutines in CLM4.5 (Koven et al., 2013; Thornton et al., 2007; Thornton & Rosenbloom, 2005). It incorporates new mechanisms of DOC fermentation, hydrogenotrophic

methanogenesis, acetoclastic methanogenesis, aerobic methanotrophy, anaerobic methanotrophy, and H_2 production based on known processes (Thauer et al., 1989; Thauer et al., 2008) and adopted from previous modeling studies (Grant, 1998; Kettunen, 2003; Riley et al., 2011; Segers & Kengen, 1998; Tian et al., 2010; Walter & Heimann, 2000; Xu et al., 2010; Zhuang et al., 2004). Detailed mathematical expressions for CH_4 production and consumption processes were organized in Xu et al. (2015). The code for the CLM-Microbe model is archived at this site (https:// github.com/email-clm/clm-microbe). The model version used in this study was checked out from GitHub on 18 June 2018.

In a previous study, the CH_4 module in the CLM-Microbe model was validated for simulating the dynamics of CH_4 and CO_2 emissions from incubation experiments on Arctic soils with invariant soil temperature and soil water content (Xu et al., 2015). In this study, we focused on the fully incorporated CLM-Microbe model, created separate model runs for each landscape type, and modified the soil hydrological setup according to landscapes' unique soil conditions. Three soil hydrological parameters, largely affected by microtopography, were selected: soil water content (*h2osoi_vol*), surface runoff (*qflx_surf*), and the inundated fraction (*finun- dated*). Because the low-elevation polygonal features, such as trough, LCP center, LCP transition, and HCP transition are poorly drained and oversaturated in summer, the parameters for soil water content were changed to a maximum of 1.0, and those for the inundated fraction and surface runoff were changed to 0.99 and 0, respectively. In contrast, the high-elevation features, such as LCP rim, HCP rim, and HCP center, are well- drained in summer. For these features, the parameters for soil water content were set at a maximum of 0.3, which is the baseline allowing the gas transport in soil profiles due to model structures; and those for surface runoff and inundated fraction were set in the default processes with dynamic changes.

The model driving data included meteorological, plant, and soil data. The meteorological data included shortwave and longwave radiation, air temperature, relative humidity, wind speed, and precipitation from 1 January 1991 to 31 December 2014, derived by *Xu and Yuan* (2016) from the Utqiaġvik, AK, station of NOAA/Earth System Laboratory, Global Monitoring Division (http://www.esrl. noaa.gov/gmd/obop/brw/). The data set is gap-filled and at a half-hour time step. The observed plant and soil data for each landscape type—including the composition of plant functional types, plant cover, and soil organic carbon density— were supplied by the NGEE Arctic project.

Model Implementation

To identify the role of microbial functions in CH_4 dynamics, we set up model simulations using the default CLM4.5 and the CLM-Microbe models separately for each landscape type. The model implementation was carried out in three stages. First, the accelerated model spin-up was set up for 2,000 years to allow the system to accumulate C. Then a final spin-up for 50 years allowed the modeled system to reach a relatively steady state. After the final spin-up, the transient model simulation was set up to cover the period of 1850–2014.

Table 1. Key parameters for model parameterization

	KAce	AceProdACmax	k_dom	k_bacteria	k_fungi	fatm_f	grperc
Default value	16	2.4e-06	0.007	0.22	0.22	0.20	0.1652
Trough	12	6.4e-06	0.014	0.05	0.05	0.15	0.0052
LCP center	12	1.8e-06	0.007	0.01	0.01	0.12	0.0052
LCP rim	12	1.2e-06	0.007	0.01	0.01	0.05	0.0052
LCP transition	16	6.4e-06	0.007	0.22	0.22	0.20	0.0052
HCP transition	16	6.4e-06	0.007	0.22	0.22	0.20	0.0052
HCP center	16	2.4e-06	0.007	0.22	0.22	0.20	0.0052
HCP rim	16	2.4e-06	0.007	0.22	0.22	0.20	0.0052

Note. LCP = low-centered polygon; HCP = high-centered polygon

For the default CLM4.5 model simulations, the parameters were set to be the default values

for each landscape type. For the CLM-Microbe model simulations, the model parameterization was initialized with the default parameters in Xu et al. (2015); it was performed within their ranges to determine the optimal values of parameters in the microbial module for simulating the observational CH_4 and CO_2 fluxes for each landscape type. For the trough, LCP center, and LCP rim, the observed CH_4 and CO_2 fluxes in 2012 were used for model parameterization, and the fluxes in 2013 were used for model validation. Based on the current knowledge of mechanisms of CH_4 and CO_2 cycling, we primarily focused on the parameters for decomposition and substrate availability for methanogenesis (e.g., *k_bacteria, k_fungi, KAce*, and *AceProdACmax*) for the CH_4 cycling. For CO_2 cycling, we focused on the parameters for plant growth respiration (*grperc*), maintenance respiration (*br_mr*), and C allocation within biogeochemical cascade (e.g., *fatm_f*). According to the values of parameters reported in the previous studies, the para- meters were calibrated empirically in the model parameterization (Table 1). Because of the lack of the observational data, most of the parameters for LCP transition, HCP center, HCP rim, and HCP transition, were set as the default values; and some parameters were modified according to the setup for the trough, LCP center, and LCP rim (Table 1). The transient simulations of 1850–2014 produced output at both daily and hourly time steps. Simple linear regression was conducted to evaluate the modeled CH_4 and CO_2 fluxes compared with measured fluxes. The error statistics were used to distinguish the difference between the modeled and measured fluxes on the platform of *R* Studio platform (version 1.1.456), such as the coefficient of determination (R^2).

Uncertainty Analysis

The uncertainties of the CO_2 and CH_4 fluxes for each landscape type were quantified using the Markov Chain Monte Carlo method based on Bayesian statistics (Gilks et al., 1998) and were determined by a large ensemble of model simulations with different parameter settings. In this

study, a total of 100 model simulations with different settings of 15 key parameters were set up for each landscape type, separately. These 15 key parameters determine the decomposition of organic carbon, methanogenesis, microbial growth, and plant photosynthesis and respiration and therefore control the CH_4 and CO_2 fluxes (Table 2). They varied within a range of 30% of their optimal values (Xu et al., 2015). Model simulations were conducted from the transient simulation to cover 1850–2014 at a daily time step.

Table 2. Key parameters chosen for uncertainty analysis and sensitivity analysis

Parameter	Ecological meaning
KAce	Half-saturation coefficient of available carbon mineralization
ACminQ10	Temperature sensitivity of available carbon mineralization
AceProdACmax	Maximum rate of acetic acid production from available carbon
H2ProdAcemax	Maximum rate of H_2 production from available acetic acid
KH2ProdAce	Half-saturation coefficient of conversion of H_2 and CO_2 to acetate
KCO2ProdAce	Assuming it is half of that for H_2 based on stoichiometry theory
KCO2ProdCH4	Half coefficient of CO_2 for methane production from H_2
GrowRAceMethanogens	Growth rate of acetoclastic methanogens
YAceMethanogens	Growth efficiency of acetoclastic methanogens
K_dom	Decomposition rate constant dissolved organic matter
K_bacteria	Decomposition rate constant biomass of bacteria
K_fungi	Decomposition rate constant biomass of fungi
flnr	Fraction of leaf N in the Rubisco enzyme
grperc	Growth respiration parameter
br_mr	Base rate of maintenance respiration

Area-Weighted Upscaling

The modeled CH_4 and CO_2 fluxes in 2013 for each landscape type were further used for upscaling to the EC tower domain based on an area-weighted average approach. Because of the limitation of the landscape classification data, the EC domain was confined to an area of 100 m × 100 m. The area-weighted average approach includes information for landscape heterogeneity in

the upscaling process. The upscaled flux was calculated by the following equation:

$$F = \sum_{i=1}^{n} f_i \times area_i \qquad (1)$$

where F is the upscaled plot flux for the EC domain, f_i is the plot-level CH_4 or CO_2 fluxes for a given land- scape type for a given time period, $area_i$ is the fraction of each major landscape type within the EC domain (Davidson et al., 2016). In addition, the average fluxes were calculated based on the CH_4 and CO_2 fluxes from the seven landscape types for comparison with the upscaled fluxes.

Sensitivity Analysis

To identify the most important process and the most sensitive parameters for CH_4 and CO_2 dynamics in Arctic tundra, a global sensitivity analysis was conducted for each microtopographic type. It focused on the 15 parameters related to plant and microbial processes that were used in the uncertainty analysis (Table 2). For each parameter, we set up model simulations with +20% and −20% changes and investigated the responses of the modeled CH_4 and CO_2 fluxes in 2013. The index S, comparing the change in the model output relative to the model response for a nominal set of parameters, was calculated based on the flowing equation (Xu et al., 2015):

$$S = \frac{(R_a - R_n)/R_n}{(P_a - P_n)/P_n} \qquad (2)$$

where S is the ratio of the standardized change in model response to the standardized change in parameter values. R_a and R_n are model responses for altered and nominal parameters, respectively, and P_a and P_n are the altered and nominal parameters, respectively. S is negative if the direction of model response opposes the direction of parameter change (Xu et al., 2015).

Results

Model-Simulated CH_4 and CO_2 Fluxes

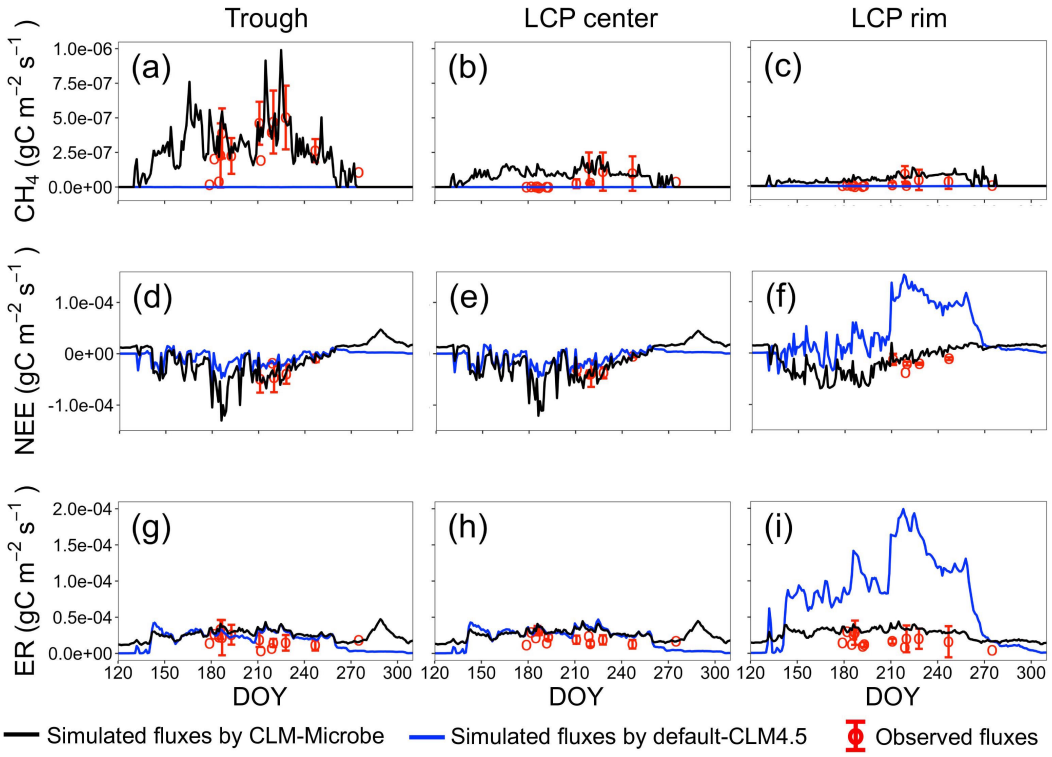

Figure 2. Simulated (a–c) CH_4 fluxes, (d–f) net ecosystem carbon exchange (NEE), and (g–i) ecosystem respiration (ER) for trough, low-centered polygon (LCP) center, and LCP rim compared with observational fluxes from static chambers (red circles with error bars) from May to September 2013 (Torn, 2016). The black lines indicate the modeled fluxes simulated by the CLM-microbe model, and the blue lines indicate the default fluxes simulated by the default CLM4.5. The blue lines are not smooth for CH_4 fluxes; the fluxes are negative and are too small to show.

The CLM-Microbe model was more accurate than the default CLM4.5 in simulating the CH_4 and CO_2 fluxes during the summer of 2013 (Figure 2). The dynamics of CH_4 was captured well by the CLM-Microbe model for the trough, LCP center, and LCP rim, but those sites were simulated as a small CH_4 sink in summer by the default CLM4.5 (Figures 2a–2c and Table 3). NEE and ER were used to represent the dynamics of CO_2 flux. In the summer months, NEE and ER had the similar patterns for the trough and LCP center but showed significant differences for LCP rim in the default CLM4.5 and CLM-Microbe models (Figures 2d–2i). For the trough and LCP center, the CLM-Microbe model simulated the NEE well, whereas the default model under-

estimated it by 47–50%; however, both of them overestimated the ER by 28–47% (Figure 3 and Table 3). The variations of NEE and ER were not captured by either the default or the CLM-Microbe models for LCP rim, but the CLM-microbe model performed slightly better than the default model (Figure 3 and Table 3).

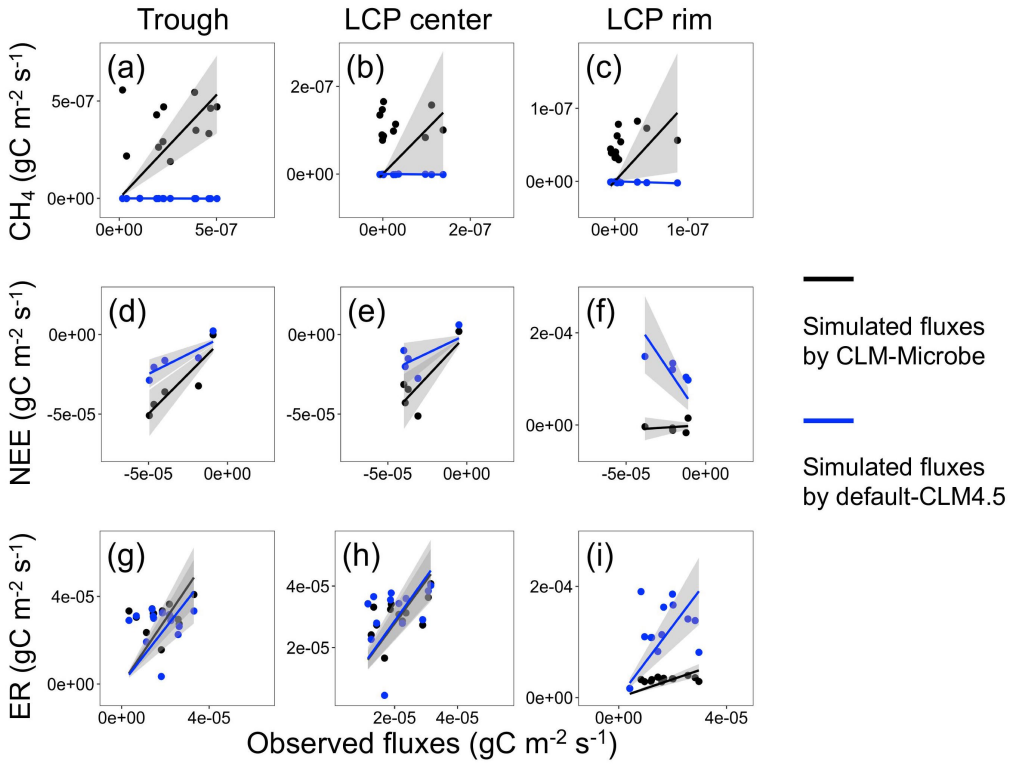

Figure 3. Scatter plots of observed versus simulated (a–c) CH_4 fluxes, (d–f) net ecosystem carbon exchange (NEE), and (g–i) ecosystem respiration (ER) for trough, low-centered polygon (LCP) center, and LCP rim, with linear lines of best fit (no interception) and 95% confidence interval for regression line shaded gray. The black lines and points indicate the relationship between observed fluxes and modeled fluxes simulated by the CLM-microbe model. The blue lines and points indicate the relationship between observed fluxes and the default fluxes simulated by the default CLM4.5.

For the simulations of the CLM-Microbe model, larger CH_4 fluxes with greater variations were observed for the trough than that for the LCP center and LCP rim (Figures 2a–2c). Additionally, modeled CH_4 fluxes were more consistent with the observational fluxes for the trough ($R^2 = 0.7381$, $p = 0.0001$) than for the LCP center ($R^2 = 0.2820$, $p = 0.0507$) and LCP rim

(R^2 = 0.3432, p = 0.0277; Table 3). For the dynamics of CO_2 fluxes, similar patterns of NEE and ER were simulated for the trough and LCP center (Figures 2d and 2e). Modeled NEE was highly consistent with the observed data for the trough (R^2 = 0.9569, p = 0.0007) and LCP center (R^2 = 0.9194, p = 0.0025); whereas ER was overestimated by 47.3% for the trough (R^2 = 0.8316, p < 0.0001) and 39.2% for the LCP center (R^2 = 0.9188, p < 0.0001; Table 3). Compared with the trough and LCP center, a slightly higher NEE (lower CO_2 uptake) was modeled for the LCP rim and it was underestimated by 78.4% (R^2 = 0.4080, p = 0.1757; Table 3). However, ER for the LCP rim was over- estimated by 64.5% (R^2 = 0.88, p < 0.0001; Table 3).

Table 3. Linear regression analysis for CH_4 flux, net ecosystem carbon exchange (NEE) and ecosystem respiration (ER) for model validation of the CLM-Microbe model and the default CLM4.5

Site	Variable	*Estimate*	*Std. Error*	*P-value*	R^2
Trough	Modeled CH_4	1.0626	0.1827	0.0001*	0.7381
	Default CH_4	-0.0027	0.0003	0.0000*	0.8388
LCP center	Modeled CH_4	1.0167	0.4683	0.0507	0.2820
	Default CH_4	-0.0090	0.0038	0.0341	0.3226
LCP rim	Modeled CH_4	1.0925	0.4363	0.0277	0.3432
	Default CH_4	-0.0309	0.0093	0.0060*	0.4802
Trough	Modeled NEE	0.9961	0.1057	0.0007*	0.9569
	Default NEE	0.4957	0.0650	0.0016*	0.9356
LCP center	Modeled NEE	1.0572	0.1565	0.0025*	0.9194
	Default NEE	0.4711	0.1216	0.0179	0.7895
LCP rim	Modeled NEE	0.2160	0.2339	0.4080	0.1757
	Default NEE	-5.1333	0.7907	0.0029*	0.9133
Trough	Modeled ER	1.4729	0.1913	0.0000*	0.8316
	Default ER	1.2800	0.2028	0.0000*	0.7685
LCP center	Modeled ER	1.3922	0.1195	0.0000*	0.9188
	Default ER	1.4301	0.1456	0.0000*	0.8893
LCP rim	Modeled ER	1.6449	0.1753	0.0000*	0.8800
	Default ER	6.4249	0.9320	0.0000*	0.7984

Note. LCP = low-centered polygon
* = the significant level < 0.01.

Variability and Seasonality of CH_4 and CO_2 Fluxes across the Landscape Types

Modeled CH_4 and CO_2 fluxes exhibited large variabilities among all seven landscape types. In the summer months, high CH_4 emissions were generally simulated, associated with low NEE (i.e., high CO_2 uptake) and high ER for all the landscape types (Figure 4). Low-elevation landscape types, such as trough, LCP transition, and HCP transition, had higher CH_4 emissions with greater variation compared with high-elevation types, such as LCP rim, HCP rim, and HCP center (Figure 4a). However, low-elevation types, including trough, LCP transition, and LCP center showed lower NEE (i.e., higher CO_2 uptake) than high-elevation types, including LCP rim and HCP rim (Figure 4b). ER was roughly higher in the HCP center and lower in the trough and LCP center in the summer months (Figure 4c).

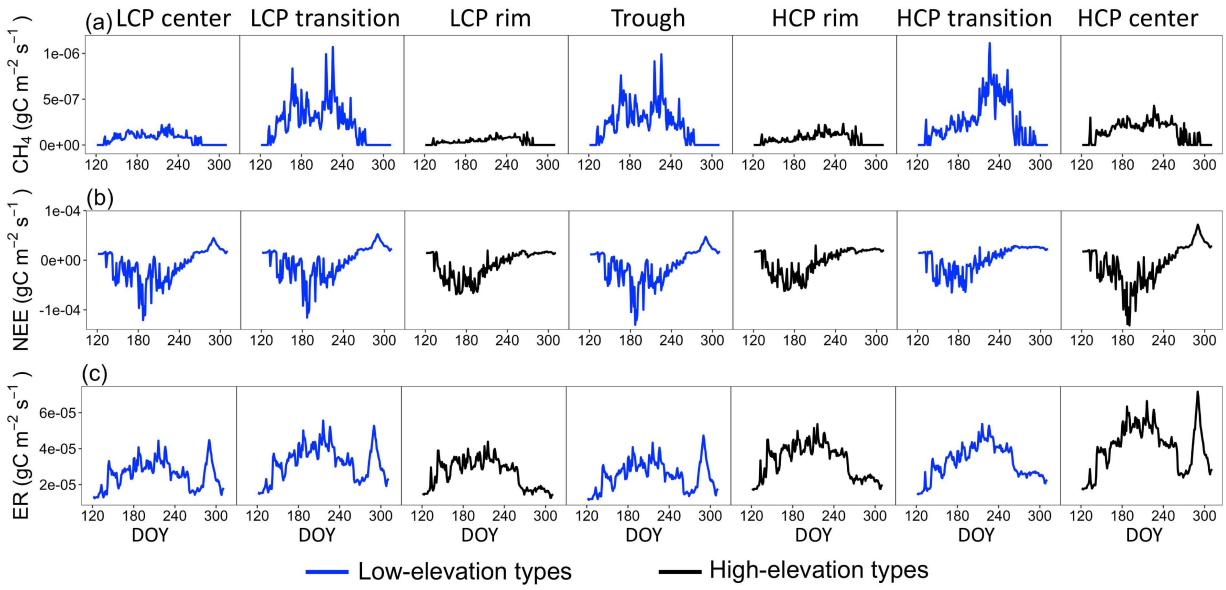

Figure 4. Modeled (a) CH_4 fluxes, (b) net ecosystem carbon exchange (NEE), and (c) ecosystem respiration (ER) for all seven landscapes types in 2013. The black lines indicate the high-elevation types, and blue lines indicate the low-elevation types. LCP = low-centered polygon; HCP = high-centered polygon.

Larger seasonal variations of CH_4 dynamics were modeled in low-elevation landscape types (e.g., trough and transitions) than high-elevation types (e.g., rim; Figure 4a). In the early

spring, most of the landscape types showed a burst release of CH_4 flux, corresponding to the early Spring thaw. During the growing seasons, the lower ground of the trough and LCP transition had similar seasonality of CH_4 and CO_2 fluxes, with the highest CH_4 emission and highest CO_2 uptake (Figure 4). The higher ground of rims tended to have smaller variations of CH_4 and NEE fluxes (Figure 4). A sudden rise was simulated in NEE for the trough, LCP transition, LCP center and HCP center, during the late growing seasons; a similar rise simultaneously was simulated in ER (Figure 4).

Annual Estimates of CH_4 and CO_2 Fluxes Across the Landscape Types

Annual CH_4 fluxes were estimated for all landscape types, resulting in a range of 0.66 to 3.97 g $C \cdot m^{-2}$ (Table 4). The HCP transition, as the largest CH_4 source, has released 5.06 times more annual CH_4 fluxes more than the smallest CH_4 sources (i.e., LCP rim). Low-elevation types, including trough and transition, contributed a larger proportion of CH_4 emissions than high-elevation types in Arctic tundra ecosystems. Based on the areal fractions, the HCPs and LCPs were estimated to have comparable annual CH_4 fluxes of 2.12 and 2.19 g $C \cdot m^{-2} \cdot year^{-1}$, respectively, both of which were smaller than the annual CH_4 fluxes of 3.63 g $C \cdot m^{-2} \cdot year^{-1}$ from the trough (Table 4).

The landscape types were found to be net sources of CO_2, except for the trough, in which 21.08 g $C \cdot m^{-2} \cdot year^{-1}$ of CO_2 was sequestered (Table 4). Large variations existed in the annual NEE, which ranged from −21.08 to 248.22 g $C \cdot m^{-2} \cdot year^{-1}$ (Table 4). The HCP transition was the largest CO_2 source to the atmosphere among the landscape types. All the landscape types had comparable ERs — ranging from 582.72 to 776.31 g $C \cdot m^{-2} \cdot year^{-1}$ — except the HCP center, which exhibited the greatest ER of 927.98 g $C \cdot m^{-2} \cdot year^{-1}$. The trough, LCP center, and LCP rim with smaller NEE estimates were also estimated to have smallest ER budget.

Table 4. Annual estimates of CH_4 fluxes, net ecosystem carbon exchange (NEE) and ecosystem respiration (ER) (g C· m^{-2}·$year^{-1}$) with the uncertainties for all seven landscape types, the average and the area-weighted average (AWA) for the EC domain based on modeled daily fluxes in 2013

Types	CH_4	NEE	ER
Trough	3.632 (3.403~3.887)	−21.083 (−26.187~−16.546)	582.715 (581.149~584.086)
LCPcenter	1.145 (1.117~1.175)	3.056 (−8.265~10.780)	598.520 (586.288~606.655)
LCPrim	0.656 (0.575~0.678)	19.579 (11.464~22.378)	617.660 (613.992~625.929)
LCPtransition	3.835 (3.714~3.971)	160.928 (157.811~165.165)	754.986 (752.519~755.857)
HCPcenter	2.384 (2.296~2.461)	137.940 (130.614~145.714)	927.981 (923.071~930.792)
HCPrim	1.075 (1.029~1.130)	180.277 (177.880~181.020)	776.309 (774.682~782.879)
HCPtransition	3.974 (3.839~4.121)	248.219 (246.895~251.471)	759.463 (758.276~761.238)
Average	2.386	104.131	716.805
AWA	2.671	73.825	692.855

Upscaling CH_4 and CO_2 Fluxes to the EC Domain

Modeled CH_4 and CO_2 fluxes were upscaled to the EC domain based on the area fraction of each landscape type. High consistency was shown between the upscaled fluxes and EC measurements (Figures 5 and 6). The regression analysis showed that more accurate simulations of CH_4 and NEE fluxes for the EC domain were obtained at daily time steps than at hourly time steps (Figure 6). CH_4 fluxes were underestimated at daily (R^2 = 0.7931, p < 0.0001) and hourly (R^2 = 0.6135, p < 0.0001) time steps by 20.08% and 24.95%, respectively. NEE was underestimated at the daily time steps by 21.44% (R^2 = 0.2843, p < 0.0001), but was overestimated at the hourly time steps by 30.01% (R^2 = 0.3464, p < 0.0001; Table 5).

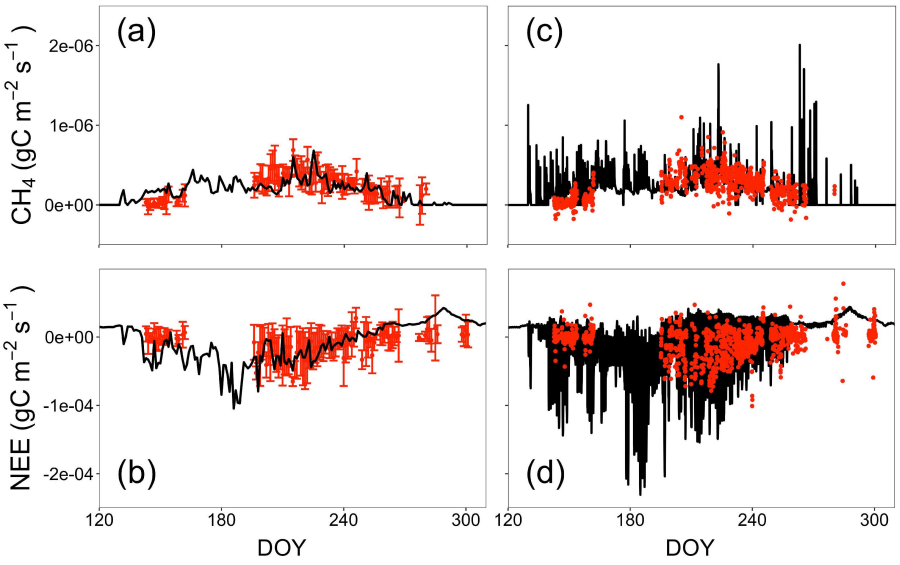

Figure 5. Upscaled (a, b) CH_4 fluxes and (c, d) net ecosystem carbon exchange (NEE) comparing with measured fluxes from an eddy covariance tower centered in the study area at the daily (a, c) and hourly (b, d) time steps in 2013. Black lines indicate the gas fluxes and red points with/without error bars indicate measured fluxes. DOY = day of year.

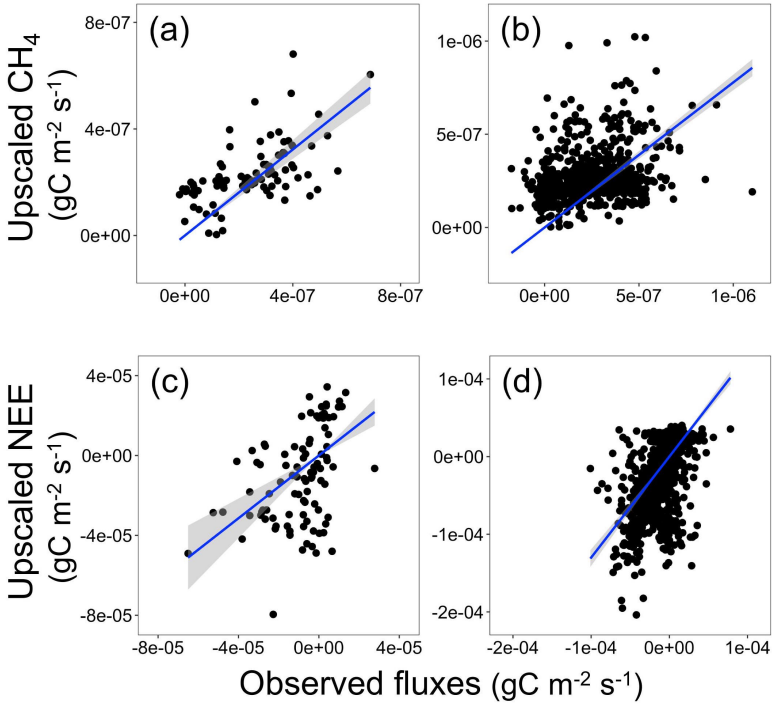

Figure 6. Scatter plots of measured versus upscaled CH_4 (a, b) and net ecosystem carbon exchange (NEE) (c, d) at daily (a, c) and hourly (b, d) time steps for the eddy covariance domain of the study area in 2013, with linear lines of best fit (no interception) and 95% confidence interval for regression line shaded gray.

Table 5. Linear regression analysis for CH_4 fluxes and net ecosystem carbon exchange (NEE) modeled and measured from the eddy covariance (EC) tower at daily and hourly time steps

Variables	Time step	*Estimate*	*Std. Error*	*P-value*	R^2
CH_4	Daily	0.7992	0.0440	0.0000[a]	0.7931
	Hourly	0.7505	0.0204	0.0000[a]	0.6135
NEE	Daily	0.7856	0.1242	0.0000[a]	0.2943
	Hourly	1.3001	0.0546	0.0000[a]	0.3464

[a]The significant level < 0.01

Annual CH_4 and CO_2 fluxes were estimated for the EC domain using the arithmetic average and area- weighted average approaches. When the proportions of different landscape types were not considered, the annual CH_4 flux was underestimated at 2.39 g $C \cdot m^{-2} \cdot year^{-1}$, compared with an annual estimate of 2.67 g $C \cdot m^{-2} \cdot year^{-1}$ based on the areal fractions. However, NEE and ER were overestimated at 104.13 g $C \cdot m^{-2} \cdot year^{-1}$ and 716.81 g $C \cdot m^{-2} \cdot year^{-1}$, respectively, compared with the annual estimates of 73.83 g $C \cdot m^{-2} \cdot year^{-1}$ and 692.86 g $C \cdot m^{-2} \cdot year^{-1}$ for NEE and ER, respectively, that considered the heterogeneity of landscapes (Table 4).

Sensitivity Analysis

CH_4 and CO_2 fluxes were sensitive to a portion of the key parameters that are related to available carbon mineralization, CH_4 production, growth of methanogens, decomposition, photosynthesis, plant growth respiration, and maintenance respiration. Specifically, the CH_4 flux was strongly sensitive to the parameters of *AceProdAcemax* and *ACMinQ10*, followed by *YAceMethanogens*, *GrowRAceMethanogens*, *KAce*, and *k_dom* for all landscape types (Figure 7a), which suggested that acetate production and available C mineralization were the key controls on CH_4 dynamics in Arctic tundra ecosystems. Growth of methanogens also regulated CH_4 flux by influencing CH_4 production. Changes in the decomposition rate of the dissolved organic matter (DOM) had a positive influence on CH_4 flux for all the landscapes except the LCP rim (Figure 7a).

In the high-elevation features LCP rim, HCP rim, and HCP center, the CH_4 flux was sensitive to the fraction of leaf nitrogen in the Rubisco enzyme functioning in photosynthesis (*flnr*). In the HCP rim, CH_4 dynamics also responded to changes in the decomposition rate of fungi biomass (*k_fungi*) and plant growth respiration (*grcep*; Figure 7a). Autotrophic respiration (e.g., plant growth respiration and maintenance respiration) and the *flnr* were also the key controlling factors for CH_4 flux in low-elevation features but exhibited opposite effects (Figure 7a).

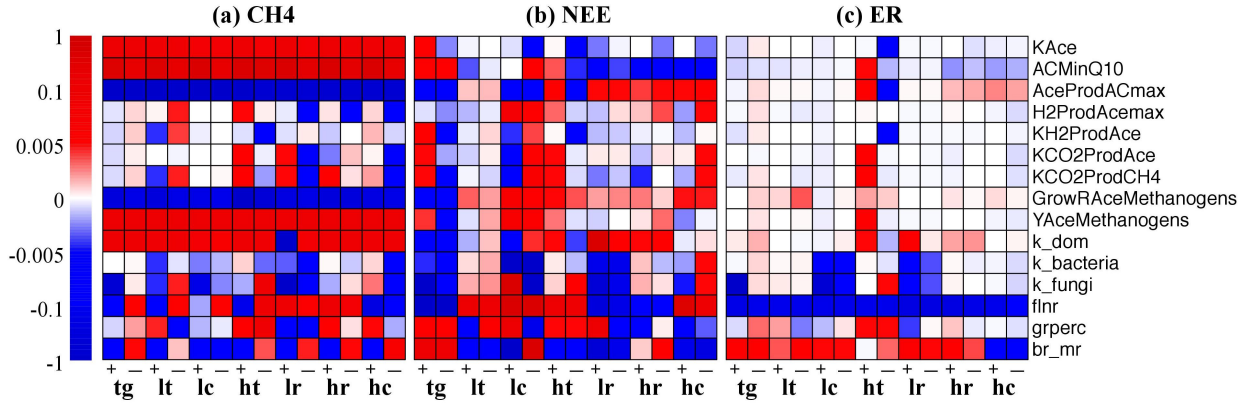

Figure 7. Sensitivity analysis for model response of (a) CH_4 fluxes, (b) net ecosystem carbon exchange (NEE), and (c) eco- system respiration (ER) to15 parameters (*KAce, ACMinQ10, AceProdACmax, H2ProdAcemax, KH2ProdAce, KCO2ProdAce, KCO2ProdCH4, GrowRAceMethanogens, YAceMethanogens, k_dom, k_bacteria, k_fungi, flnr, grperc, and br_mr*) for trough (tg), LCP transition (lt), LCP center (lc), HCP transition (ht), LCP rim (lr), HCP rim (hr), and HCP center (hc). The symbols "+" and "-" indicate a 20% increase or 20% decrease of parameter values. Darker red and darker blue indicate a stronger positive or negative model response to parameter change. *S* is negative if the direction of model response opposes the direction of parameter change. LCP = low-centered polygon; HCP = high-centered polygon.

The most important processes of CO_2 dynamics are related to photosynthesis and respiration, which control CO_2 uptake and release across the Arctic landscape types. The *flnr* was identified as the primary factor for NEE and ER (Figure 7b and 7c). An increase in the *flnr* lead to a rise in NEE in the trough, LCP rim, and HCP rim but a NEE reduction in the LCP center, LCP transition, HCP transition, and HCP center. There was a significant decrease in ER for all landscapes with increased *flnr* (Figure 7b and 7c). For high-elevation features, including LCP rim,

HCP rim, and HCP center, NEE dynamics showed negative responses to *ACMinQ10* and positive responses to *AceProdACmax*, suggesting that acetate production is also important for CO_2 uptake from the atmosphere (Figure 7b). In the trough, NEE was sensitive to many other parameters related to acetate production, decomposition, and respiration (Figure 7b). Beside the *flnr*, ER dynamics was sensible to maintenance respiration (*br_mr*) in both high-elevation and low-elevation landscape types (Figure 7c). Additionally, changes in the decomposition rates of bacteria and fungi biomass for the LCP center could also result in changes in ER (Figure 7c).

Discussions

Microtopographic Impacts on CH_4 and CO_2 Fluxes

Microtopography determines CH_4 and CO_2 dynamics in Arctic polygonal tundra by affecting the hydrological processes and thereby the soil water content, active layer depth, vegetation, and microbial functional groups in ecosystem C exchange (Davidson et al., 2016; Grant, Mekonnen, Riley, Arora, & Torn, 2017a; Lipson et al., 2012; Throckmorton et al., 2015; *D*. Zona et al., 2011). Soil water content was greater in the low-elevation ground of trough, LCP transition, LCP center, and HCP transition than in the high-elevation ground of the LCP rim, HCP rim, and HCP center; this discrepancy largely explained the variability in CH_4 fluxes among the heterogeneous landscape types in the Arctic (Grant, Mekonnen, Riley, Wainwright, et al., 2017b; Lu & Zhuang, 2012). In summer, larger CH_4 emissions were observed and modeled in the trough than in higher-elevation rims and centers because of the trough's higher soil water content and oversaturated soils, which is consistent with previous studies (Grant, Mekonnen, Riley, Arora, & Torn, 2017a; Schrier-Uijl et al., 2010). Saturated and oversaturated soils create an anoxic condition facilitating methanogenesis to produce CH_4 (von Fischer et al., 2010; Von Fischer & Hedin, 2007).

Higher CH_4 emissions were also modeled for other low-elevation types, including LCP center, LCP transition, and HCP transition, a finding that supported the promotion effects of high soil water content on CH_4 production.

CH_4 flux is strictly produced by methanogens at very low O_2 concentration in soils, mainly converted from acetate and $CO_2 + H_2$ (Nazaries et al., 2013). The sensitivity analysis suggested that the substrate availability for methanogenesis resulting from acetate production and DOM decomposition was the key constraint for CH_4 dynamics in Arctic polygonal landscapes (Xu et al., 2015). In summer months, higher CO_2 uptake (i.e., lower NEE) and stronger photosynthesis (i.e., increased *flnr*) were modeled associated with the higher CH_4 emissions in the low-elevation ground. The results implied that a positive correlation existed between the CO_2 uptake and CH_4 emission. Stronger CO_2 uptake refers to a higher amount of plant biomass, which

facilitates the emission of large CH_4 fluxes emitting to the atmosphere via plant-mediated transport (von Fischer et al., 2010). Additionally, high CO_2 uptake can provide abundant C input into soils as litter for microbial decomposition, which in turn produces a high amount of available C for methanogenesis. However, the field study reported that no relationship was observed between instantaneous GPP (i.e., CO_2 uptake) and CH_4 fluxes (Davidson et al., 2016), suggesting that the processes from decomposition of organic matter to substrates for methanogenesis are very complicated and need to be considered cautiously in CH_4 models.

Microtopographic effects on CO_2 dynamics are caused primarily by changes in soil hydrological conditions and hence CO_2 diffusion (Davidson et al., 2016; Olivas et al., 2010). Low-elevation landscape types, especially the trough and LCP center, were shown by modeling to have the largest CO_2 uptake in summer. Additionally, the ER via roots and microbial communities was suppressed by the low dissolved O_2 concentration in the saturated soils (Olivas et al., 2010; Zona

et al., 2011). These results suggested that high soil moisture in Arctic tundra promotes the plant growth and suppresses the ER, eventually increasing the strength of the CO_2 sink in low-elevation landscapes. In contrast, lower CO_2 uptake and greater ER in summer were simulated for the rims and HCP center, confirming that the high-elevation ground in the Arctic acts as a smaller CO_2 sink (Zona et al., 2011). The ER variations in low-elevation and high-elevation land- scape types in the summer months were caused largely by the difference in the availability of soil O_2 for microbial respiration. The strength of the CO_2 sink in Arctic tundra can be biased by the effects of microtopography on soil water and O_2 conditions. However, most landscape models have not incorporated microtopographic effects in simulating CO_2 fluxes. Not considering those effects might cause large biases; therefore, better simulation of microtopographic impacts is critical for model applications to C cycling in the Arctic.

NEE and CH_4 Flux at Daily and Hourly Time Steps

Biological processes occur instantaneously, on a time scale inconsistent with field measurements normally undertaken at hourly or daily scales. Ecosystem functions are more apparent at the hourly, daily, monthly, and annual scales, at which the CLM-Microbe performs. The model performance was more consistent with observed CH_4 and CO_2 fluxes for the EC domain on the daily than on the hourly scale, indicating that the model did not perform well in capturing some pulse fluxes on an hourly scale. Since the "CH_4 pulse" in the spring season has been widely recognized as an important component for ecosystem models in recent decades (Lu & Zhuang, 2012; Song et al., 2012; Tokida et al., 2007), an improvement of the CLM-Microbe model for better simulation of these outbreak events is needed.

In general, upscaled CH_4 and CO_2 fluxes based on modeled plot-level fluxes were able to capture most variations of measured EC fluxes at both daily and hourly time steps. We conclude

that the CLM-Microbe model can be used to estimate CH_4 and CO_2 fluxes at landscape scale if fluxes are scaled by different landscape types (Schrier-Uijl et al., 2010). Moreover, the dynamics of CH_4 and CO_2 fluxes was modeled more accurately at daily than at hourly time steps. This is probably because the key factors or processes controlling CH_4 and CO_2 dynamics are slightly different across the temporal scales; but they are well defined with stable priorities in the model according to the extant knowledge, usually from observations at long time scales. Another rea- son for the underestimation of CO_2 flux might be the unexplained CO_2 uptake during the non-growing season (i.e., October) in the Alaska tundra ecosystem (Figures 5b and 5d). Until confirmed mechanisms are found for the underestimation, it has no clear implications for the model performance.

Model Implications

This study has three implications for model development and scientific understanding of the C dynamic in the Arctic. First, the CLM-Microbe model performed well in capturing the variabilities in CH_4 and CO_2 fluxes among primary polygonal landscapes in Arctic tundra, which emphasizes the importance of spatial heterogeneity in simulating CO_2 and CH_4 fluxes in ecosystem CH_4 models. The model simulations indicate that the trough and transitions had estimated CH_4 emissions of 3.6 – 4.0 g $C \cdot m^{-2} \cdot$ $year^{-1}$ annually, and the rims had a smaller annual CH_4 emissions of 0.7 – 1.1 g $C \cdot$ $m^{-2} \cdot year^{-1}$. Differences in the annual estimates were likely due to the saturated and anoxic conditions in low-elevation ground that promote anaerobic methanogenesis, leading to a higher CH_4 emission. However, the annual CH_4 fluxes for the seven landscape types may be greatly underestimated because of the low estimates for the cold season in model simulations. Many studies have reported that >50% of annual CH_4 emissions occur during the cold season in Alaskan tundra (September to May; Kittler et al., 2017; Zona et al., 2016). Moreover, our estimate

of annual CH_4 fluxes for the entire study area was smaller compared with similar studies in Arctic tundra (Reeburgh et al., 1998; Wille et al., 2008). This discrepancy might be explained by the lower organic matter density or less plant cover in our study area. For example, the less abundant plant cover reduces the plant-mediated transport of CH_4 and therefore lowers CH_4 emissions (Bhullar et al., 2013). The variations in our estimates for seven landscape types were potentially biased because they ignored the lateral surface hydrologic and thermal processes. The spatial variability in soil moisture and soil temperature can be over-predicted if the lateral subsurface hydrologic and thermal processes are excluded (Bisht et al., 2018), and the same is true for the spatial variability in CH_4 emissions in Arctic polygonal landscapes. By incorporating these surface processes, the CH_4models can improve the representation of lateral hydrologic and thermal transport, and thereby improve the accuracy of estimations (Aas et al., 2019).

Table 6. The comparison between modeled and observed concentrations of belowground dissolved organic carbon (DOC), CO_2, and CH_4 (g C m^{-3}) along soil profiles for the trough, LCP center and LCP rim in 2013–2014

DOY	Site	Sample depth (cm)	Soil layer (CLM-Microbe)	DOC		CO_2		CH_4	
				modeled	observed	modeled	observed	modeled	observed
183	Trough	28	6	448.11	282.84	16.08	156.60	0.55	0.11
240	Trough	22	5	478.20	283.92	0.00	33.00	0.08	0.14
240	Trough	29	6	458.43	222.84	16.15	NA	0.59	NA
606	Trough	20	5	483.29	118.08	0.00	48.84	0.01	0.50
606	Trough	37	6	462.32	184.80	16.25	35.16	0.57	2.06
183	Center	26	5	1419.74	30.60	0.00	NA	0.04	NA
240	Center	49	6	1422.88	1015.32	13.33	NA	0.28	NA
606	Center	10	4	1674.68	25.68	0.00	NA	0.02	NA
183	Rim	29	6	1064.58	NA	4.13	NA	0.09	NA
183	Rim	7	3	1120.60	29.16	618.30	NA	0.05	NA
240	Rim	7	3	1178.37	30.72	618.34	NA	0.14	NA
240	Rim	37	6	1073.85	66.72	4.20	NA	0.20	NA

Second, the potential shifts in Arctic tundra ecosystems as C sinks or sources is valuable information for climate projections. This study showed that the trough is the only net CO_2 sink among all landscape types and plays a key role in ecosystem C storage because of its 35% areal share of the entire study area. CO_2 dynamics in the trough were very sensitive to many processes related to photosynthesis, plant and soil respiration, and C mineralization and distribution. It is possible for trough shifting to being net C sources from net C sinks, even with a tiny change in CO_2 processes under climate changes. Annual estimates indicated that the HCPs were 310% greater CO_2 sources than the LCPs. Additionally, greater ER was estimated in the HCPs than in the LCPs. The HCP center, in particular, had an ER of 928.0 g $C \cdot m^{-2}$, the highest among the landscape types. Because LCPs may eventually subside into HCPs, CO_2 emissions from Arctic soils tend to increase rapidly not only because of the effects of climate changes but also because of the changes in landscape patterns.

Finally, this study advocates the mechanistic modeling of C cycling to better estimate CO_2 and CH_4 fluxes across the Arctic tundra ecosystems. It is well known that differences in CH_4 and CO_2 emissions across the Arctic landscapes are directly led by the mechanisms and dynamics of microbial activities in relation to C mineralization, decomposition, respiration, methanogenesis, and methanotrophy. By including these microbial processes, the CLM-Microbe model allows us to understand the mechanisms of Arctic C cycling according to the production and consumption processes of CO_2 and CH_4. Soil DOC, CH_4, and CO_2 concentrations were modeled and compared with the measured concentrations for the landscape types and soil depths for a few data points (Table 6). Modeled DOC concentrations were ~1.6 times the measurements at the middle layer of soils in the trough on day of year (DOY) 183 and DOY 240 of 2013; these results suggested that the model could be useful for simulating the concentrations of C compounds. In Arctic ecosystems,

high CH_4 emissions in saturated soils were modeled with high CH_4 production, which was consistent with the large amount of modeled acetoclastic methanogens. CH_4 oxidation was strengthened by high O_2 availability in the topsoil of the rims and HCP center compared with saturated trough and transitions. Moreover, differences in CH_4 transport via diffusion, ebullition, and plant-mediated transport were modeled with seasonal variations. Large CH_4 fluxes emitted from soils were associated with the fast plant growth in summer. Furthermore, soil microbial structure and biomass were simulated to understand the CO_2 and CH_4 dynamics, which suggested the importance of belowground microbial mechanisms in modeling surface CO_2 and CH_4 fluxes.

The Way Forward

The CLM-Microbe model can simulate the belowground microbial processes for surface CO_2 and CH_4 fluxes. Although promising results proved the robustness of the CLM-Microbe model in simulating surface CO_2 and CH_4 fluxes, a number of tasks were identified as follow-up efforts to this study. First, although the upscaling results with an area-weighted approach seems promising, the dominant roles of landscape types weakened the variations in C flux. Upscaling with a mechanistic model should provide more accurate quantification of the C flux on a regional scale, as well as a finer-resolution C flux at both the spatial and the temporal scales (Watts et al., 2014). Second, belowground C dynamics — for example, DOC, acetate, CO_2, and CH_4 concentrations—are important variables and precursors for observed surface gas fluxes. We call for a data-model integration approach to better integrate the observational data and better simulate belowground processes and surface flux. Third, hydrological dynamics is the key control for biogeochemical processes, particularly for the changing Arctic. Improving the model's ability to simulate hydrology is an important cornerstone for simulating soil biogeochemistry. Fourth, microbial genomic information is the most accurate information for microbial functions, yet it has

not been well utilized for model parameterization. The CLM-Microbe model is capable of simulating the relative abundance of methanogenesis; thus, it is worth- while to improve the model to better simulate the microbial functional groups responsible for CH_4 production and consumption. Fifth, although C flux data, particularly the CH_4 flux, have been scarce across the Arctic tundra ecosystem, recent projects and technical improvements have allowed year-round measurements. Those data can serve as a good constraint for the CLM-Microbe model at multiple scales; a multiscale "MODEX" (model-observation-experiment) framework to better integrate multiple observational data to quantify gas flux and understand its mechanisms in the Arctic is much needed.

Conclusions

This study reported the application of the CLM-Microbe model to seven microtopographic landscape types in the Arctic tundra near Utqiagvik, AK. The model results were promising and consistent with the observational gas fluxes. The modeled results showed that low-elevation landscape types (e.g. trough, transitions, and LCP center) have higher CH_4 emission with greater seasonal variations than high-elevation landscape types (e.g. rims and HCP center), as a result of the greater soil saturation in the low-elevation landscape types. Model sensitivity analysis determined that the substrate (e.g. acetate, $CO_2 + H_2$) availability for methanogens was the most important factor in controlling CH_4 emissions in Arctic ecosystems, and plant photosynthesis greatly affected the NEE and ER. The model performed more accurately in simulating the daily EC fluxes than hourly fluxes, indicating the importance of the time scale in simulating gas fluxes.

The large spatial heterogeneity in CO_2 and CH_4 fluxes across the Arctic landscape requires explicit consideration and modeling of microtopography, as well as of the mechanisms controlling C biogeochemistry in response to hydrology dynamics. As the climate continues to warm rapidly

in the Arctic, large variations at both the spatial and the temporal scales are anticipated across the Arctic landscape. Dramatic changes in land surface CO_2 and CH_4 fluxes might alter the land–atmosphere feedback in the Arctic. An insightful regional-scale investigation of the thermal conditions, hydrology, and biogeochemistry across the pan- Arctic is urgently needed and will benefit the entire scientific community and the public.

References

Aas, K. S., Martin, L., Nitzbon, J., Langer, M., Boike, J., Lee, H., et al. (2019). Thaw processes in ice-rich permafrost landscapes represented with laterally coupled tiles in a land surface model. *The Cryosphere*, *13*(2), 591–609. https://doi.org/10.5194/tc-13-591-2019

Abolt, C. J., Young, M. H., Atchley, A. L., & Harp, D. R. (2018). Microtopographic control on the ground thermal regime in ice wedge polygons. *The Cryosphere*, *12*(6), 1957–1968. https://doi.org/10.5194/tc-12-1957-2018

Atchley, A. L., Coon, E. T., Painter, S. L., Harp, D. R., & Wilson, C. J. (2016). Influences and interactions of inundation, peat, and snow on active layer thickness. *Geophysical Research Letters*, *43*, 5116–5123. https://doi.org/10.1002/2016gl068550

Belshe, E. F., Schuur, E. A. G., & Bolker, B. M. (2013). Tundra ecosystems observed to be CO_2 sources due to differential amplification of the carbon cycle. *Ecology Letters*, *16*(10), 1307–1315. https://doi.org/10.1111/ele.12164

Bhullar, G. S., Edwards, P. J., & Olde Venterink, H. (2013). Variation in the plant-mediated methane transport and its importance for methane emission from intact wetland peat mesocosms. *Journal of Plant Ecology*, *6*(4), 298–304. https://doi.org/10.1093/jpe/ rts045

Bisht, G., Riley, W. J., Wainwright, H. M., Dafflon, B., Yuan, F., & Romanovsky, V. E. (2018). Impacts of microtopographic snow redistribution and lateral subsurface processes on hydrologic and thermal states in an Arctic polygonal ground ecosystem: A case study using ELM-3D v1. 0. *Geoscientific Model Development*, *11*(1). https://doi.org/10.5194/gmd-11-61-2018

Bridgham, S. D., Cadillo-Quiroz, H., Keller, J. K., & Zhuang, Q. (2013). Methane emissions from wetlands: Biogeochemical, microbial, and modeling perspectives from local to global scales. *Global Change Biology*, *19*(5), 1325–1346. https://doi.org/10.1111/gcb.12131

Davidson, S. J., Sloan, V. L., Phoenix, G. K., Wagner, R., Fisher, J. P., Oechel, W. C., & Zona, D. (2016). Vegetation type dominates the spatial variability in CH_4 emissions across multiple Arctic tundra landscapes. *Ecosystems*, *19*(6), 1116–1132. https://doi.org/10.1007/ s10021-016-9991-0

Ebrahimi, A., & Or, D. (2017). Mechanistic modeling of microbial interactions at pore to profile scale resolve methane emission dynamics from permafrost soil. *Journal of Geophysical Research: Biogeosciences*, *122*, 1216–1238. https://doi.org/10.1002/2016jg003674

Gilks, W. R., Richardson, S., & Spiegelhalter, D. J. (1998). *Markov chain Monte Carlo in practice*, (Vol. xvii, p. 486). Boca RatonFla.: Chapman & Hall. https://doi.org/10.1201/b14835

Grant, R. F. (1998). Simulation of methanogenesis in the mathematical model *ecosys*. *Soil Biology and Biochemistry*, *30*, 883–896. https:// doi.org/10.1016/S0038-0717(97)00218-6

Grant, R. F., Mekonnen, Z. A., Riley, W. J., Arora, B., & Torn, M. S. (2017a). Mathematical modelling of Arctic polygonal tundra with Ecosys: 2. Microtopography determines how CO_2 and CH_4 exchange responds to changes in temperature and precipitation. *Journal of Geophysical Research: Biogeosciences*, *122*, 3174–3187. https://doi.org/10.1002/2017jg004037

Grant, R. F., Mekonnen, Z. A., Riley, W. J., Wainwright, H. M., Graham, D., & Torn, M. S. (2017b). Mathematical modelling of Arctic polygonal tundra with Ecosys: 1. Microtopography determines how active layer depths respond to changes in temperature

and preci- pitation. *Journal of Geophysical Research: Biogeosciences*, *122*, 3161–3173. https://doi.org/10.1002/2017jg004035

Herndon, E. M., Mann, B. F., Roy Chowdhury, T., Yang, Z., Wullschleger, S. D., Graham, D., et al. (2015a). Pathways of anaerobic organic matter decomposition in tundra soils from Barrow, Alaska. *Journal of Geophysical Research: Biogeosciences*, *120*, 2345–2359. https://doi. org/10.1002/2015JG003147

Herndon, E. M., Yang, Z., Bargar, J., Janot, N., Regier, T. Z., Graham, D. E., et al. (2015). Geochemical drivers of organic matter decom- position in Arctic tundra soils. *Biogeochemistry*, *126*(3), 397–414. https://doi.org/10.1007/s10533-015-0165-5

Hinkel, K. M., Frohn, R. C., Nelson, F. E., Eisner, W. R., & Beck, R. A. (2005). Morphometric and spatial analysis of thaw lakes and drained thaw lake basins in the western Arctic coastal plain, Alaska. *Permafrost and Periglacial Processes*, *16*(4), 327–341. https://doi.org/ 10.1002/ppp.532

Jørgensen, C. J., Lund Johansen, K. M., Westergaard-Nielsen, A., & Elberling, B. (2014). Net regional methane sink in high Arctic soils of Northeast Greenland. *Nature Geoscience*, *8*(1), 20–23. https://doi.org/10.1038/ngeo2305

Kaiser, S., Göckede, M., Castro-Morales, K., Knoblauch, C., Ekici, A., Kleinen, T., et al. (2017). Process-based modelling of the methane balance in periglacial landscapes (JSBACH-methane). *Geoscientific Model Development*, *10*(1), 333–358. https://doi.org/10.5194/gmd-10- 333-2017

Kettunen, A. (2003). Connecting methane fluxes to vegetation cover and water table fluctuations at microsite level: A modeling study. *Global Biogeochemical Cycles*, *17*(2), 1051. https://doi.org/10.1029/2002GB001958

Kittler, F., Heimann, M., Kolle, O., Zimov, N., Zimov, S., & Göckede, M. (2017). Long-term drainage reduces CO_2 uptake and CH_4 emissions in a Siberian permafrost ecosystem. *Global Biogeochemical Cycles*, *31*, 1704–1717. https://doi.org/10.1002/2017gb005774

Koven, C. D., Riley, W., Subin, Z. M., Tang, J., Torn, M. S., Collins, W. D., et al. (2013). The effect of vertically-resolved soil biogeochemistry and alternate soil C and N models on C dynamics of CLM4. *Biogeosciences*, *10*, 7109–7131. https://doi.org/10.5194/bg-10-7109-2013

Kumar, J., Collier, N., Bisht, G., Mills, R. T., Thornton, P. E., Iversen, C. M., & Romanovsky, V. (2016). Modeling the spatiotemporal variability in subsurface thermal regimes across a low-relief polygonal tundra landscape. *The Cryosphere*, *10*, 2241–2274. https://doi.org/ 10.5194/tc-10-2241-2016

Langford, Z., Kumar, J., Hoffman, F., Norby, R., Wullschleger, S., Sloan, V., & Iversen, C. (2016). Mapping arctic plant functional type distributions in the barrow environmental observatory using WorldView-2 and LiDAR datasets. *Remote Sensing*, *8*, 733. https://doi.org/ 10.3390/rs8090733

Liljedahl, A. K., Hinzman, L. D., Harazono, Y., Zona, D., Tweedie, C. E., Hollister, R. D., et al. (2011). Nonlinear controls on evapotranspiration in arctic coastal wetlands. *Biogeosciences*, *8*(11), 3375–3389. https://doi.org/10.5194/bg-8-3375-2011

Lipson, D. A., Raab, T. K., Goria, D., & Zlamal, J. (2013). The contribution of Fe (III) and humic acid reduction to ecosystem respiration in drained thaw lake basins of the Arctic coastal plain. *Global Biogeochemical Cycles*, *27*, 399–409. https://doi.org/10.1002/gbc.20038

Lipson, D. A., Zona, D., Raab, T. K., Bozzolo, F., Mauritz, M., & Oechel, W. C. (2012). Water

table height and microtopography control biogeochemical cycling in an Arctic coastal tundra ecosystem. *Biogeosciences*, *9*, 577–591. https://doi.org/10.1002/gbc.20038

Lu, X. L., & Zhuang, Q. L. (2012). Modeling methane emissions from the Alaskan Yukon River basin, 1986–2005, by coupling a large-scale hydrological model and a process-based methane model. *Journal of Geophysical Research – Biogeosciences*, *117*, G02010. https://doi.org/ 10.1029/2011jg001843

Nauta, A. L., Heijmans, M. M., Blok, D., Limpens, J., Elberling, B., Gallagher, A., et al. (2015). Permafrost collapse after shrub removal shifts tundra ecosystem to a methane source. *Nature Climate Change*, *5*, 67–70. https://doi.org/10.1038/nclimate2446

Nazaries, L., Murrell, J. C., Millard, P., Baggs, L., & Singh, B. K. (2013). Methane, microbes and models: Fundamental understanding of the soil methane cycle for future predictions. *Environmental Microbiology*, *15*, 2395–2417. https://doi.org/10.1111/1462-2920.12149

Newman, B. D., Throckmorton, H. M., Graham, D. E., Gu, B., Hubbard, S. S., Liang, L., et al. (2015). Microtopographic and depth controls on active layer chemistry in Arctic polygonal ground. *Geophysical Research Letters*, *42*, 1808–1817. https://doi.org/10.1002/ 2014gl062804

Oechel, W. C., Hastings, S. J., Vourlitis, G., Jenkins, M., Riechers, G., & Grulke, N. (1993). Recent change of Arctic tundra ecosystems from a net carbon-dioxide sink to a source. *Nature*, *361*, 520–523. https://doi.org/10.1038/361520a0

Oh, Y., Stackhouse, B., Lau, M. C. Y., Xu, X., Trugman, A. T., Moch, J., et al. (2016). A scalable model for methane consumption in arctic mineral soils. *Geophysical Research Letters*, *43*, 5143–5150. https://doi.org/10.1002/2016gl069049

Olivas, P. C., Oberbauer, S. F., Tweedie, C. E., Oechel, W. C., & Kuchy, A. (2010). Responses of CO_2 flux components of Alaskan coastal plain tundra to shifts in water table. *Journal of Geophysical Research – Biogeosciences*, *115*, G00I05. https://doi.org/10.1029/ 2009jg001254

Raz-Yaseef, N. Billesbach, D., Torn M. (2013). Eddy-covariance and auxiliary measurements, NGEE-Barrow, 2012-2013. Next generation ecosystem experiments Arctic data collection, oak Ridge National Laboratory, U.S. Department of Energy, oak ridge, Tennessee, USA. Dataset accessed on July 1st 2015 at https://doi.org/10.5440/1362279.

Reeburgh, W. S., King, J. Y., Regli, S. K., Kling, G. W., Auerbach, N. A., & Walker, D. A. (1998). A CH_4 emission estimate for the Kuparuk River basin, Alaska. *Journal of Geophysical Research-Atmospheres*, *103*, 29,005–29,013. https://doi.org/10.1029/98jd00993

Riley, W. J., Subin, Z. M., Lawrence, D. M., Swenson, S. C., Torn, M. S., Meng, L., et al. (2011). Barriers to predicting changes in global terrestrial methane fluxes: Analyses using CLM4Me, a methane biogeochemistry model integrated in CESM. *Biogeosciences*, *8*, 1925–1953. https://doi.org/10.5194/bg-8-1925-2011

Schrier-Uijl, A. P., Kroon, P. S., Hensen, A., Leffelaar, P. A., Berendse, F., & Veenendaal, E. M. (2010). Comparison of chamber and eddy covariance-based CO_2 and CH_4 emission estimates in a heterogeneous grass ecosystem on peat. *Agricultural and Forest Meteorology*, *150*, 825–831. https://doi.org/10.1016/j.agrformet.2009.11.007

Segers, R., & Kengen, S. W. M. (1998). Methane production as a function of anaerobic carbon mineralization: A process model. *Soil Biology and Biochemistry*, *30*, 1107–1117. https://doi.org/10.1016/S0038-0717(97)00198-3

Semenchuk, P. R., Elberling, B., Amtorp, C., Winkler, J., Rumpf, S., Michelsen, A., & Cooper,

E. J. (2015). Deeper snow alters soil nutrient availability and leaf nutrient status in high Arctic tundra. *Biogeochemistry*, *124*, 81–94. https://doi.org/10.1007/s10533-015-0082-7

Song, C., Xu, X., Sun, X., Tian, H., Sun, L., Miao, Y., et al. (2012). Large methane emission upon spring thaw from natural wetlands in the northern permafrost region. *Environmental Research Letters*, *7*, 34009. https://doi.org/10.1088/1748-9326/7/3/034009

Sturtevant, C. S., & Oechel, W. C. (2013). Spatial variation in landscape-level CO_2 and CH_4 fluxes from arctic coastal tundra: Influence from vegetation, wetness, and the thaw lake cycle. *Global Change Biology*, *19*(9), 2853–2866. https://doi.org/10.1111/gcb.12247

Tan, Z., Zhuang, Q., Henze, D. K., Frankenberg, C., Dlugokencky, E., Sweeney, C., & Turner, A. J. (2015). Mapping pan-Arctic methane emissions at high spatial resolution using an adjoint atmospheric transport and inversion method and process-based wetland and lake biogeochemical models. *Atmospheric Chemistry and Physics Discussions*, *15*, 32,469–32,518. https://doi.org/10.5194/acpd-15- 32469-2015

Tas, N., Prestat, E., Wang, S., Wu, Y., Ulrich, C., Kneafsey, T., et al. (2018). Landscape topography structures the soil microbiome in arctic polygonal tundra. *Nature Communications*, *9*(1), 777. https://doi.org/10.1038/s41467-018-03089-z

Thauer, R. K., Kaster, A.-K., Seedorf, H., Buckel, W., & Hedderich, R. (2008). Methanogenic archaea: Ecologically relevant differences in energy conservation. *Nature Reviews Microbiology*, *6*(8), 579–591. https://doi.org/10.1038/nrmicro1931

Thauer, R. K., Zinkhan, D., & Spormann, A. (1989). Biochemistry of acetate catabolism in anaerobic chemotrophic bacteria. *Annual Reviews in Microbiology*, *43*, 43–67. https://doi.org/10.1146/annurev.mi.43.100189.000355

Thornton, P. E., Lamarque, J.-F., Rosenbloom, N. A., & Mahowald, N. M. (2007). Influence of carbon-nitrogen cycle coupling on land model response to CO_2 fertilization and climate variability. *Global Biogeochemical Cycles*, *21*, GB4018. https://doi.org/10.1029/ 2006gb002868

Thornton, P. E., & Rosenbloom, N. A. (2005). Ecosystem model spin-up: Estimating steady state conditions in a coupled terrestrial carbon and nitrogen cycle model. *Ecological Modelling*, *189*, 25–48. https://doi.org/10.1016/j.ecolmodel.2005.04.008

Throckmorton, H. M., Heikoop, J. M., Newman, B. D., Altmann, G. L., Conrad, M. S., Muss, J. D., & Wilson, C. J. (2015). Pathways and transformations of dissolved methane and dissolved inorganic carbon in Arctic tundra watersheds: Evidence from analysis of stable isotopes. *Global Biogeochemical Cycles*, *29*, 1893–1910. https://doi.org/10.1002/2014GB005044

Tian, H., Xu, X., Liu, M., Ren, W., Zhang, C., Chen, G., & Lu, C. (2010). Spatial and temporal patterns of CH_4 and N_2O fluxes in terrestrial ecosystems of North America during 1979-2008: Application of a global biogeochemistry model. *Biogeosciences*, *7*, 2673–2694. https:// doi.org/10.5194/bg-7-2673-2010

Tokida, T., Mizoguchi, M., Miyazaki, T., Kagemoto, A., Nagata, O., & Hatano, R. (2007). Episodic release of methane bubbles from peatland during spring thaw. *Chemosphere*, *70*(2), 165–171. https://doi.org/10.1016/j.chemosphere.2007.06.042

Torn, M. S. (2016). CO_2 CH_4 flux air temperature soil temperature and soil moisture, Barrow, Alaska 2013 ver. 1. Retrieved from: http:// ngee-arctic.ornl.gov/

Von Fischer, J. C., & Hedin, L. O. (2007). Controls on soil methane fluxes: Tests of biophysical mechanisms using stable isotope tracers. *Global Biogeochemical Cycles*, *21*, GB2007. https://doi.org/10.1029/2006GB002687

von Fischer, J. C., Rhew, R. C., Ames, G. M., Fosdick, B. K., & von Fischer, P. E. (2010). Vegetation height and other controls of spatial variability in methane emissions from the Arctic coastal tundra at Barrow, Alaska. *Journal of Geophysical Research, Biogeosciences (2005–2012)*, *115*, G00I03. https://doi.org/10.1029/2009JG001283

Wagner, R., Zona, D., Oechel, W., & Lipson, D. (2017). Microbial community structure and soil pH correspond to methane production in Arctic Alaska soils. *Environmental Microbiology*, *19*, 3398–3410. https://doi.org/10.1111/1462-2920.13854

Wainwright, H. M., Liljedahl, A. K., Dafflon, B., Ulrich, C., Peterson, J. E., Gusmeroli, A., & Hubbard, S. S. (2017). Mapping snow depth within a tundra ecosystem using multiscale observations and Bayesian methods. *The Cryosphere*, *11*(2), 857–875. https://doi.org/10.5194/tc-11-857-2017

Walter, B. P., & Heimann, M. (2000). A process-based, climate-sensitive model to derive methane emissions from natural wetlands: Application to five wetland sites, sensitivity to model parameters, and climate. *Global Biogeochemical Cycles*, *14*, 745–765. https://doi.org/10.1029/1999GB001204

Wania, R., Ross, I., & Prentice, I. C. (2010). Implementation and evaluation of a new methane model within a dynamic global vegetation model: LPJ-WHyMe v1.3.1. *Geoscientific Model Development*, *3*, 565–584. https://doi.org/10.5194/gmd-3-565-2010

Watts, J. D., Kimball, J. S., Parmentier, F. J. W., Sachs, T., Rinne, J., Zona, D., et al. (2014). A satellite data driven biophysical modeling approach for estimating northern peatland and tundra CO_2 and CH_4 fluxes. *Biogeosciences*, *11*, 1961–1980. https://doi.org/10.5194/bg-11-1961-2014

Wille, C., Kutzbach, L., Sachs, T., Wagner, D., & Pfeiffer, E.-M. (2008). Methane emission from Siberian arctic polygonal tundra: Eddy covariance measurements and modeling. *Global Change Biology*, *14*, 1395–1408. https://doi.org/10.1111/j.1365-2486.2008.01586.x

Xu, X., & Yuan, F. (2016). *Meteorological forcing at Barrow AK 1981–2013*. Retrieved from http://ngee-arctic.ornl.gov/ Xu, X., Yuan, F., Hanson, P. J., Wullschleger, S. D., Thornton, P. E., Riley, W. J., et al. (2016). Review and synthesis: Four decades of modeling methane cycling within terrestrial ecosystems. *Biogeosciences*, *13*, 3735–3755. https://doi.org/10.5194/bg-13-3735-2016

Xu, X. F., Elias, D. A., Graham, D. E., Phelps, T. J., Carrol, S. L., Wullschleger, S. D., & Thornton, P. E. (2015). A microbial functional group based module for simulating methane production and consumption: Application to an incubation permafrost soil. *Journal of Geophysical Research: Biogeosciences*, *120*, 1315–1333. https://doi.org/10.1002/2015JG002935

Xu, X. F, Hahn, M. S., Kumar, J., Yuan, F., Tang, G., Thornton, P., et al. (2014), Upscaling Plot-Scale Methane Flux to a Eddy Covariance Tower Domain in Barrow, AK: Integrating in-situ data with a microbial functional group-based model, paper presented at AGU Fall Meeting Abstracts.

Xu, X. F., Tian, H. Q., Zhang, C., Liu, M. L., Ren, W., Chen, G. S., et al. (2010). Attribution of spatial and temporal variations in terrestrial methane flux over North America. *Biogeosciences*, *7*, 3637–3655. https://doi.org/10.5194/bg-7-3637-2010

Yuan, F., Wang, G., Painter, S. L., Tang, G., Xu, X., Kumar, J., et al. (2017). *Effect of Freeze-Thaw Cycles on Soil Nitrogen Reactive Transport in a Polygonal Arctic Tundra Ecosystem at Barrow AK Using 3-D Coupled ALM-PFLOTRAN*. In AGU Fall Meeting

Abstracts.
Zhang, Y., Sachs, T., Li, C., & Boike, J. (2012). Upscaling methane fluxes from closed chambers to eddy covariance based on a permafrost biogeochemistry integrated model. *Global Change Biology*, *18*, 1428–1440. https://doi.org/10.1111/j.1365-2486.2011.02587.x
Zhuang, Q., Melillo, J. M., Kicklighter, D. W., Prinn, R. G., McGuire, A. D., Steudler, P. A., et al. (2004). Methane fluxes between terrestrial ecosystems and the atmosphere at northern high latitudes during the past century: A retrospective analysis with a process-based biogeochemistry model. *Global Biogeochemical Cycles*, *18*, GB3010. https://doi.org/10.1029/2004GB002239
Zona, D., Gioli, B., Commane, R., Lindaas, J., Wofsy, S. C., Miller, C. E., et al. (2016). Cold season emissions dominate the Arctic tundra methane budget. *Proceedings of the National Academy of Sciences*, *113*(1), 40–45. https://doi.org/10.1073/pnas.1516017113
Zona, D., Lipson, D. A., Zulueta, R. C., Oberbauer, S. F., & Oechel, W. C. (2011). Microtopographic controls on ecosystem functioning in the Arctic coastal plain. *Journal of Geophysical Research–Biogeosciences*, *116*, G00I08. https://doi.org/10.1029/2009jg001241

Chapter 2

Upscaling Methane Flux from Plot Level to Eddy Covariance Tower Domains in Five Alaskan Tundra Ecosystems

This chapter has already been published by Frontiers Media SA.

Yihui Wang, Fengming Yuan, Kyle A. Arndt, Jianzhao Liu, Liyuan He, Yunjiang Zuo, Donatella Zona, David A. Lipson, Walter C. Oechel, Daniel M. Ricciuto, Stan D. Wullschleger, Peter E. Thornton, and Xiaofeng Xu. 2022. Upscaling Methane Flux from Plot Level to Eddy Covariance Tower Domains in Five Alaskan Tundra Ecosystems. Frontiers in Environmental Science. doi: 10.3389/fenvs.2022.939238.

Abstract

Spatial heterogeneity in methane (CH_4) flux requires a reliable upscaling approach to reach accurate regional CH_4 budgets in the Arctic tundra. In this study, we combined the CLM-Microbe model with three footprint algorithms to scale up CH_4 flux from a plot level to eddy covariance (EC) tower domains (200 m × 200 m) in the Alaska North Slope, for three sites in Utqiaġvik (US-Beo, US-Bes, and US-Brw), one in Atqasuk (US-Atq) and one in Ivotuk (US-Ivo), for a period of 2013-2015. Three footprint algorithms were the homogenous footprint (HF) that assumes even contribution of all grid cells, the gradient footprint (GF) that assumes gradually declining contribution from center grid cells to edges, and the dynamic footprint (DF) that considers the impacts of wind and heterogeneity of land surface. Simulated annual CH_4 flux was highly consistent with the EC measurements at US-Beo and US-Bes. In contrast, flux was overestimated at US-Brw, US-Atq, and US-Ivo due to the higher simulated CH_4 flux in early growing seasons. The simulated monthly CH_4 flux was consistent to EC measurements but with different accuracies among footprint algorithms. At US-Bes in Sep 2013, RMSE and NNSE were 0.002 $\mu mol \cdot m^{-2} \cdot s^{-1}$ and 0.782 using the DF algorithm, but 0.007 $\mu mol \cdot m^{-2} \cdot s^{-1}$ and 0.758 using HF and 0.007 $\mu mol \cdot m^{-2} \cdot s^{-1}$ and 0.765 using GF, respectively. DF algorithm performed better than HF and GF algorithms

in capturing the temporal variation in daily CH_4 flux in each month, while the model accuracy was similar among the three algorithms due to flat landscapes. Temporal variations in CH_4 flux during 2013-2015 were predominately explained by air temperature (67-74%), followed by precipitation (22-36%). Spatial heterogeneities in vegetation fraction and elevation dominated the spatial variations in CH_4 flux for all five tower domains despite relatively weak differences in simulated CH_4 flux among three footprint algorithms. The CLM-Microbe model can simulate CH_4 flux at both plot and landscape scales at a high temporal resolution, which should be applicable for other landscapes. Integrating land surface models with an appropriate algorithm provides a powerful tool for upscaling CH_4 flux in terrestrial ecosystems.

Introduction

Northern Arctic tundra is characterized by polygonal patterns due to freeze-thaw cycles with large spatial heterogeneity in vegetation and soil water table (Budishchev et al., 2014b; Lara et al., 2020; Petrescu et al., 2015). This heterogeneity leads to large spatial variability of methane (CH_4) flux (Budishchev et al., 2014b; Xu et al., 2010), as the production, consumption, and transport processes of CH_4 are primarily related to hydrology, vegetation, and microbial activities (Vaughn et al., 2016). Modeling and predicting the spatial variability of CH_4 emissions at broader scales depend on the upscaling algorithms that consider heterogeneous landscapes (Davidson et al., 2016; Xu et al., 2016). At the plot scale (10^{-2} - 1 m^2), closed chambers are commonly employed to measure CH_4 flux for dominant topography and/or vegetation types (Davidson et al., 2016; Fox et al., 2008). Numerous empirical and mechanistic modeling studies have attempted to upscale these measurements to the landscape scale (10^4 - 10^5 m^2) and evaluated against eddy covariance (EC) flux (Baldocchi, 2008; Chen et al., 2012; Davidson et al., 2017; Xu and Tian, 2012). Yet, these estimates ignored the impacts of the spatial variability of CH_4 flux within the source area.

Accurate regional estimations of CH_4 flux require an upscaling approach that considers the mechanistic CH_4 processes, including the key factors that control CH_4 flux across time and space (Xu et al., 2016).

Factors affecting Arctic CH_4 emission vary substantially across spatial scales (Mer and Roger, 2001; Serrano-Silva et al., 2014; Xu et al., 2016). Soil water table has been identified as a key factor determining the CH_4 flux (Funk et al., 1994; Pirk et al., 2017). In addition, plant coverage and composition play an important role in CH_4 emission by affecting CH_4 transport pathway and providing substrate for methanogens (Bhullar et al., 2013; Davidson et al., 2016; McEwing et al., 2015; von Fischer et al., 2010). Greater vascular plant coverage and density were linked to higher CH_4 emission (Andresen et al., 2017; McEwing et al., 2015), and vegetation types can explain a large proportion of the variation in CH_4 flux in Arctic tundra (Davidson et al., 2016; Sturtevant and Oechel, 2013). This is because sedges and vascular wetland plants not only exist in waterlogged areas prime for CH_4 production, but they also transport CH_4 through their tissue straight to the atmosphere(Lai, 2009). Therefore, it is critically important to include vegetation characteristics within an EC footprint for improving the accuracy of CH_4 estimation at the landscape scale. In most CH_4 models (Xu et al., 2016), vegetation is represented as plant functional types (PFTs) and in each PFT group, plant species share similar responses to environmental factors (Langford et al., 2016). Therefore, it is critically important to integrate mechanistic models of CH_4 cycling with high-resolution spatial datasets of vegetation coverage and environmental factors to improve the accuracy of estimations of CH_4 flux at the landscape scale.

The process-based CLM-Microbe model has been tested for simulating plot-scale CH_4 flux by validating with different polygonal characteristics' (e.g. troughs, rims, and centers) flux at Utqiagvik, Alaska (Wang et al., 2019). In the previous study, we upscaled model-simulated flux

from the plot to landscape scales and validated with EC measurements using the area-weighted average approach (Wang et al., 2019). However, this approach can be rather inaccurate because the contribution of areas in upscaling might be different within the EC tower footprint, leading to a significant mismatch (Fox et al., 2008; Oechel et al., 1998). Accurate knowledge of footprints is of crucial importance for upscaling from plot-scale flux measurements to the landscape scale. Flux footprint algorithms generate the spatial extent and position of the probable source area for EC flux measurements by integrating effects of wind direction and speed, roughness at a specific time point, thereby they are widely used for understanding EC estimates and improving greenhouse gas budgets (Heidbach et al., 2017; Horst and Weil, 1992; Kljun et al., 2015; Kormann and Meixner, 2001). In our study, we combined the CLM-Microbe model with three footprint algorithms to better scale up to the landscape-scale CH_4 flux. The CLM-Microbe model represents 17 PFTs for vegetation across the globe (He et al., 2021a; He et al., 2021b; Wang et al., 2019), adding Arctic- and boreal-specific PFTs in its vegetation modules makes it more appropriate to capture Arctic vegetation processes.

This study was designed to apply the CLM-Microbe model to simulate plot-scale CH_4 flux with a fine spatial resolution for five study sites in Alaskan Arctic tundra. By incorporating with different footprint algorithms, we upscaled the simulated plot-scale flux to the EC domain and validated with the EC measurements. In this study, we aim to 1) evaluate the accuracy of CH_4 estimates simulated by the CLM-Microbe model with different footprint algorithms, 2) compare the homogenous footprint algorithm (HF), gradient footprint algorithm (GF), and dynamic footprint algorithm (DF) for assisting upscaling CH_4 flux, and 3) investigate the primary controlling factors of CH_4 emission at the landscape scale in the Arctic tundra ecosystems.

Methodology

Site Description

We performed our study at five sites in the northern Alaskan tundra (**Figure 1**), and detailed information of sites and measurements is available in (Arndt et al., 2020; Arndt et al., 2019). Three of these sites are located in Utqiaġvik (formerly Barrow), including US-Beo (71.2810°N, 156.6124°W), US-Bes (71.2809°N, 156.5965°W), and US-Brw (71.3225°N, 156.6093°W) (Zona et al., 2016). US-Beo is a polygonal coastal tundra site on the Barrow Environmental Observatory; and US-Bes is an inundated wet coastal tundra site at the southern end of the previous Biocomplexity Experiment, usually with a water table above the surface of the soil due to its low elevation (Zona et al., 2009). US-Brw is a well-drained moist coastal tundra site, and its vegetation is dominated by graminoids (Kwon et al., 2006). The US-Atq site (70.4696°N, 157.4089°W) in Atqasuk is located about 100 km south of Utqiaġvik; and the US-Ivo site (68.4805°N, 155.7569°W) in Ivotuk is located about 300 km south of Utqiaġvik in the northern foothills of the Brooks Range (**Figure 1**) (Davidson et al., 2016). US-Atq is characterized by polygonised tussock tundra and sandy soils (Walker et al., 1989), and US-Ivo, the most inland site, is the warmest and gently sloping tussock tundra (Davidson et al., 2016). The sensors are located between 2.0 – 4.17 m above the ground (3.12 m at US-Beo, 2.20 m at US-Bes, 4.17 m at US-Brw, 2.42 m at US-Atq and 3.42 m at US-Ivo) (Arndt et al., 2019).These study sites have a polar maritime climate with the majority of precipitation falling during summer months (June-August). Detailed meteorological and vegetation information for these sites is posted in the Oak Ridge National Laboratory Distributed Active Archive Center (ORNL DAAC) (https://doi.org/10.3334/ORNLDAAC/1562 and https://doi.org/10.3334/ORNLDAAC/1546).

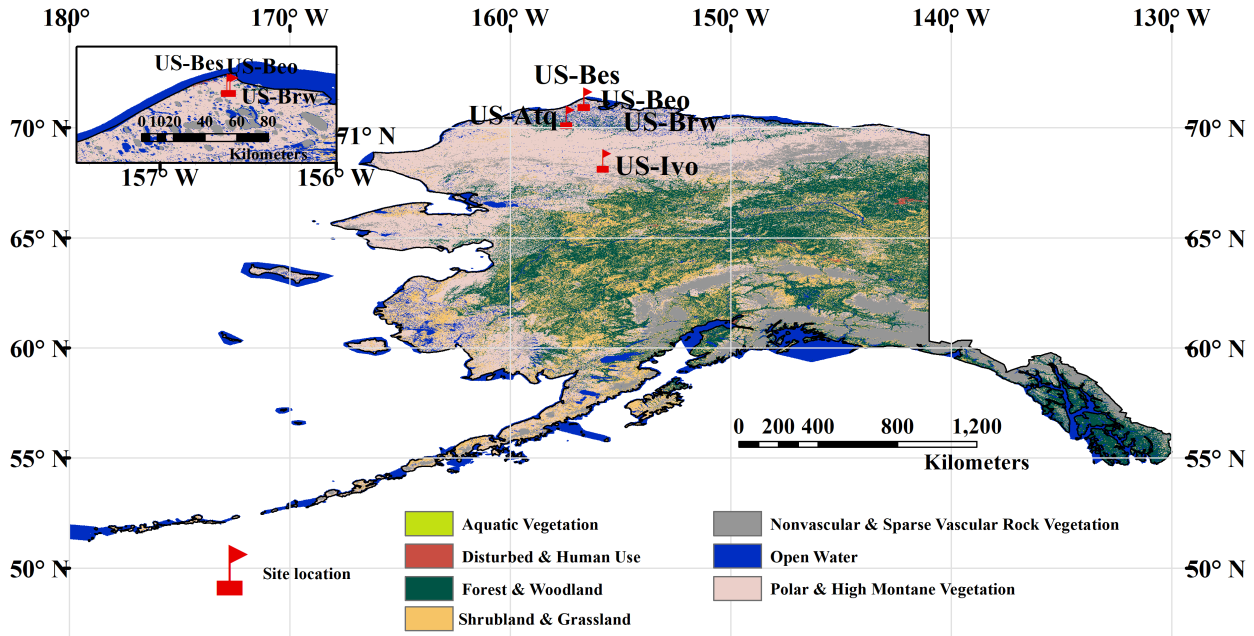

Figure 1. The land cover in Alaskan region and an inset showing the location of the eddy covariance tower sites and National Oceanic and Atmospheric Administration (NOAA) BRW station in Alaska. The land cover in Alaskan region were from GAP/LANDFIRE National Terrestrial Ecosystems data for U.S. and provided by United States Geological Survey (https://www.usgs.gov/). The US-Brw, US-Bes, and US-Beo are overlapped as three sites are close in distance; two site labels are shown in the inset.

Data Source for CH_4 Flux

CH_4 flux were monitored at a half-hourly time step using an EC tower at each study site for the period of 2013 – 2015 and half-hourly flux were calculated from raw data using the EddyPro software by LI-COR while missing data were gap-filled (Oechel and Kalhori, 2018). Winter CH_4 flux were difficult to monitor due to the frozen equipment and frozen soil (Goodrich et al., 2016; Zona et al., 2016). Daily CH_4 flux were calculated as the mean of half-hourly EC flux. Detailed information about the measurement protocols is available at https://daac.ornl.gov/ABOVE/guides/AK_North_Slope_NEE_CH4_Flux.html.

Model Description and Driving data

The CLM-Microbe model branches from the framework of default CLM 4.5 in 2013. Therefore, the CLM-Microbe has default decomposition subroutines in CLM4.5 (Koven et al.,

2013; Thornton and Rosenbloom, 2005; Thornton and Zimmermann, 2007). The improvements in the CLM-Microbe model include a new microbial-functional-group based CH_4 module (Wang et al., 2019; Xu et al., 2015), and a new framework for microbial controls on the carbon mineralization (He et al., 2021b; Xu et al., 2014). Detailed mathematical expressions for CH_4 production, consumption, and transport processes were organized in (Wang et al., 2019; Xu et al., 2015). The code for the CLM-Microbe model has been archived at https://github.com/email-clm/CLM-Microbe since 2015. The model version used in this study was obtained from GitHub on 27 May 2020.

The CLM-Microbe model considers the dynamics of dissolved organic carbon, acetate, O_2, H_2, CH_4, CO_2, and the processes of fermentation, homoacetogenesis, and methanogenesis and methanotrophy (Xu et al., 2015). The four key mechanisms for CH_4 production and consumption are methanogenesis from acetate or from single-carbon compounds and CH_4 oxidation using molecular oxygen or other inorganic electron acceptors. Four microbial functional groups perform these processes: acetoclastic methanogens, hydrogenotrophic methanogens, aerobic methanotrophs, and anaerobic methanotrophs (Xu et al., 2015; Wang et al., 2019). The soil profile is the same as the CLM4.5 (Oleson et al., 2013).

In our previous study (Wang et al., 2019), this module was validated with incubation flux and closed-chamber flux, and further compared with EC flux using an area-weighted average approach for upscaling. In this study, we considered the spatial heterogeneity of vegetation and elevation within the EC domain for each study site and conducted the model simulations at a spatial resolution of 4 m × 4 m with a domain of 40000 m^2 with the EC tower at the center. Meteorological variables driving the model include shortwave and longwave radiation, air temperature, relative humidity, wind speed and precipitation. US-Beo, US-Bes, and US-Brw shared the same

meteorological parameters due to the small distance between sites, which were generated by Xu and Yuan (2016) for the period of 1991-2015 and can be obtained from the Utqiaġvik, AK, station of NOAA/Earth System Laboratory, Global Monitoring Division (http://www.esrl.noaa.gov/gmd/obop/brw/). The data set is gap-filled and at a half-hourly time step. Meteorological variables for US-Atq and US-Ivo were extracted from the half-hourly, gap-filled CRUNCEP dataset version 4.0 with a resolution of 0.5° × 0.5° longitude/latitude resolution for a period of 1991-2014 (https://rda.ucar.edu/datasets/ds314.3/).

Other model parameters include spatial distribution of vegetation and a digital elevation model with a resolution of 4 m covering the tower domain at each site, and soil organic carbon (SOC) concentration at ten soil layers defined in CLM4.5 (Koven et al., 2013; Thornton et al., 2007; Thornton and Rosenbloom, 2005). Vegetation distribution in the source area for US-Brw, US-Beo, and US-Bes was determined using a random forest algorithm using the plant functional type (PFT) from Langford et al. (2019) as training data (Figure S2). Four PFTs were classified among five areas, including Arctic C3 grass, bare soil, broadleaf evergreen shrub and broadleaf deciduous boreal shrub. The former three PFTs dominated and accounted for > 80% of the domain of each area. A World-View3 image (Maxar Technologies) of the Barrow area collected on July 24, 2016, was used with the plant functional type map overlain to predict plant functional types at the other Barrow sites. The model was trained using 1,000 pixels at random, and then applying the trained models to the World-View3 image near the sites of interest. For the US-Atq and US-Ivo sites, an unsupervised linear spectral unmixing was performed in in ENVI V5.2 (L3Harris Geospatial) using the vegetation classes from a previous publication (Davidson et al., 2016) to inform the number of classes, with an additional open water category. Following the unmixing, vegetation classes were applied according to (Davidson et al., 2016). A 0.5 m (vertical resolution)

digital elevation model (DEM) was used for elevation data at the US-Beo, US-Bes, and US-Brw sites (Wilson, 2012). Elevation maps for US-Atq and US-Ivo were download from ArcticDEM (v3.0 Pan-Arctic) with a high resolution of 2 m based on the geographic information of these two sites, and further processed to maps with a resolution of 4 m using the MATLAB software (R2018a, the MatWorks, Inc.). SOC concentrations at 0-10, 10-20, 20-30 and 30-40 cm at US-Bes, US-Atq, and US-Ivo were derived from the Northern Circumpolar Soil Carbon Database (Hugelius et al., 2013). Due to the lack of SOC data, we assumed that US-Beo and US-Brw shared the same SOC data with BES since these sites are adjacent. In addition, since there were no spatial data of SOC, we assumed that all the grid cells within a domain of 40000 m^2 had the same vertical distribution of SOC. To calculate SOC at each soil layer for model simulation, we assumed the cumulative SOC fraction follows an asymptotic equation (Guo et al., 2020; Jackson et al., 1996; Xu et al., 2013); therefore, SOC concentration for each soil layer was estimated by an exponential equation:

$$Y = a * \beta^d,$$

where the Y is SOC concentration at the soil depth d (m) and a and β are the fitted 'coefficient' (Table S1). The SOC dataset used for model simulation was shown in Table 1.

Table 1. Concentration of soil organic carbon (SOC) (kg ·C ·m^{-3}) for model initialization for all study sites

Layer	Depth (m)	US-Beo	US-Bes	US-Brw	US-Atq	US-Ivo
1	0.007	44.6	44.6	44.6	51.6	50.8
2	0.028	45.4	45.4	45.4	51.4	49.6
3	0.062	46.6	46.6	46.6	51.0	47.6
4	0.119	48.8	48.8	48.8	50.5	44.6
5	0.212	52.6	52.6	52.6	49.5	40.1
6	0.366	59.4	59.4	59.4	48.0	33.5
7	0.620	72.8	72.8	72.8	45.7	25.0
8	1.038	101.7	101.7	101.7	42.0	15.4
9	1.728	101.7	101.7	101.7	42.0	15.4
10	2.865	101.7	101.7	101.7	42.0	15.4

Model Implementation

Model implementation was carried out in three stages, similar to the default CLM4.5 protocols (Oleson et al., 2013). The first phase is accelerated model spin-up that was set up for 2,000 years to allow the system to an accumulate C and reach steady state. We set the accelerated model spin-up for 2,000 years to allow more carbon accumulation as Arctic tundra has a low rate and long period of carbon sequestration. Then a final spin-up was set up to 50 years to allow the modeled system to reach a relatively steady state. After the final spin-up, the transient model simulation was set to cover the period of 1850–2015 for US-Beo, US-Bes, and US-Brw, and the period of 1850-2014 for US-Atq and US-Ivo. The difference in model duration was determined by the available meteorological data for each site. The climate data of 1850-2015 and 1850-2014 were covered as the CLM-Microbe model can be set to cycle the extant climate data.

For the model simulations, parameters for microbial community and hydrological processes were set to default values in the CLM-Microbe model for each study site (Oleson et al., 2013; Wang et al., 2019; Xu et al., 2015). To simulate the actual hydrological processes in this area, we modified the soil hydrology module and changed parameters for the inundated fraction to guarantee soil inundated below the 5^{th} soil layer (2 m) in the CLM-Microbe model. In addition, the parameter for plant-mediated transport of CH_4 was changed to allow CH_4 emission from soil. The transient simulations for each site produced output at the daily time step. The same model parameters and settings were applied for all five study sites.

Footprint Algorithms

In this study, we upscaled the simulated CH_4 flux to the landscape scale using three footprint algorithms. The first algorithm was the "homogeneous" footprint (HF) algorithm, which assumes the footprint is a circular area with a radius of 100 m and the EC tower as the center and

each grid cell in the footprint contributes equally (Figure 2a). The second algorithm was the "gradient" footprint (GF) algorithm, which assumes the footprint is also a circle area with a radius of 100 m and the EC tower as the center, but grid cells contribute distinctly and their contribution weights decrease from 1 at the center to 0 at the edge in the footprint (Figure 2b). Both HF and GF were constant over time. The third algorithm was the "dynamic" footprint (DF) algorithm, which considered the influence of wind direction, wind velocity, air temperature, sensible heat, precipitation, and the landscape roughness to rigorously characterize the actual EC footprint (Chen et al., 2012; Kim et al., 2006; Kormann and Meixner, 2001) (Figure 2c). The DF was developed to estimate the probability of flux originated from a particular location surrounding the flux tower (Chen et al., 2012).

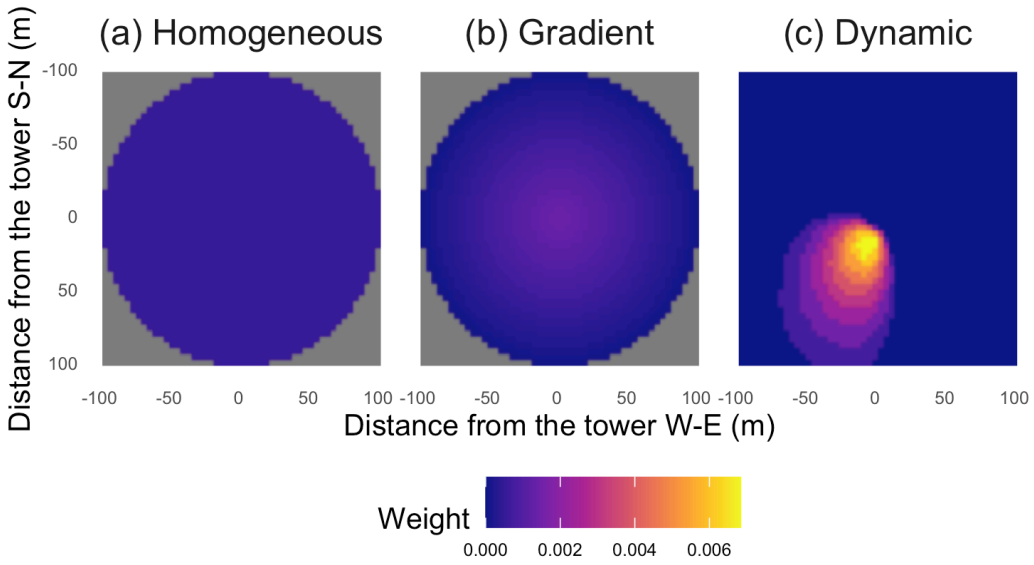

Figure 2. Source area and weight distribution for different footprint algorithms within an area of 200 m × 200 m and the EC tower as center (50 latitude grids × 50 longitude grids): (a) the "homogeneous" footprint (HF) algorithm regards each grid cell contributes evenly to total EC flux, (b) the "gradient" footprint (GF) algorithm regards the contribution of grid cells gradually decrease from center to edge; and (c) the "dynamic" footprint (DF) algorithm considers the environmental influence to generate dynamic EC footprints at daily time step. Figure (a) and (b) are constant through the year. Figure (c) shows a sample of EC footprints produced for ATQ on 22 September 2013. Grey indicates the data are unavailable. Relative weights are shown and the weights for all grids within the entire domain sum to one.

We produced the footprint with HF and GF algorithms using R, version 3.6 (R Core Team, 2020), and implemented the DF following the protocols using the MATLAB software (R2018a, MatWorks, Inc.) (Kormann and Meixner, 2001). The DF was generated at a daily time step and only for the days with no precipitation. Meteorological data for the DF were derived by the EC technique, including friction velocity, crosswind covariance, Monin-Obukhov length, roughness length, displacement height, and wind direction available at the half-hourly time step for the period of 2013-2015 (https://daac.ornl.gov/ABOVE/guides/AK_North_Slope_NEE_CH4_Flux.html).

Model Evaluation

Model evaluation was performed for the combined use of the CLM-Microbe model with each footprint model. The upscaled flux was calculated by the grid-cell CH_4 flux and its weight in the footprint and validated with the measured EC flux in 2013-2015 for each site. The coefficient of determination (R^2) and root mean square error (RMSE) were calculated for comparing upscaled and observed daily CH_4 flux at monthly and annual time steps using R, version 3.6 (R Core Team, 2020). The coefficients cannot be calculated for all months because of insufficient observations and limited DF. To further quantify the model accuracy, we adopted an index of Normalized Nash-Sutcliffe Efficiency (*NNSE*). The t is the time series of data, T is the total sample size, Q_o and Q_m are the observed and modeled data, respectively. The *NNSE* has a range of [0, 1], higher values indicate better model performance. Noted that the *NNSE* is different from R^2 as the *NNSE* takes heavy consideration of absolute values of individual data points, while R^2 relies on the covariance between observational data and modeled outputs.

$$NNSE = \frac{1}{1 + \frac{\sum_{t=1}^{T}(Q_o^t - Q_m^t)^2}{\sum_{t=1}^{T}(Q_o^t - \overline{Q_o})^2}}$$

Statistical Analysis

Annual estimates of CH_4 flux at each site were calculated based on observed and upscaled flux. Because some observed flux and DF estimates were missing, we interpolated those data with a linear method at daily time scales using R, version 3.6 (R Core Team, 2020). This approach has been applied to gap-fill the missing data, ranging from 10% for US-Beo, 21% for US-Bes, 42% for US-Brw, 43% for US-Atq, and 24% for US-Ivo. Additionally, in the current version of the CLM-Microbe model, CH_4 emission does not occur when the surface water is frozen. Hence, we only used the flux for the period of from DOY (day of year) 121 to DOY 280 for annual estimates for all study sites. Therefore, annual CH_4 flux for those areas can be underestimated by the model, since cold season flux can contribute up to 50% of annual flux (Zona et al., 2016). We also investigated the effects of air temperature, precipitation, vegetation composition and elevation on temporal and spatial variations of CH_4 flux for each site. Correlation analysis was conducted for quantifying controls of daily air temperature and precipitation on daily CH_4 flux in 2013-2015. Correlations between vegetation composition and elevation and CH_4 flux were analyzed based on the spatial distribution of those variables in 2013-2015. Pearson's correlation coefficients (r_p) are shown in Table 4 and Table S5. All statistical analyses were conducted using R scripts developed in house (version 3.6).

Results

Simulated CH_4 Flux Based on Footprint Algorithms

Compared with EC measurements, the estimates using DF algorithm were similar to those using HF and GF across study sites in 2013 – 2015, with a R^2 range of 0.210 - 0.629 (Table S3, Figure S1). A total of 61 – 63% of the variations in observed flux was explained by the simulated

flux at US-Bes and US-Atq using different footprint algorithms, while only 21% was explained for US-Ivo (Table S3, Figure S1). Values of RMSE were comparably small (0.008 - 0.011 $\mu mol \cdot m^{-2} \cdot s^{-1}$) for all sites, except 0.023 at US-Ivo (Table S3). At the monthly scale, the temporal variations of simulated CH_4 flux were improved using the DF algorithm compared with HF and GF algorithms, especially in the summer months (July - September), whereas the accuracy of estimates was similar using the HF and GF algorithms (Table 2). In the months when the DF algorithm performed better, the correlation (R^2) between observed and modeled flux was greatly increased compared with HF and GF algorithms (Table 2). However, we also observed a decreased accuracy of 36% using the DF algorithm compared with HF and GF algorithms at US-Ivo in September 2013. In the majority of the study period, the accuracy of estimated CH_4 flux was consistent among DF, HF, and GF algorithms as shown by the similar NNSE values among the three algorithms (Table 2). Overall, the three footprint algorithms were consistent for all sites (Table 2). For instance, the NNSE value was 0.758 for the HF algorithm, 0.765 for the GF algorithm, and 0.782 for the DF algorithm at the US-Bes site in September 2013, indicating a slightly better performance of the DF algorithm than the other two algorithms.

Table 2. Coefficients for simulated daily CH_4 flux for each month using the homogeneous footprint (HF), gradient footprint (GF) and dynamic footprint (DF) algorithms compared with observed flux for all study sites. (RMSE: root mean square error; Bolded values are significant at P = 0.5; NNSE: the Normalized Nash-Sutcliffe Efficiency)

Site	Year	Month	R^2			RMSE			NNSE		
			HF	GF	DF	HF	GF	DF	HF	GF	DF
US-Beo	2015	**May**	0.103	0.103	**0.384**	0.007	0.007	0.008	0.072	0.071	0.071
	2015	Jun	**0.699**	0.696	0.631	0.006	0.006	0.004	0.731	0.732	0.724
	2015	**Jul**	0.312	0.310	**0.391**	0.014	0.014	0.015	0.389	0.394	0.411
	2015	**Sep**	0.181	0.182	**0.566**	0.007	0.007	0.006	0.271	0.262	0.247
US-Bes	2013	**Jul**	0.745	0.740	**0.989**	0.016	0.016	0.019	0.181	0.178	0.177
	2013	Aug	**0.521**	0.517	0.394	0.008	0.009	0.009	0.323	0.314	0.314
	2013	**Sep**	0.461	0.459	**0.758**	0.007	0.007	0.002	0.758	0.765	0.782
	2013	**Oct**	0.015	0.015	**0.309**	0.012	0.012	0.012	0.025	0.025	0.025
	2014	Jun	**0.527**	0.520	0.419	0.007	0.007	0.007	0.502	0.498	0.495
	2014	**Aug**	0.373	0.373	**0.420**	0.01	0.01	0.012	0.133	0.129	0.127
	2015	Jun	0.617	**0.623**	0.605	0.012	0.012	0.01	0.576	0.569	0.569
	2015	Aug	**0.247**	0.242	0.173	0.007	0.006	0.006	0.310	0.322	0.318
	2015	**Sep**	0.096	0.101	**0.810**	0.01	0.01	0.01	0.156	0.162	0.170
US-Brw	2013	**Sep**	0.712	0.712	**1.000**	0.004	0.004	0.002	0.157	0.154	0.158
	2014	Jun	0.584	**0.585**	0.524	0.005	0.005	0.005	0.112	0.112	0.112
	2015	**Jun**	0.598	0.602	**0.735**	0.013	0.013	0.012	0.092	0.092	0.092
US-Atq	2013	**Aug**	0.004	0.005	**0.841**	0.005	0.005	0.005	0.012	0.012	0.010
	2014	Jun	0.352	**0.361**	0.271	0.019	0.019	0.018	0.090	0.090	0.086
	2014	**Sep**	0.506	0.504	**0.560**	0.006	0.006	0.006	0.022	0.022	0.019
US-Ivo	2013	Jul	**0.442**	0.438	0.423	0.015	0.015	0.016	0.012	0.012	0.013
	2013	Sep	**0.364**	0.364	0.234	0.049	0.049	0.046	0.049	0.049	0.048
	2014	**Aug**	0.002	0.002	**0.408**	0.023	0.023	0.022	0.098	0.099	0.091

Simulated CH_4 Flux Among Study Sites

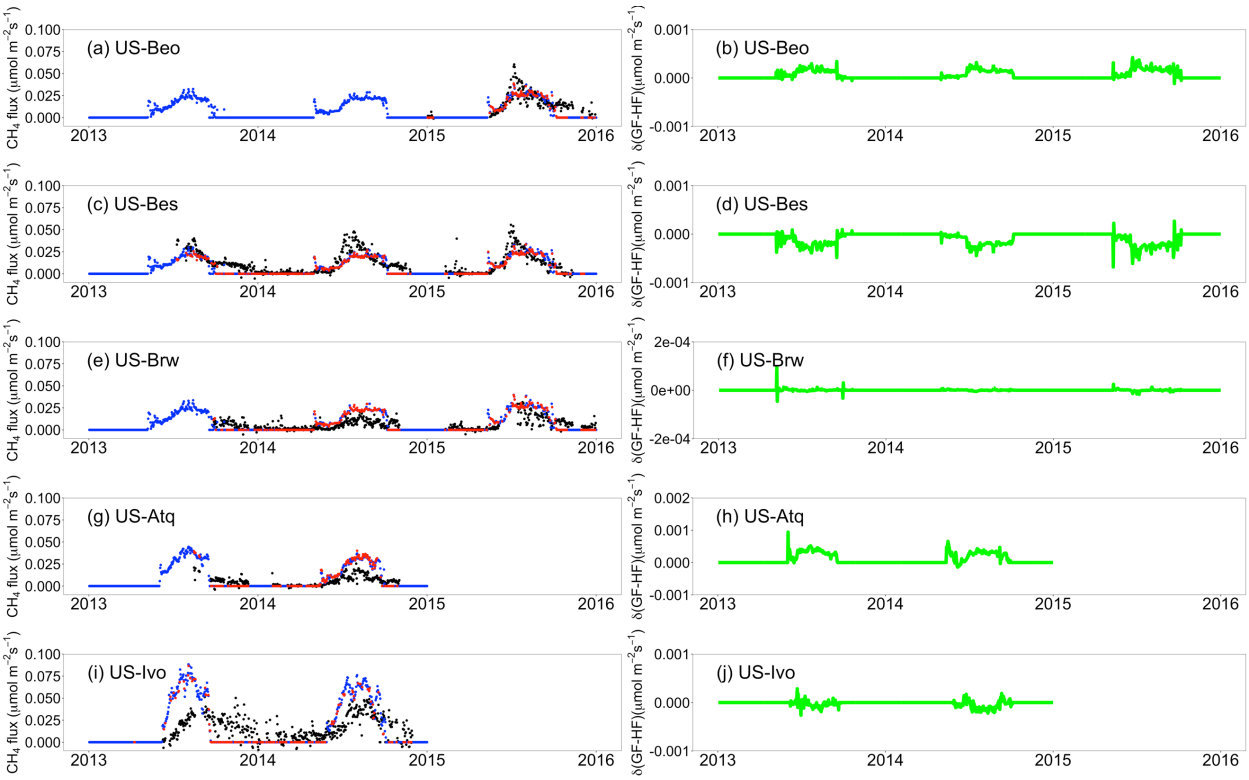

Figure 3. Left column shows the comparison of upscaled CH_4 flux using the homogeneous footprint (HF) algorithm (green points), the gradient footprint (GF) algorithm (blue points) and the dynamic footprint (DF) algorithm (red points) with the EC observed flux (black points) for (a) US-Beo, (c) US-Bes, (e) US-Brw, (g) US-Atq, and (i) US-Ivo at daily time step during a period of 2013-2015. Right column shows the differences of CH_4 flux between GF and HF for (b) US-Beo, (d) US-Bes, (f) US-Brw, (h) US-Atq, and (j) US-Ivo.

The CLM-Microbe model captured the starts, peaks, and seasonal trajectory of CH_4 flux across study sites using different footprint algorithms (Figure 3). US-Beo, US-Bes, and US-Brw showed similar trends for CH_4 emission with comparable average daily flux, even with different footprints in 2015 (Figure 3). The average CH_4 flux of the growing seasons (DOY 121 - 280) at these three sites was in a range of 0.017 - 0.020 $\mu mol \cdot m^{-2} \cdot s^{-1}$ in 2015. US-Atq and US-Ivo had higher average flux than US-Bes and US-Brw across footprints in 2013 – 2014. Average CH_4 flux at US-Atq was 0.020 $\mu mol \cdot m^{-2} \cdot s^{-1}$ in 2013, and 0.019 $\mu mol \cdot m^{-2} \cdot s^{-1}$ in 2014 using different

footprints. At US-Ivo, the average CH_4 flux in 2013 - 2014 was 0.036 - 0.037 $\mu mol \cdot m^{-2} \cdot s^{-1}$ using HF and GF algorithms, and 0.040 - 0.051 $\mu mol \cdot m^{-2} \cdot s^{-1}$ using the DF algorithm.

Table 3. Annual estimates of observed and upscaled CH_4 flux using the homogeneous footprint (HF), gradient footprint (GF) and dynamic footprint (DF) algorithms for all study sites in 2013-2015 (Unit: g C $\cdot m^{-2} \cdot year^{-1}$, n.a.: not available)

	Site	2013	2014	2015
Observed	US-Beo	n.a.	n.a.	4.1
	US-Bes	n.a.	3.8	3.7
	US-Brw	n.a.	1.5	2.7
	US-Atq	n.a.	1.7	n.a.
	US-Ivo	n.a.	4.6	n.a.
HF	US-Beo	n.a.	n.a.	4.1
	US-Bes	3.0	3.2	3.7
	US-Brw	3.4	3.6	4.3
	US-Atq	4.4	4.0	n.a.
	US-Ivo	8.0	8.3	n.a.
GF	US-Beo	n.a.	n.a.	4.1
	US-Bes	3.0	3.1	3.7
	US-Brw	3.4	3.6	4.3
	US-Atq	4.5	4.0	n.a.
	US-Ivo	8.0	8.2	n.a.
DF	US-Beo	n.a.	n.a.	4.1
	US-Bes	n.a.	3.1	3.7
	US-Brw	n.a.	3.6	4.3
	US-Atq	n.a.	4.0	n.a.
	US-Ivo	8.1	7.7	n.a.

Annual estimates of upscaled CH_4 flux were comparable using different footprints for each study site in the same year with a range of 3.0 - 8.3 g $C \cdot m^{-2}$ (Table 3). Moreover, annual estimates of upscaled CH_4 flux were consistent with estimates of observed flux for US-Beo and US-Bes in 2015, but were overestimated for US-Brw, US-Atq, and US-Ivo in 2014-2015. A small difference in annual estimates of CH_4 flux was found among US-Beo, US-Bes, and US-Brw with a range of 3.7 - 4.3 g $C \cdot m^{-2}$ using different footprint algorithms in 2015. Annual flux at US-Atq was overestimated as 4.0 g $C \cdot m^{-2}$ by all footprint algorithms, which was 2.4 times of the observed flux.

In addition, annual estimate of observed flux at US-Ivo in 2014 was 4.6 g C·m^{-2}, which was overestimated by 1.67 - 1.8 times using footprint algorithms (Table 3).

Spatial Patterns of Simulated CH_4 Flux within Study Domains

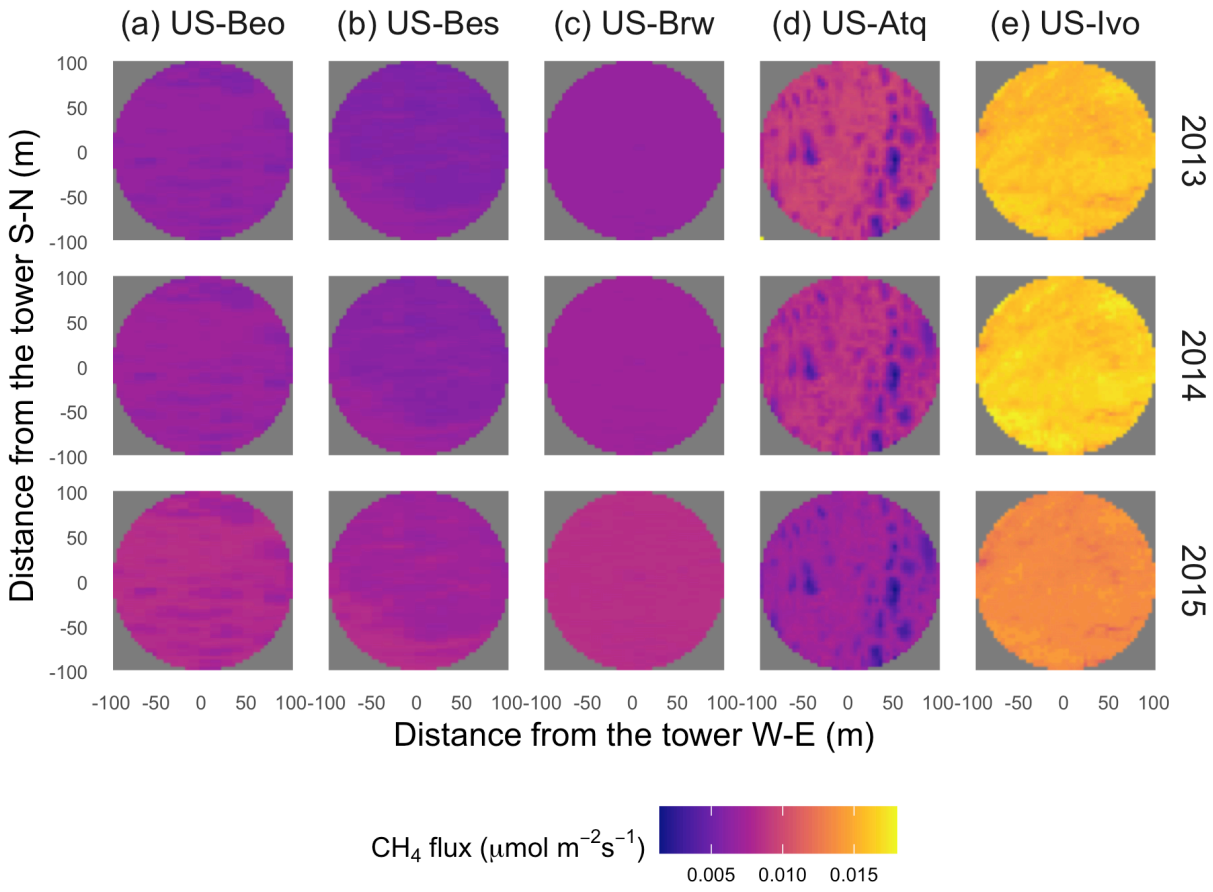

Figure 4. Spatial patterns of upscaled CH_4 emission rates based on the homogeneous footprint (HF) algorithm in an area of 200 m × 200 m during a period of 2013-2015 for all study sites

Spatial patterns of simulated CH_4 flux varied among study sites at annual and monthly scales using different footprints (Figure 4 and S3-S19, Table S4). Generally, the spatial variations were greatest using the HF algorithm across sites, which were 1.6 times of using the GF algorithm and 3.2 - 28 times of using the DF algorithm (Table S4). Similar to spatial variations, spatial averages for each study site using the GF and DF algorithms were comparable but were about half of spatial averages using the HF algorithm (Table S4). US-Ivo had the highest spatial averages

compared with other sites (unit = $\mu mol \cdot m^{-2} \cdot s^{-1}$): 0.0125 - 0.129 using the HF algorithm, 0.0044 - 0.0046 using the GF algorithm and 0.0012 - 0.0017 using the DF algorithm (Figure 4, S3 and S4, Table S4). US-Atq had the second-highest spatial averages and variations (unit = $\mu mol \cdot m^{-2} \cdot s^{-1}$): 0.0062 - 0.0069 using the HF algorithm, 0.0022 - 0.0025 using the GF algorithm, and 0.0002 - 0.0004 using the DF algorithm (Figure 4, S3 and S4, Table S4). US-Beo, US-Bes, and US-Brw had similar spatial averages using different footprint algorithms, which were 0.0047 - 0.0007 using the HF algorithm, 0.0016 - 0.0024 using the GF algorithm, and 0.0001 - 0.0005 using the DF algorithm (Figure 4, S3 and S4, Table S4). Spatial patterns of CH_4 flux were scaled up by three footprint algorithms (Figure 4, S3 and S4), but they cannot be verified because there is no available observation for spatial distribution of CH_4.

Controls on the Variations in CH_4 Flux

Air temperature and precipitation were the primary factors determining CH_4 flux at the temporal scale (Table 4). The influences of air temperature and precipitation on CH_4 flux were highly dependent on footprint algorithms across study sites. In summary, air temperature explained 67.3 - 74.3% whereas precipitation explained 22.3 - 35.6% of the temporal variations in CH_4 flux among the five study sites (Table 4). At the spatial scale, CH_4 flux was negatively correlated with bare soil percentage and positively correlated with Arctic C3 grass percentage using different footprint algorithms among the five sites, except for US-Bes; in other words, higher vegetation cover was associated with greater CH_4 emission (Table S5). Arctic C3 grass percentage was strongly related with CH_4 flux at US-Beo using the HF ($r_p = 0.385$, $P < 0.0001$), GF ($r_p = 0.284$, $P < 0.0001$) and DF ($r_p = 0.265$, $P < 0.0001$) algorithms; at US-Atq using the HF ($r_p = 0.718$, $P < 0.0001$), GF ($r_p = 0.305$, $P < 0.0001$) and DF ($r_p = 0.280$, $P < 0.0001$) algorithms; and at US-Bes ($r_p = 0.488$, $P < 0.0001$) and US-Ivo ($r_p = 0.305$, $P < 0.0001$) using the HF algorithm. More Arctic

C3 grasses facilitated CH_4 emission among five study sites (Table S5). Generally, soil temperature and soil water content were positively correlated with CH_4 fluxes using different footprint algorithms (Table S5); however, their correlations seemed to be overlaid by Arctic C3 grass and bare soils. CH_4 fluxes were positively correlated with soil temperature (r_p = 0.265, P < 0.0001) and soil water content (r_p = 0.249, P < 0.0001), but these direction of correlation was changed using GF (r_p = -0.242, P < 0.0001 for soil temperature; r_p = -0.210, P < 0.0001 for soil water content) and DF (r_p = -0.229, P < 0.0001 for soil temperature; r_p = -0.200, P < 0.0001 for soil water content) algorithms (Table S5).

Table 4. Pearson's correlation coefficients (r_p) for relationships between air temperature, precipitation and upscaled CH_4 flux using the homogeneous footprint (HF), gradient footprint (GF) and dynamic footprint (DF) for all study sites (Bold indicates | r_p | > 0.2; * indicates P <0.05, ** P < 0.01)

Footprint algorithms	Site	Air temperature (K)	Precipitation (mm)
HF	US-Beo	**0.743****	**0.222****
	US-Bes	**0.742****	**0.222****
	US-Brw	**0.743****	**0.222****
	US-Atq	**0.717****	**0.342****
	US-Ivo	**0.720****	**0.252****
GF	US-Beo	**0.743****	**0.222****
	US-Bes	**0.742****	**0.222****
	US-Brw	**0.743****	**0.222****
	US-Atq	**0.717****	**0.342****
	US-Ivo	**0.720****	**0.251****
DF	US-Beo	**0.694****	0.204
	US-Bes	**0.736****	**0.248****
	US-Brw	**0.734****	**0.261****
	US-Atq	**0.673****	**0.231****
	US-Ivo	**0.711****	**0.356****

Discussion

Importance of Footprint Algorithms in Upscaling CH_4 Emission to Landscape Scales

In this study, we integrated three footprint algorithms with a microbial functional group-based CH_4 model for upscaling plot-scale CH_4 flux to the landscape scale. Generally, the simulated flux was consistent with the observed CH_4 flux at the five study sites during 2013-2015 (Figure 3). This confirmed that the CLM-Microbe model is capable of simulating the temporal pattern of landscape-scale CH_4 emission in Arctic tundra (Wang et al., 2019). Additionally, Arctic tundra (about 11,563,300 km^2) was estimated to emit 7.54 - 20.87 Tg CH_4 per year based on our maximum and minimum of annual estimates using different footprints among all study sites, which were comparable to previous estimates (Zona et al., 2016). However, our model generally overestimated CH_4 emission for US-Brw, US-Atq, and US-Ivo in 2014-2015 and underestimated flux for US-Bes in 2014, regardless of footprint algorithms (Table 2). GF and DF algorithms narrowed the discrepancies between simulated and observed flux for US-Ivo compared with the HF algorithm, and their effects were small and upscaled fluxes were still 1.67 – 1.78 times annual estimates of observed flux. It is probably due to the relatively homogeneous surface of the source area, which led to small spatial variations in CH_4 flux at US-Ivo and further weakened the influence of footprints on upscaled fluxes (Figure 4).

The footprint algorithms can be a key factor for the regional quantification of the CH_4 flux. For example, at US-Bes in Sep 2013, the R^2 of the DF algorithm was almost double of the R^2 for the GF algorithm. This is because the upscaled flux can be simulated to be zero using the GF algorithm which can lead to a huge difference between measured and upscaled data. But upscaled flux using the DF algorithm can only be calculated when measured flux was not zero which guarantees that the upscaled flux using the DF algorithm would not be zero and maybe close to

measured flux. This is why the differences in upscaled flux between the DF algorithm and GF algorithm seem to be tiny in Figure 3 but the R^2 using DF and GF can be largely different in Table 3. Previous research found that footprint algorithms were of considerable importance for improving greenhouse gas budgeting (Chi et al., 2021; Kljun et al., 2015), and footprints provide useful information about the spatial representativeness of flux in the case that footprint size and position determine the distribution of individual sinks or sources in the study areas with large heterogeneity (Chu et al., 2021; Heidbach et al., 2017; Reuss-Schmidt et al., 2019). Thus, it is reasonable to have a small effect from footprints on improving CH_4 estimates in homogenous area, suggesting that footprint estimates are more important when validating CH_4 emission models with EC fluxes for areas with a heterogeneous and irregular vegetation pattern (Budishchev et al., 2014b). A study reported the footprint for 214 AmeriFlux sites and found that the upscaling with fixed-extent target area can lead to up to 20% of biases. A recent review paper highly recommended the footprint algorithm as a key task for the flux community (Helbig et al., 2021). This study added another evidence of the importance of dynamic footprint in predicting CH_4 flux at the regional scale.

The footprint algorithms varied among temporal scales; for example, the DF algorithm had better performance in upscaling the CH_4 flux at the monthly scale than at the annual scale. The DF algorithm performed better or comparable to improve the accuracy of CH_4 annual estimates compared with the HF and GF algorithms. The HF and GF algorithms were immutable over time, whereas the DF algorithm considers the impact of turbulence in releasing CH_4 from ecosystems (Kljun et al., 2015). Strong atmospheric turbulence can facilitate the instantaneous release of CH_4 bubbles trapped within the soil or on surfaces below the water table (Sturtevant et al., 2012). Moreover, friction velocity, which is strongly correlated with wind speed, has been reported to be

positively correlated to CH_4 emission in Arctic and sub-Arctic tundra (Sachs et al., 2008; Sturtevant et al., 2012). The DF algorithm performed better in summer months (July – September). This may be explained by the enhanced preformation of dynamic footprint estimates over heterogeneous ground, and in summer months the unstable conditions of atmospheric turbulence and vegetation cause a higher spatial heterogeneity than in winter (Sturtevant et al., 2012).

Factors Controlling Landscape-scale CH_4 Emission

In this study, air temperature was the dominant factor controlling CH_4 emission in the Arctic tundra, which explained 67.3 - 74.3% of the temporal variation in CH_4 flux. Three study sites in Utqiaġvik (US-Beo, US-Bes, and US-Brw) exhibited the same trend, start, peak, and end of CH_4 emission, since they experienced the same climate conditions (Figure 3). The annual average of air temperature was highest at US-Ivo, the southernmost study site, which correspondingly had the greatest CH_4 emission (Arndt et al., 2020; Arndt et al., 2019). The key role of temperature affecting Arctic CH_4 emission has been illustrated in numerous studies (Chistensen et al., 1993, 1995, 2004; Morrissey et al., 1992; Nielsen et al., 2016): 1) warmer temperature leads to a deeper active layer, allowing a greater soil volume to produce CH_4; 2) temperature directly affects microbial activities and efficiency of converting substrates to produce CH_4; and 3) temperature influences the plant growth and biomass in the ecosystem that impact CH_4 transport via plants. Further, precipitation explained 22.3 - 35.6% of the temporal variations in CH_4 flux among different sites. This is because CH_4 is produced by methanogens in inundated soils with no oxygen, and is oxidized in soils above the water table or in while diffusing through open water (MacDonald et al., 1998).

Spatial variations of CH_4 emission were influenced by vegetation distribution in Arctic tundra ecosystems. Higher vegetation cover was associated with larger CH_4 emission within study

sites due to the stronger plant-mediated transport of CH_4 (King et al., 1998; Waddington and Roulet, 1996). In contrast, the US-Bes displayed a positive relationship between non-vegetation proportion and CH_4 emission within the source area, which may be because inundated areas inhibited plant growth, but accelerated ebullition and production of CH_4. C_3 grasses dominate the landscape of the Arctic tundra and are known to provide a conduit for CH_4 to transport to the atmosphere. As a result, CH_4 emissions are strongly correlated with vascular species cover and root density (Davidson et al., 2016; Joabsson and Christensen, 2001; Sturtevant et al., 2012). Further, Bellisario et al. (1999) found an inverse relationship between water table position and CH_4 flux in a Canadian northern peatland, and a greater vascular plant cover was most responsible for higher emissions. A few comprehensive analyses with the FLUXNET-CH4 data have confirmed the substrate and water table as key controlling factors for CH_4 flux (Chang et al., 2021; Delwiche et al., 2021; Knox et al., 2021). More mechanistic analysis with our model for quantitative understanding of those factors on CH_4 flux is deemed as future work.

Combining the controls on temporal and spatial variations in CH_4 flux, we found that climate and seasonal drivers dominated the temporal variability while the spatial heterogeneity in land surface property dominated the spatial variability in CH_4 flux. This is consistent with two studies in the Arctic (Hashemi et al., 2021; Treat et al., 2018). Considering the small differences among the three algorithms in upscaling CH_4 flux, it suggested that the variation in CH_4 flux over months is larger than that the variation across space in the Arctic (Hashemi et al., 2021), indicating that maybe the coarser scale models are suitable in capturing total budget but not finer scale temporal rends in the Arctic (Melton et al., 2013).

The Implications

This study has three major implications for model development and upscaling CH_4 emission in the Arctic. First, the CLM-Microbe model performed well in capturing the temporal variabilities in CH_4 flux among different landscapes in the Arctic tundra, thereby improving the simulation accuracy for CH_4 flux with appropriate footprint algorithms. This study infers that the DF algorithm had similar performance to HF and GF algorithms if the landscape is flat. Second, this study emphasizes the importance of vegetation composition in influencing the spatial heterogeneity of CH_4 emission in agreement with many prior studies (Davidson et al., 2016; McEwing et al., 2015; Waddington and Roulet, 1996). However, the proportions of different plant function types are defined as unchanged during model simulation. The CLM-Microbe model could improve estimates by developing a more advanced vegetation module to improve the simulation performance for vegetation effects on CH_4 flux that have been observed to change over decadal timescales (Arndt et al., 2019; Liljedahl et al., 2016). Third, this study infers the importance of topography in driving CH_4 flux across the heterogeneous landscape. This study adopted a spatial resolution of 4 m × 4 m for the tower domain, yet soil heterogeneity is observed within a sub-meter scale. Finer resolution of soil and vegetation data might be critical for better simulating CH_4 flux at a sub-meter scale in Arctic tundra landscapes.

The Way Forward

Previous and current results demonstrate the robustness of the CLM-Microbe model to simulate the landscape-scale CH_4 emission in the Arctic tundra by incorporating different upscaling techniques (Wang et al., 2019). Here we identify several tasks required to further advance the modeling of landscape-level CH_4 emission in Arctic tundra. First, CH_4 emission during the cold season is very important, which possibly contributes up to ~50% of annual estimates in Arctic tundra (Arndt et al., 2020; Hashemi et al., 2021; Zona et al., 2016). The

formation of a zero curtain during the cold season thereby contributes to a large underestimation of CH_4 production (Mastepanov et al., 2008; Mastepanov et al., 2013; Zona et al., 2016). The current version of CLM-Microbe allows CH_4 release from a frozen soil surface, and the model does not effectively simulate the CH_4 dynamics associated with the zero-curtain in Arctic tundra. Hence, a more accurate representative of the actual soil hydrological and physical condition is warranted. Second, estimation of the Arctic CH_4 budget can be improved by the CLM-Microbe model, owing to the simulation of different microbial functional groups (methanogens vs. methanotrophs) acting in CH_4 processes. Based on current study, it is feasible to conduct the model simulation of CH_4 for Arctic regions using the Circumpolar Arctic map. Extrapolating to the entire Arctic by combining a relatively high-resolution vegetation maps and topography data would tremendously improve the accuracy of the CH_4 emission estimates. Third, the "hot moments" may represent a disproportionate contribution to the annual CH_4 flux in the permafrost region (Mastepanov et al., 2013; Pirk et al., 2015; Raz-Yaseef et al., 2016; Song et al., 2012), yet no landscape and regional modeling studies have fully taken it into consideration these "hot moments" events (Xu et al., 2016). Although our model showed a high pulse in the early growing season, more mechanistic evaluation of the CH_4 pulse dynamics should be included in our future work. Fourth, selection of footprint algorithms for upscaling plot-level CH_4 flux is important for landscape-scale CH_4 estimates. Currently, various models have been used to estimate the source area of flux measurements (Budishchev et al., 2014a; Zhang et al., 2012). This study compared three footprint algorithms for upscaling CH_4 flux. Other footprint algorithms such as Lagrangian particle models (Heidbach et al., 2017) and the development of complex "full flow" large eddy simulations may need to be considered for a more comprehensive evaluation.

Conclusions

This study reported applying the CLM-Microbe model to landscape-scale CH_4 emission in the Arctic tundra in association with three footprint algorithms. The model captured the temporal dynamics of CH_4 emission for different study sites, even when using the same model settings and parameters. The DF algorithm improved the accuracy of temporal variations in CH_4 flux compared with the HF and GF algorithms by considering the influence of wind and soil surface conditions. It performed better on the monthly scale than on an annual scale. Due to the relatively flat landscape in the Arctic, the three footprint algorithms did not lead to substantial differences in the magnitudes of observed CH_4 flux within a portion of the study sites. Air temperature explained 67 - 74% of temporal variations of CH_4 flux, whereas precipitation explained 22 - 36% of temporal variations. Concerning spatial dynamics, vegetation cover was positively related to Arctic CH_4 emission from soil to atmosphere. In particular, the C_3 arctic grasses played an essential role in facilitating CH_4 transport from soil to the atmosphere. Extrapolating our modeling results to the northern Arctic tundra ecosystems led to an annual CH_4 emission of 7.54 - 20.87 Tg CH_4 per year. This study suggested that the approach adopted in this study is applicable for other ecosystem types around the globe. The selection of an appropriate footprint model for upscaling CH_4 flux depends on the landscape characteristics of the study domains.

References

Andresen, C. G., Lara, M. J., Tweedie, C. E., and Lougheed, V. L. (2017). Rising Plant-Mediated Methane Emissions from Arctic Wetlands. *Glob. Change Biol.* 23 (3), 1128–1139. doi:10.1111/gcb.13469

Arndt, K. A., Oechel, W. C., Goodrich, J. P., Bailey, B. A., Kalhori, A., Hashemi, J., et al. (2019). Sensitivity of Methane Emissions to Later Soil Freezing in Arctic Tundra Ecosystems. *J. Geophys. Res. Biogeosci.* 124 (8), 2595–2609. doi:10.1029/2019jg005242

Arndt, K. A., Lipson, D. A., Hashemi, J., Oechel, W. C., and Zona, D. (2020). Snow Melt Stimulates Ecosystem Respiration in Arctic Ecosystems. *Glob. Change Biol.* 26 (9), 5042–5051. doi:10.1111/gcb.15193

Baldocchi, D. (2008). 'Breathing' of the Terrestrial Biosphere: Lessons Learned from a Global Network of Carbon Dioxide Flux Measurement Systems. *Aust. J. Bot.* 56 (1), 1–26. doi:10.1071/bt07151

Bellisario, L. M., Bubier, J. L., Moore, T. R., and Chanton, J. P. (1999). Controls on CH_4 Emissions from a Northern Peatland. *Glob. Biogeochem. Cycl.* 13 (1), 81–91. doi:10.1029/1998gb900021

Bhullar, G. S., Iravani, M., Edwards, P. J., and Olde Venterink, H. (2013). Methane Transport and Emissions from Soil as Affected by Water Table and Vascular Plants. *BMC Ecol.* 13 (1), 32–39. doi:10.1186/1472-6785-13-32

Budishchev, A., Mi, Y., van Huissteden, J., Belelli-Marchesini, L., Schaepman- Strub, G., Parmentier, F. J. W., et al. (2014). Evaluation of a Plot-Scale Methane Emission Model Using Eddy Covariance Observations and Footprint Modelling. Biogeosciences 11 (17), 4651–4664. doi:10.5194/bg-11-4651-2014

Chang, K.-Y., Riley, W. J., Knox, S. H., Jackson, R. B., McNicol, G., Poulter, B., et al. (2021). Substantial Hysteresis in Emergent Temperature Sensitivity of Global Wetland CH4 Emissions. *Nat. Commun.* 12 (1), 1–10. doi:10.1038/s41467-021-22452-1

Chen, B., Coops, N. C., Fu, D., Margolis, H. A., Amiro, B. D., Black, T. A., et al. (2012). Characterizing Spatial Representativeness of Flux Tower Eddy- Covariance Measurements across the Canadian Carbon Program Network Using Remote Sensing and Footprint Analysis. *Remote Sens. Environ.* 124, 742–755. doi:10.1016/j.rse.2012.06.007

Chi, J., Zhao, P., Klosterhalfen, A., Jocher, G., Kljun, N., Nilsson, M. B., et al. (2021). Forest Floor Fluxes Drive Differences in the Carbon Balance of Contrasting Boreal Forest Stands. *Agric. For. Meteorol.* 306, 108454. doi:10.1016/j. agrformet.2021.108454

Christensen, T. R., and Cox, P. (1995). Response of Methane Emission from Arctic Tundra to Climatic Change: Results from a Model Simulation. *Tellus B Chem. Phys. Meteorol*. 47 (3), 301–309. doi:10.3402/tellusb.v47i3.16049

Christensen, T. R., Johansson, T., Åkerman, H. J., Mastepanov, M., Malmer, N., Friborg, T., and Svensson, B. H. (2004). Thawing Sub-arctic Permafrost: Effects on Vegetation and Methane Emissions. Geophys. Res. Lett. 31, L04501. doi:10.1029/ 2003gl018680

Christensen, T. R. (1993). Methane Emission from Arctic Tundra. *Biogeochemistry* 21 (2), 117–139. doi:10.1007/bf00000874

Chu, H., Luo, X., Ouyang, Z., Chan, W. S., Dengel, S., Biraud, S. C., et al. (2021). Representativeness of Eddy-Covariance Flux Footprints for Areas Surrounding AmeriFlux Sites. *Agric. For. Meteorol*. 301-302, 108350. doi:10.1016/j. agrformet.2021.108350

Davidson, S. J., Sloan, V. L., Phoenix, G. K., Wagner, R., Fisher, J. P., Oechel, W. C., et al. (2016). Vegetation Type Dominates the Spatial Variability in CH4 Emissions across Multiple Arctic Tundra Landscapes. *Ecosystems* 19 (6), 1116–1132. doi:10.1007/s10021-016-9991-0

Davidson, S., Santos, M., Sloan, V., Reuss-Schmidt, K., Phoenix, G., Oechel, W., et al. (2017). Upscaling CH4 Fluxes Using High-Resolution Imagery in Arctic Tundra Ecosystems. *Remote Sens*. 9 (12), 1227. doi:10.3390/rs9121227

Delwiche, K. B., Knox, S. H., Malhotra, A., Fluet-Chouinard, E., McNicol, G., Feron, S., et al. (2021). FLUXNET-CH4: a Global, Multi-Ecosystem Dataset and Analysis of Methane Seasonality from Freshwater Wetlands. *Earth Syst. Sci. Data* 13 (7), 3607–3689. doi: 10.5194/essd-2020-307

Fox, A. M., Huntley, B., Lloyd, C. R., Williams, M., and Baxter, R. (2008). Net Ecosystem Exchange over Heterogeneous Arctic Tundra: Scaling between Chamber and Eddy Covariance Measurements. *Glob. Biogeochem. Cycl*. 22, GB2027. doi:10.1029/2007gb003027

Funk, D. W., Pullman, E. R., Peterson, K. M., Crill, P. M., and Billings, W. D. (1994). Influence of Water Table on Carbon Dioxide, Carbon Monoxide, and Methane Fluxes from Taiga Bog Microcosms. *Glob. Biogeochem. Cycl.* 8 (3), 271–278. doi:10.1029/94gb01229

Goodrich, J. P., Oechel, W. C., Gioli, B., Moreaux, V., Murphy, P. C., Burba, G., et al. (2016). Impact of Different Eddy Covariance Sensors, Site Set-Up, and Maintenance on the Annual Balance of CO2 and CH4 in the Harsh Arctic Environment. *Agric. For. Meteorol.* 228-229, 239–251. doi:10.1016/j.agrformet.2016.07.008

Guo, Z., Wang, Y., Wan, Z., Zuo, Y., He, L., Li, D., et al. (2020). Soil Dissolved Organic Carbon in Terrestrial Ecosystems: Global Budget, Spatial Distribution and Controls. *Glob. Ecol. Biogeogr*. 29 (12), 2159–2175. doi:10.1111/geb.13186

Hashemi, J., Zona, D., Arndt, K. A., Kalhori, A., and Oechel, W. C. (2021). Seasonality Buffers Carbon Budget Variability across Heterogeneous Landscapes in Alaskan Arctic Tundra. *Environ. Res. Lett.* 16 (3), 035008. doi:10.1088/1748-9326/abe2d1

He, L., Lai, C. T., Mayes, M. A., Murayama, S., and Xu, X. (2021a). Microbial Seasonality Promotes Soil Respiratory Carbon Emission in Natural Ecosystems: a Modeling Study. *Glob. Change Biol*. 27, 3035–3051. doi:10.1111/gcb.15627

He, L., Lipson, D. A., Mazza Rodrigues, J. L., Mayes, M., Björk, R. G., Glaser, B., et al. (2021b). Dynamics of Fungal and Bacterial Biomass Carbon in Natural Ecosystems: Site-Level Applications of the CLM-Microbe Model. *J. Adv. Model. Earth Syst*. 13, e2020MS002283

Heidbach, K., Schmid, H. P., and Mauder, M. (2017). Experimental Evaluation of Flux Footprint Models. *Agric. For. Meteorol.* 246, 142–153. doi:10.1016/j.agrformet.2017.06.008

Helbig, M., Gerken, T., Beamesderfer, E. R., Baldocchi, D. D., Banerjee, T., Biraud, S. C., et al. (2021). Integrating Continuous Atmospheric Boundary Layer and Tower-Based Flux Measurements to Advance Understanding of Land- Atmosphere Interactions. *Agric. For. Meteorol.* 307, 108509. doi:10.1016/j.agrformet.2021.108509

Horst, T. W., and Weil, J. C. (1992). Footprint Estimation for Scalar Flux Measurements in the Atmospheric Surface Layer. *Boundary-Layer Meteorol.* 59 (3), 279–296. doi:10.1007/bf00119817

Hugelius, G., Tarnocai, C., Broll, G., Canadell, J. G., Kuhry, P., and Swanson, D. K. (2013). The Northern Circumpolar Soil Carbon Database: Spatially Distributed Datasets of Soil

Coverage and Soil Carbon Storage in the Northern Permafrost Regions. *Earth Syst. Sci.* Data 5 (1), 3–13. doi:10.5194/essd-5-3-2013

Jackson, R. B., Canadell, J., Ehleringer, J. R., Mooney, H. A., Sala, O. E., and Schulze, E. D. (1996). A Global Analysis of Root Distributions for Terrestrial Biomes. *Oecologia* 108, 389–411. doi:10.1007/bf00333714

Joabsson, A., and Christensen, T. R. (2001). Methane Emissions from Wetlands and Their Relationship with Vascular Plants: an Arctic Example. *Glob. Change Biol.* 7 (8), 919–932. doi:10.1046/j.1354-1013.2001.00044.x

Kim, J., Guo, Q., Baldocchi, D., Leclerc, M., Xu, L., and Schmid, H. (2006). Upscaling Fluxes from Tower to Landscape: Overlaying Flux Footprints on High-Resolution (IKONOS) Images of Vegetation Cover. *Agric. For. Meteorol.* 136 (3-4), 132–146. doi:10.1016/j.agrformet.2004.11.015

King, J. Y., Reeburgh, W. S., and Regli, S. K. (1998). Methane Emission and Transport by Arctic Sedges in Alaska: Results of a Vegetation Removal Experiment. *J. Geophys. Res.* 103 (D22), 29083–29092. doi:10.1029/98jd00052

Kljun, N., Calanca, P., Rotach, M. W., and Schmid, H. P. (2015). A Simple Two- Dimensional Parameterisation for Flux Footprint Prediction (FFP). *Geosci. Model Dev.* 8 (11), 3695–3713. doi:10.5194/gmd-8-3695-2015

Knox, S. H., Bansal, S., McNicol, G., Schafer, K., Sturtevant, C., Ueyama, W. D., et al. (2021). Identifying Dominant Environmental Predictors of Freshwater Wetland Methane Fluxes across Diurnal to Seasonal Time Scales. *Glob. Change Biol.* 27, 3582–3604. doi:10.1111/gcb.15661

Kormann, R., and Meixner, F. X. (2001). An Analytical Footprint Model for Non-neutral Stratification. *Boundary-Layer Meteorol.* 99 (2), 207–224. doi:10.1023/a:1018991015119

Koven, C. D., Riley, W. J., Subin, Z. M., Tang, J. Y., Torn, M. S., Collins, W. D., et al. (2013). The Effect of Vertically Resolved Soil Biogeochemistry and Alternate Soil C and N Models on C Dynamics of CLM4. *Biogeosciences* 10, 7109–7131. doi:10.5194/bg-10-7109-2013

Kwon, H. J., Oechel, W. C., Zulueta, R. C., and Hastings, S. J. (2006). Effects of Climate Variability on Carbon Sequestration Among Adjacent Wet Sedge Tundra and Moist Tussock Tundra Ecosystems. *J. Geophys. Res. Biogeosci.* 111, G03014.

Lai, D. Y. F. (2009). Methane Dynamics in Northern Peatlands: A Review. *Pedosphere* 19 (4), 409–421. doi:10.1016/s1002-0160(09)00003-4

Langford, Z., Kumar, J., Hoffman, F., Norby, R., Wullschleger, S., Sloan, V., et al. (2016). Mapping Arctic Plant Functional Type Distributions in the Barrow Environmental Observatory Using WorldView-2 and LiDAR Datasets. *Remote Sens.* 8 (9), 733. doi:10.3390/rs8090733

Langford, Z. L., Kumar, J., Hoffman, F. M., Breen, A. L., and Iversen, C. M. (2019). Arctic Vegetation Mapping Using Unsupervised Training Datasets and Convolutional Neural Networks. *Remote Sens*. 11 (1), 69. doi:10.3390/rs11010069

Lara, M. J., McGuire, A. D., Euskirchen, E. S., Genet, H., Yi, S., Rutter, R., et al. (2020). Local-scale Arctic Tundra Heterogeneity Affects Regional-Scale Carbon Dynamics. *Nat. Commun*. 11 (1), 4925–5010. doi:10.1038/s41467-020-18768-z

Liljedahl, A. K., Boike, J., Daanen, R. P., Fedorov, A. N., Frost, G. V., Grosse, G., et al. (2016). Pan-Arctic Ice-Wedge Degradation in Warming Permafrost and its Influence on Tundra Hydrology. *Nat. Geosci*. 9 (4), 312–318. doi:10.1038/ngeo

MacDonald, J. A., Fowler, D., Hargreaves, K. J., Skiba, U., Leith, I. D., and Murray, M. B. (1998). Methane Emission Rates from a Northern Wetland; Response to Temperature, Water Table and Transport. *Atmos. Environ.* 32 (19), 3219–3227. doi:10.1016/s1352-2310(97)00464-0

Mastepanov, M., Sigsgaard, C., Dlugokencky, E. J., Houweling, S., Ström, L., Tamstorf, M. P., et al. (2008). Large Tundra Methane Burst during Onset of Freezing. *Nature* 456 (7222), 628–630. doi:10.1038/nature07464

Mastepanov, M., Sigsgaard, C., Tagesson, T., Ström, L., Tamstorf, M. P., Lund, M., et al. (2013). Revisiting Factors Controlling Methane Emissions from High-Arctic Tundra. *Biogeosciences* 10 (7), 5139–5158. doi:10.5194/ bg-10-5139-2013

McEwing, K. R., Fisher, J. P., and Zona, D. (2015). Environmental and Vegetation Controls on the Spatial Variability of CH4 Emission from Wet-Sedge and Tussock Tundra Ecosystems in the Arctic. *Plant Soil* 388 (1-2), 37–52. doi:10. 1007/s11104-014-2377-1

Melton, J. R., Wania, R., Hodson, E. L., Poulter, B., Ringeval, B., Spahni, R., et al. (2013). Present State of Global Wetland Extent and Wetland Methane Modelling: Conclusions from a Model Inter-comparison Project (WETCHIMP). *Biogeosciences* 10, 753–788. doi:10.5194/bg-10-753-2013

Mer, J. L., and Roger, P. (2001). Production, Oxidation, Emission and Consumption of Methane by Soils: a Review. Eur. J. Soil Biol. 37, 25–50. doi:10.1016/s1164-5563(01)01067-6

Morrissey, L. A., and Livingston, G. P. (1992). Methane Emissions from Alaska Arctic Tundra: An Assessment of Local Spatial Variability. *J. Geophys. Res.* 97 (D15), 16661–16670. doi:10.1029/92jd00063

Nielsen, C. S., Michelsen, A., Strobel, B. W., Wulff, K., Banyasz, I., and Elberling, B. (2017). Correlations between Substrate Availability, Dissolved CH4, and CH4 Emissions in an Arctic Wetland Subject to Warming and Plant Removal. *J. Geophys. Res. Biogeosci.* 122 (3), 645–660. doi:10.1002/2016jg003511

Oechel, W., and A. Kalhori (2018). in *ABoVE: CO_2 and CH_4 Fluxes and Meteorology at Flux Tower Sites, Alaska, 2015-2017*. ORNL DAAC, Oak Ridge, Tennessee, USA. doi: 10.3334/ORNLDAAC/1562

Oechel, W. C., Vourlitis, G. L., Brooks, S., Crawford, T. L., and Dumas, E. (1998). Intercomparison Among Chamber, Tower, and Aircraft Net CO2 and Energy Fluxes Measured during the Arctic System Science Land-Atmosphere-Ice Interactions (ARCSS-LAII) Flux Study. *J. Geophys. Res.* 103 (D22), 28993–29003. doi:10.1029/1998jd200015

Oleson, K., Lawrence, D., Bonan, G. B., Drewniak, B. A., Huang, M., Koven, C. D., et al. (2013). *Technical Description of Version 4.5 of the Community Land Model (CLM).* Bounder, Colorado: National Center for Atmospheric Research.

Petrescu, A. M. R., Lohila, A., Tuovinen, J.-P., Baldocchi, D. D., Desai, A. R., Roulet, N. T., et al. (2015). The Uncertain Climate Footprint of Wetlands under Human Pressure. *Proc. Natl. Acad. Sci. U.S.A.* 112 (15), 4594–4599. doi:10.1073/pnas. 1416267112

Pirk, N., Santos, T., Gustafson, C., Johansson, A. J., Tufvesson, F., Parmentier, F. J. W., et al. (2015). Methane Emission Bursts from Permafrost Environments during Autumn Freeze-in: New Insights from Ground-penetrating Radar. *Geophys. Res. Lett.* 42 (16), 6732–6738. doi:10.1002/2015gl065034

Pirk, N., Mastepanov, M., López-Blanco, E., Christensen, L. H., Christiansen, H. H., Hansen, B. U., et al. (2017). Toward a Statistical Description of Methane Emissions from Arctic Wetlands. *Ambio* 46 (1), 70–80. doi:10.1007/s13280- 016-0893-3

R Core Team (2020). in *R: A language and environment for statistical computing*. R foundation for statistical computing (Vienna, Austria). http://www.R-project.org.

Raz-Yaseef, N., Torn, M. S., Wu, Y., Billesbach, D. P., Liljedahl, A. K., Kneafsey, T. J., et al. (2016). Large CO2 and CH4 Emissions from Polygonal Tundra during Spring Thaw in Northern Alaska. *Geophys. Res. Lett.* 44, 504–513. doi:10.1002/ 2016GL071220

Reuss-Schmidt, K., Levy, P., Oechel, W., Tweedie, C., Wilson, C., and Zona, D. (2019). Understanding Spatial Variability of Methane Fluxes in Arctic Wetlands through Footprint Modelling. *Environ. Res. Lett.* 14 (12), 125010. doi:10.1088/1748-9326/ab4d32

Sachs, T., Wille, C., Boike, J., and Kutzbach, L. (2008). Environmental Controls on Ecosystem-scale CH4 Emission from Polygonal Tundra in the Lena River Delta, Siberia. *J. Geophys. Res. Biogeosci.* 113 (G3).

Serrano-Silva, N., Sarria-guzmán, Y., Dendooven, L., and Luna-Guido, M. (2014). Methanogenesis and Methanotrophy in Soil: a Review. *Pedosphere* 24 (3), 291–307. doi:10.1016/s1002-0160(14)60016-3

Song, C., Xu, X., Sun, X., Tian, H., Sun, L., Miao, Y., et al. (2012). Large Methane Emission upon Spring Thaw from Natural Wetlands in the Northern Permafrost Region. *Environ. Res. Lett.* 7 (3), 034009. doi:10.1088/1748-9326/7/3/034009

Sturtevant, C. S., and Oechel, W. C. (2013). Spatial Variation in Landscape-level CO2 and CH4 Fluxes from Arctic Coastal Tundra: Influence from Vegetation, Wetness, and the Thaw Lake Cycle. *Glob. Change Biol.* 19 (9), 2853–2866. doi:10.1111/gcb.12247

Sturtevant, C. S., Oechel, W. C., Zona, D., Kim, Y., and Emerson, C. E. (2012). Soil Moisture Control over Autumn Season Methane Flux, Arctic Coastal Plain of Alaska. *Biogeosciences* 9 (4), 1423–1440. doi:10.5194/bg-9-1423-2012

Thornton, P. E., and Rosenbloom, N. A. (2005). Ecosystem Model Spin-Up: Estimating Steady State Conditions in a Coupled Terrestrial Carbon and Nitrogen Cycle Model. *Ecol. Model*. 189, 25–48. doi:10.1016/j.ecolmodel.2005.04.008

Thornton, P. E., and Zimmermann, N. E. (2007). An Improved Canopy Integration Scheme for a Land Surface Model with Prognostic Canopy Structure. *J. Clim.* 20, 3902–3923. doi:10.1175/jcli4222.1

Thornton, P. E., Lamarque, J. F., Rosenbloom, N. A., and Mahowald, N. M. (2007). Influence of Carbon-Nitrogen Cycle Coupling on Land Model Response to CO2 Fertilization and Climate Variability. *Glob. Biogeochem. Cycl.* 21 (4), GB4018. doi:10.1029/2006gb002868

Treat, C. C., Marushchak, M. E., Voigt, C., Zhang, Y., Tan, Z., Zhuang, Q., et al. (2018). Tundra Landscape Heterogeneity, Not Interannual Variability, Controls the Decadal Regional Carbon Balance in the Western Russian Arctic. *Glob. Change Biol.* 24 (11), 5188–5204. doi:10.1111/gcb.14421

Vaughn, L. J. S., Conrad, M. E., Bill, M., and Torn, M. S. (2016). Isotopic Insights into Methane Production, Oxidation, and Emissions in Arctic Polygon Tundra. *Glob. Change Biol.* 22 (10), 3487–3502. doi:10.1111/gcb.13281

von Fischer, J. C., Rhew, R. C., Ames, G. M., Fosdick, B. K., and von Fischer, P. E. (2010). Vegetation Height and Other Controls of Spatial Variability in Methane Emissions from the Arctic Coastal Tundra at Barrow, Alaska. *J. Geophys. Res. Biogeosci.* 115 (G4). doi:10.1029/2009jg001283

Waddington, J. M., and Roulet, N. T. (1996). Atmosphere-wetland Carbon 1455 Exchanges: Scale Dependency of CO2 and CH4 Exchange on the Developmental Topography of a Peatland. *Glob. Biogeochem. Cycl.* 10 (2), 233–245. doi:10.1029/95gb03871

Walker, D. A., Binnian, E., Evans, B. M., Lederer, N. D., Nordstrand, E., and 1458 Webber, P. J. (1989). Terrain, Vegetation and Landscape Evolution of the R4D Research Site, Brooks Range Foothills, Alaska. *Ecography* 12 (3), 238–261. doi:10.1111/j.1600-0587.1989.tb00844.x

Wang, Y., Yuan, F., Yuan, F., Gu, B., Hahn, M. S., Torn, M. S., et al. (2019). Mechanistic Modeling of Microtopographic Impacts on CO2 and CH4 Fluxes in an Alaskan Tundra Ecosystem Using the CLM-Microbe Model. *J. Adv. Model. Earth Syst.* 11, 4228–4304. doi:10.1029/2019ms001771

Wilson, J. P. (2012). Digital Terrain Modeling. *Geomorphology* 137 (1), 107–121. doi:10.1016/j.geomorph.2011.03.012

Xu, X., and Tian, H. (2012). Methane Exchange between Marshland and the Atmosphere over China during 1949-2008. *Glob. Biogeochem. Cycl.* 26. doi:10.1029/2010gb003946

Xu, X., and Yuan, F. (2016). Meteorological Forcing at Barrow AK 1981–2013. Available at: http://ngee-arctic.ornl.gov.

Xu, X. F., Tian, H. Q., Zhang, C., Liu, M. L., Ren, W., Chen, G. S., et al. (2010). Attribution of Spatial and Temporal Variations in Terrestrial Methane Flux over North America. *Biogeosciences* 7 (11), 3637–3655. doi:10.5194/bg-7-3637-2010

Xu, X., Thornton, P. E., and Post, W. M. (2013). A Global Analysis of Soil Microbial Biomass Carbon, Nitrogen and Phosphorus in Terrestrial Ecosystems. *Glob. Ecol. Biogeogr.* 22 (6), 737–749. doi:10.1111/geb.12029

Xu, X., Schimel, J. P., Thornton, P. E., Song, X., Yuan, F., and Goswami, S. (2014). Substrate and Environmental Controls on Microbial Assimilation of Soil Organic Carbon: a Framework for Earth System Models. *Ecol. Lett.* 17 (5), 547–555. doi:10.1111/ele.12254

Xu, X., Elias, D. A., Graham, D. E., Phelps, T. J., Carroll, S. L., Wullschleger, S. D., et al. (2015). A Microbial Functional Group Based Module for Simulating Methane Production and Consumption: Application to an Incubation Permafrost Soil. *J. Geophys. Res. Biogeosci.* 120 (6), 1315–1333. doi:10.1002/2015jg002935

Xu, X., Yuan, F., Hanson, P. J., Wullschleger, S. D., Thornton, P. E., Riley, W. J., et al. (2016). Reviews and Syntheses: Four Decades of Modeling Methane Cycling in Terrestrial Ecosystems. *Biogeosciences* 13, 3735–3755. doi:10.5194/bg-13-3735-2016

Zhang, Y., Sachs, T., Li, C., and Boike, J. (2012). Upscaling Methane Fluxes from Closed Chambers to Eddy Covariance Based on a Permafrost Biogeochemistry Integrated Model. *Glob. Change Biol.* 18 (4), 1428–1440. doi:10.1111/j.1365-2486.2011.02587.x

Zona, D., Oechel, W. C., Kochendorfer, J., Paw U, K. T., Salyuk, A. N., Olivas, P. C., et al. (2009). Methane Fluxes during the Initiation of a Large-Scale Water Table Manipulation Experiment in the Alaskan Arctic Tundra. *Glob. Biogeochem. Cycl.* 23, GB2013. doi:10.1029/2009gb003487

Zona, D., Gioli, B., Commane, R., Lindaas, J., Wofsy, S. C., Miller, C. E., et al. (2016). Cold Season Emissions Dominate the Arctic Tundra Methane Budget.Proc. *Natl. Acad. Sci. U.S.A.* 113 (1), 40–45. doi:10.1073/pnas.1516017113

Chapter 2: Supporting Information

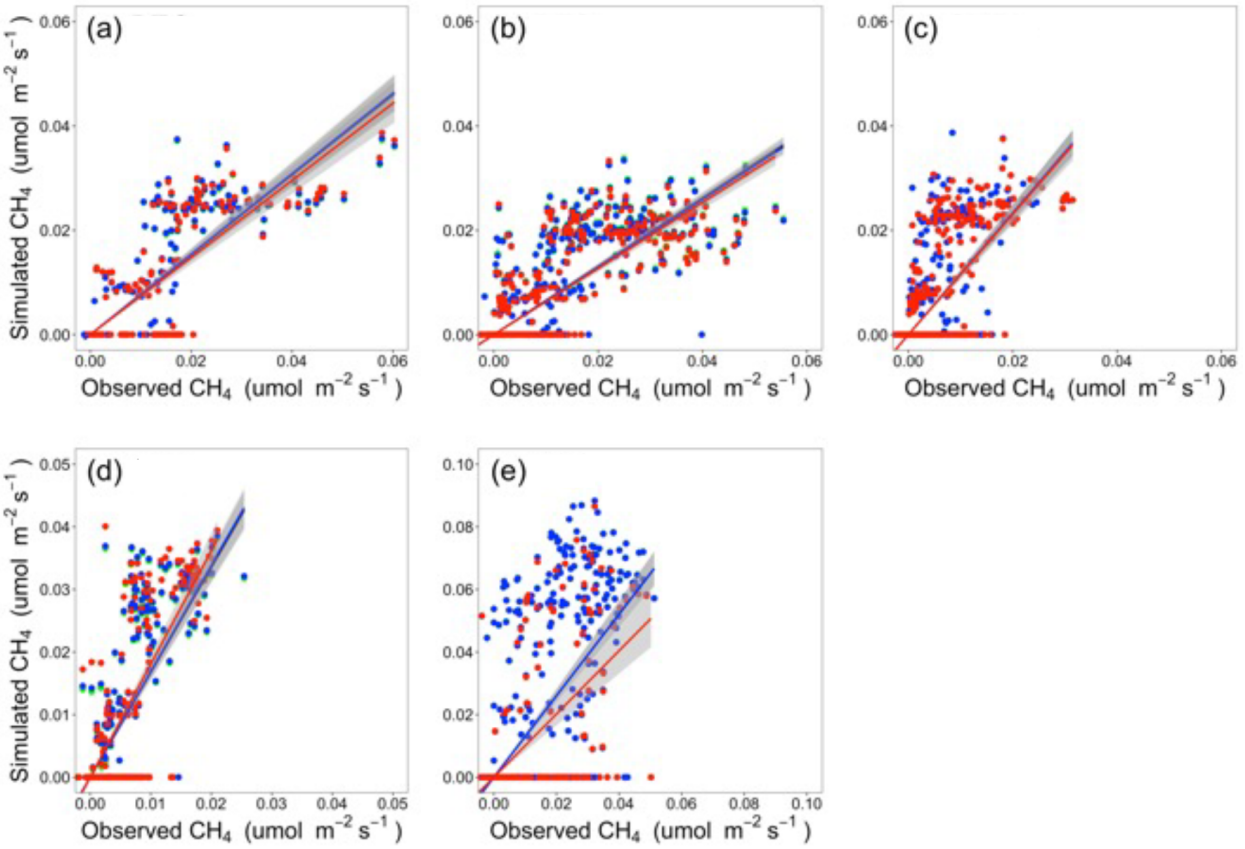

Figure S1. Scatter plots of observed versus simulated CH_4 flux for (a) US-Beo, (b) US-Bes, (c) US-Brw, (d) US-Atq, and (e) US-Ivo in 2013-2015 with linear lines of best fit (no interception) and 95% confidence interval for regression line shaded gray. The green lines and points indicate the relationship between observed fluxes and upscaled fluxes using the homogeneous footprint (HF) algorithm overlapped by blue lines and points. The blue lines and points indicate the relationship between observed fluxes and upscaled fluxes using the gradient footprint (GF) algorithm. The red lines and points indicate the relationship between observed fluxes and upscaled fluxes using dynamic footprint (DF) algorithm. Most of green lines and points were overlapped by the blue lines and points.

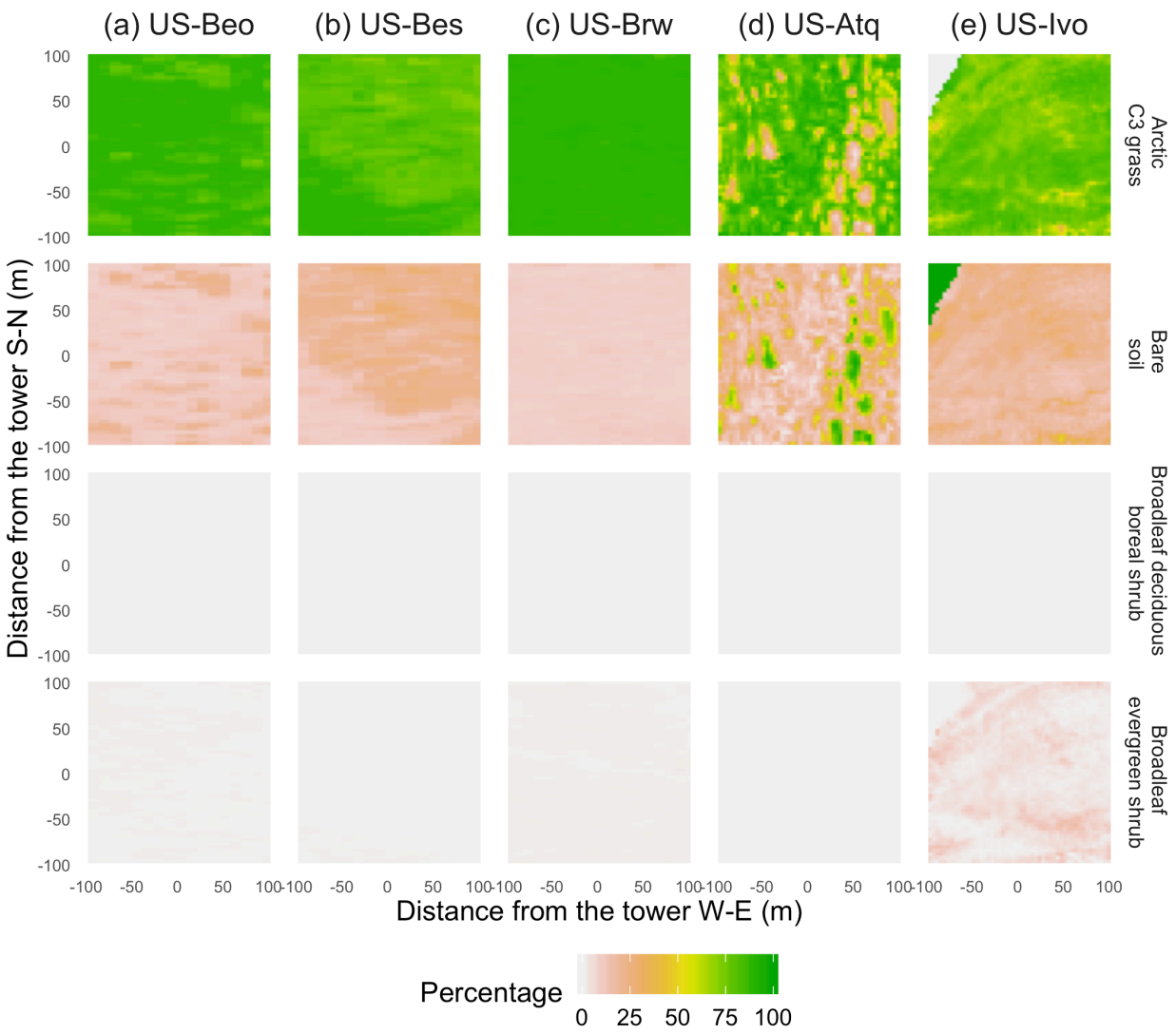

Figure S2. Vegetation maps of four plant functional types defined in the CLM-Microbe model in an area of 200 m × 200 m for all study sites

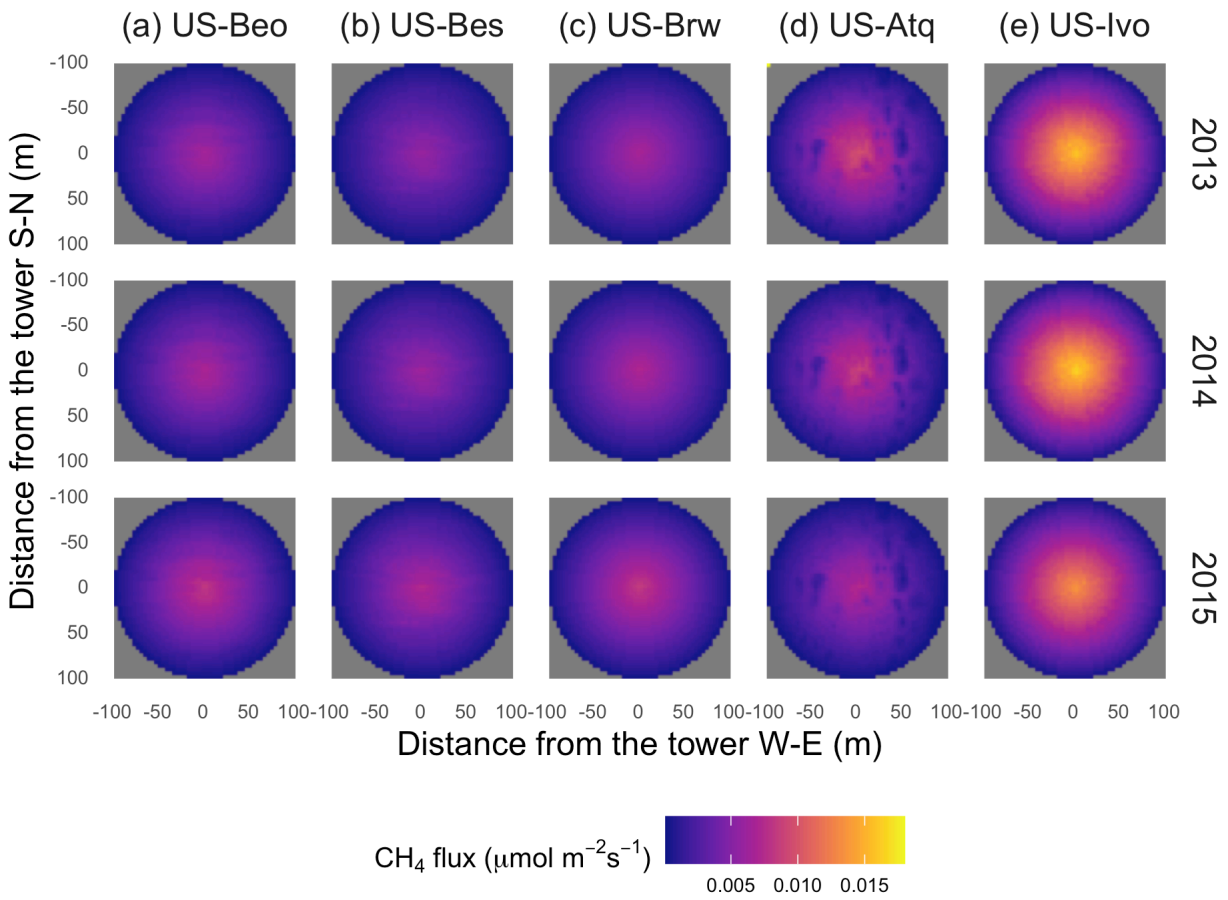

Figure S3. Spatial patterns of upscaled CH_4 emission rates based on the "gradient" footprint (GF) algorithm in an area of 200 m × 200 m from 2013 to 2015 for all study sites

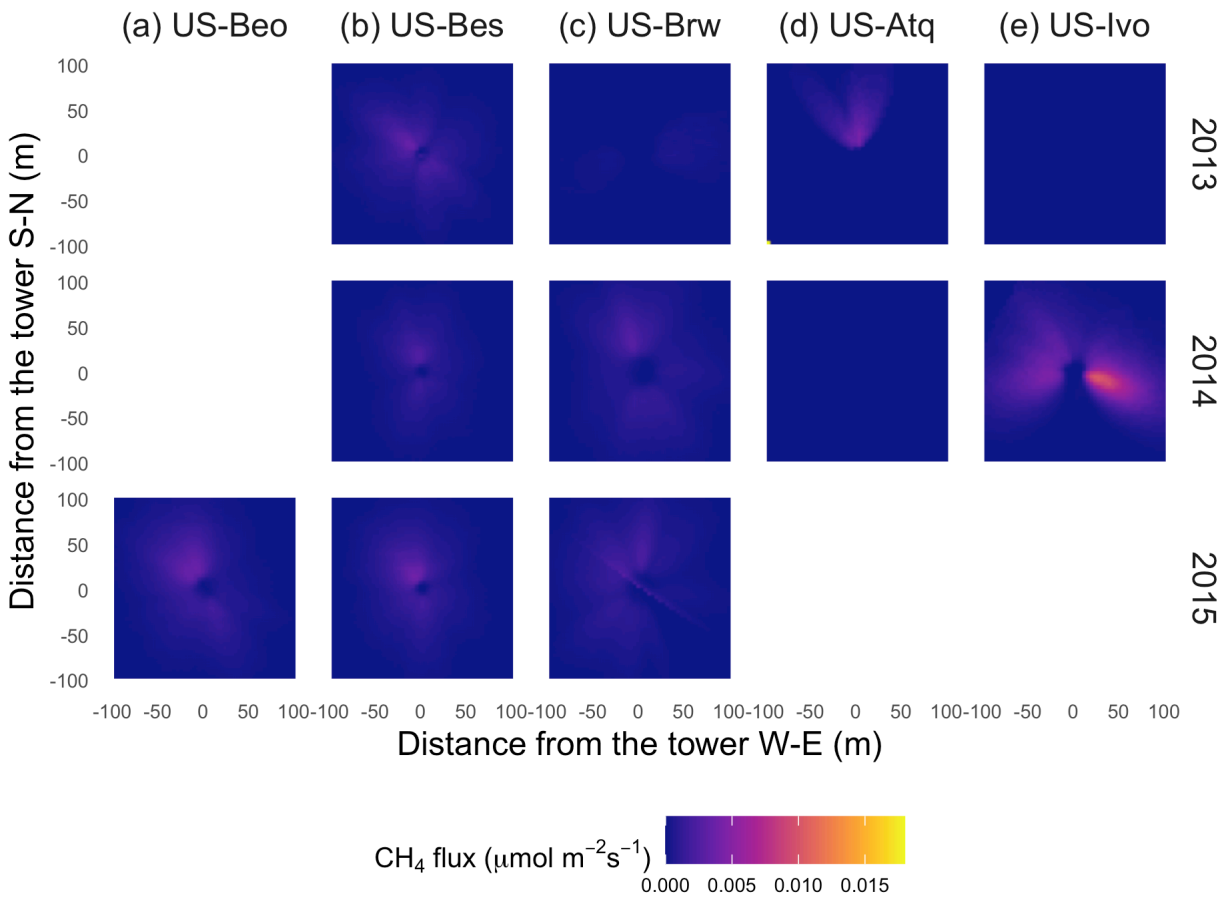

Figure S4. Spatial patterns of upscaled CH_4 emission rates based on the "dynamic" footprint (DF) algorithm in an area of 200 m × 200 m from 2013 to 2015 for all study sites

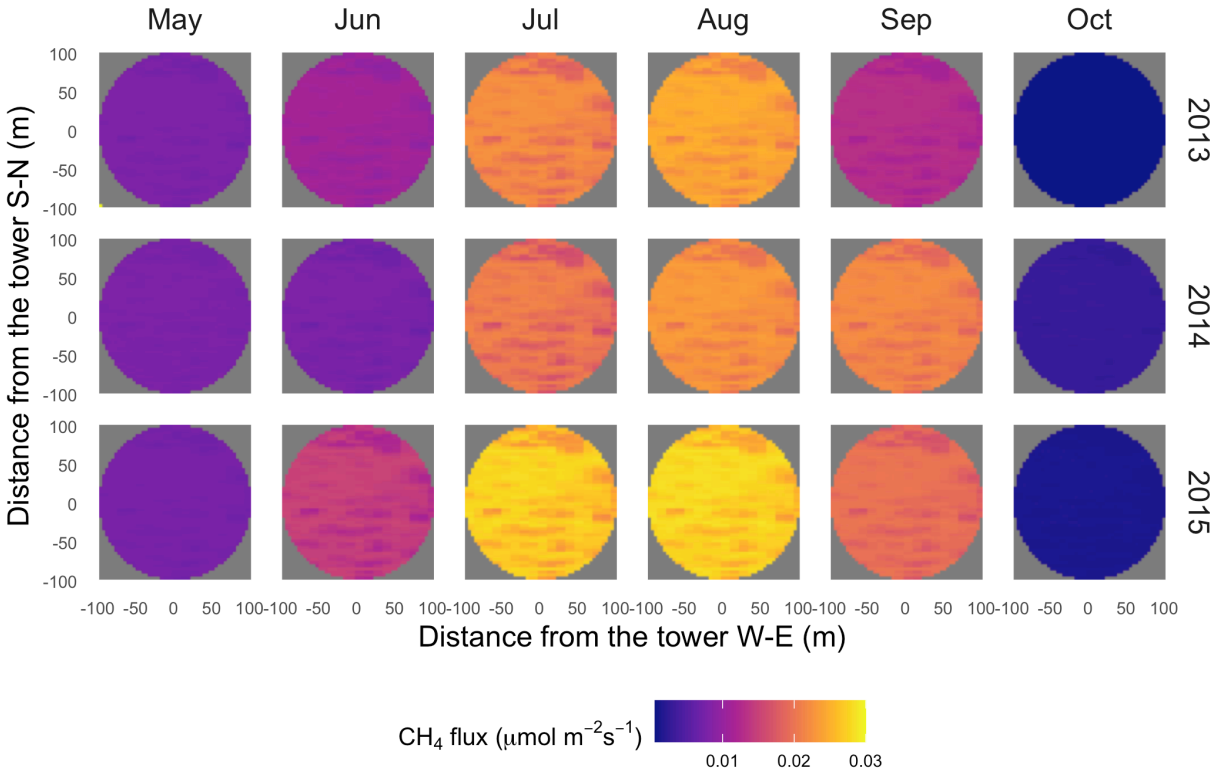

Figure S5. Spatial distribution of upscaled CH_4 flux using the homogeneous footprint (HF) algorithm for each month in 2013-2015 for US-Beo (flux was zero in January, February, March, April, November, and December)

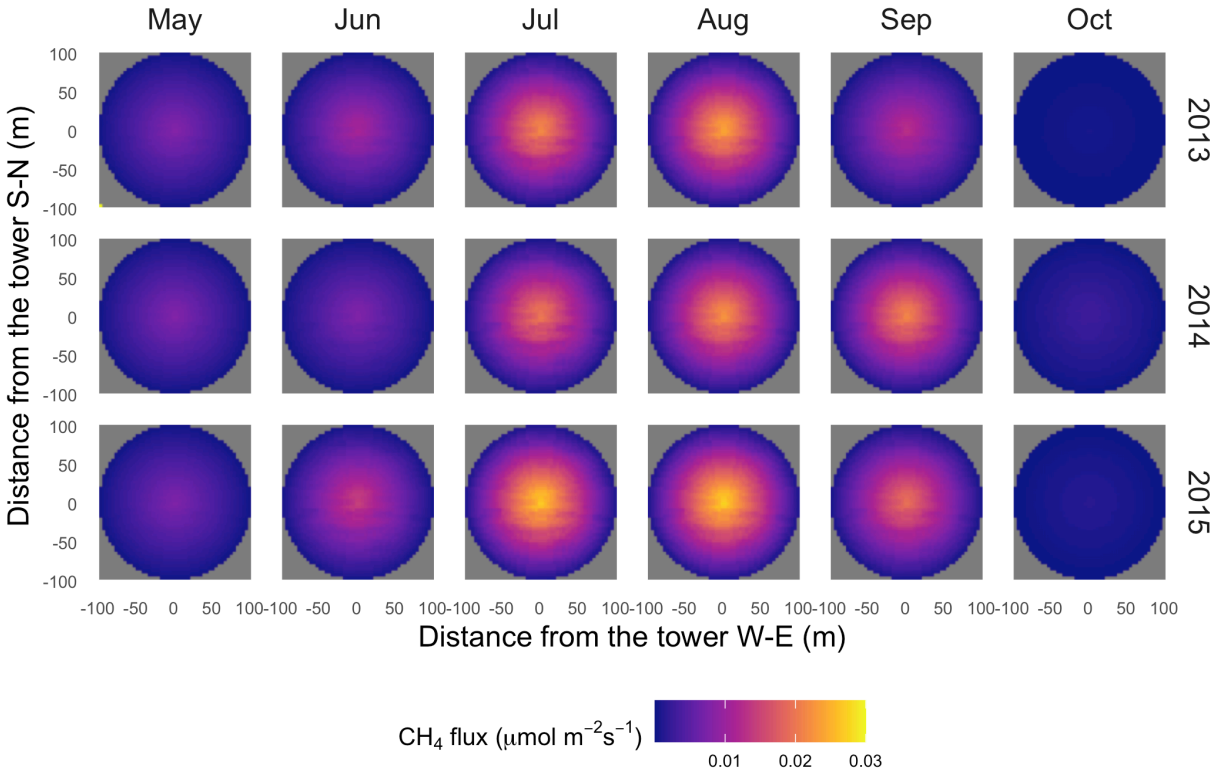

Figure S6. Spatial distribution of upscaled CH_4 flux using the gradient footprint (GF) algorithm for each month in 2013-2015 for US-Beo (flux was zero in January, February, March, April, November, and December)

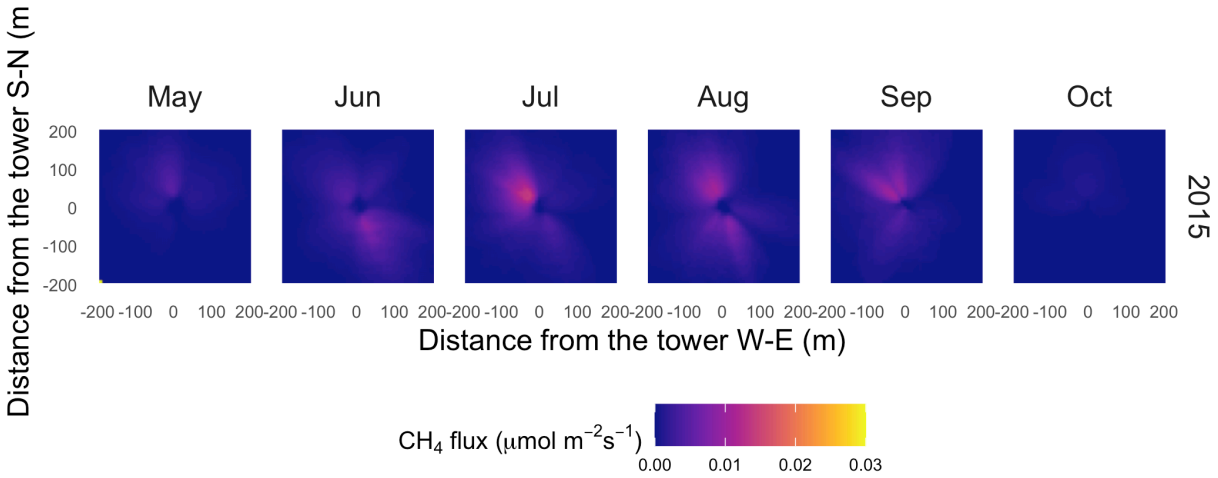

Figure S7. Spatial distribution of upscaled CH_4 flux using the dynamic footprint (DF) algorithm for each month in 2015 for US-Beo (flux was zero in January, February, March, April, November, and December)

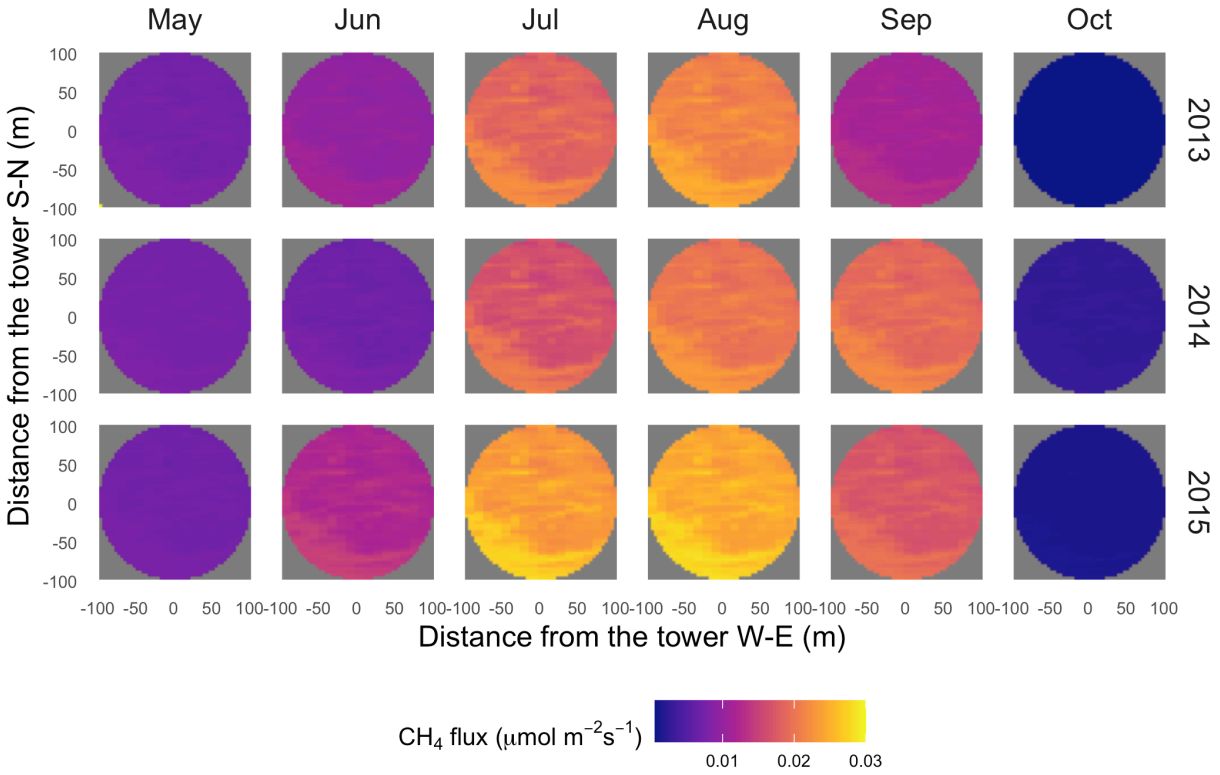

Figure S8. Spatial distribution of upscaled CH_4 flux using the homogeneous footprint (HF) algorithm for each month in 2013-2015 for US-Bes (flux was zero in January, February, March, April, November, and December)

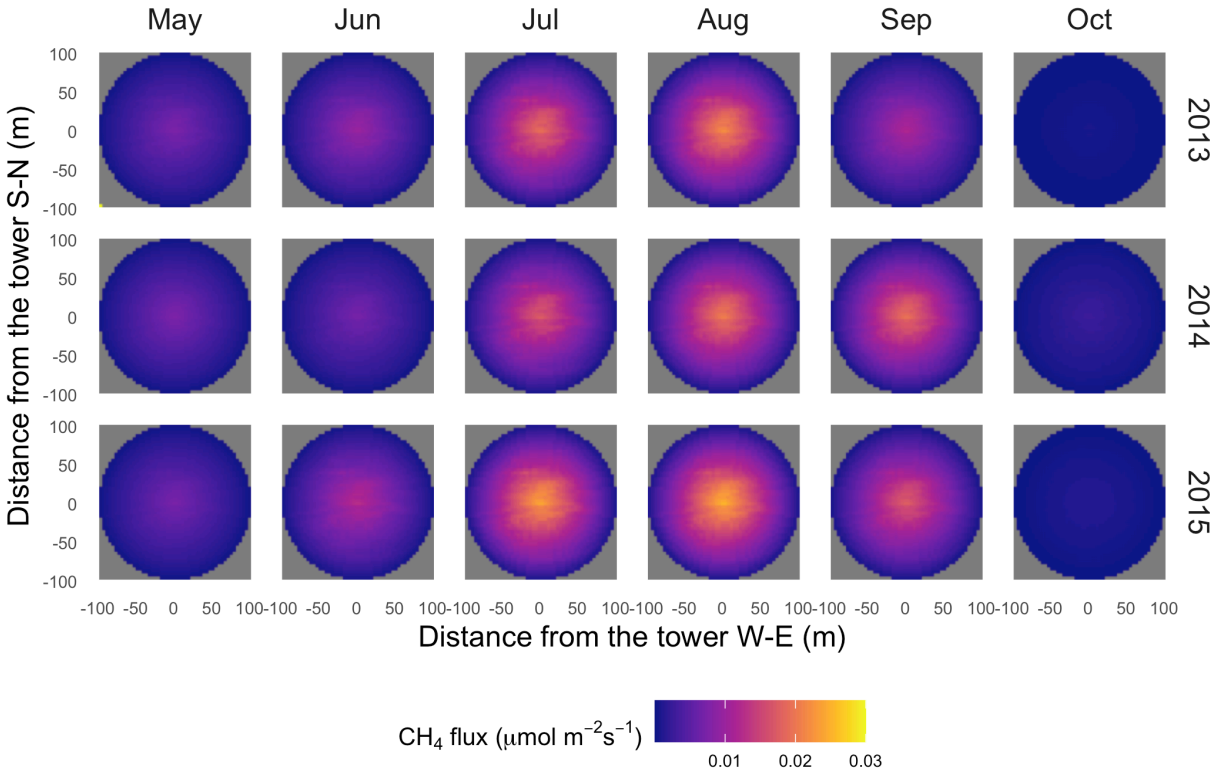

Figure S9. Spatial distribution of upscaled CH_4 flux using the gradient footprint (GF) algorithm for each month in 2013-2015 for US-Bes (flux was zero in January, February, March, April, November, and December)

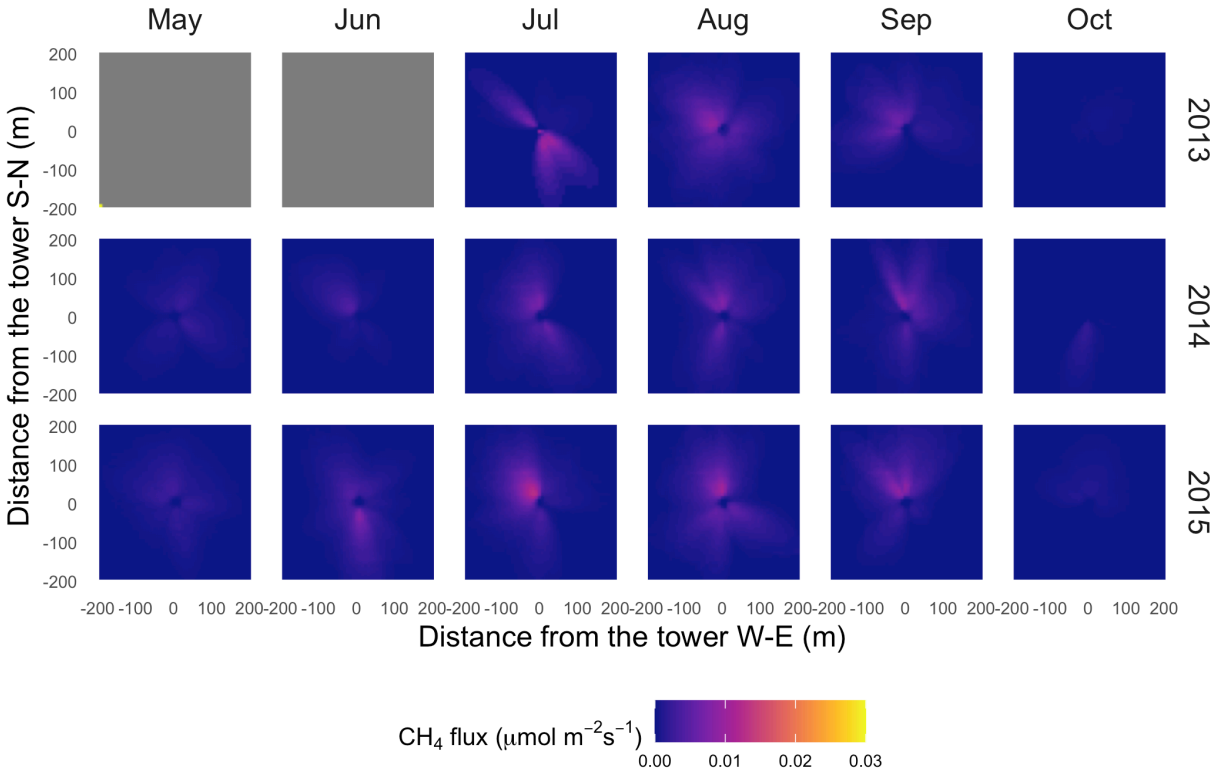

Figure S10. Spatial distribution of upscaled CH_4 flux using the dynamic footprint (DF) algorithm for each month in 2013-2015 for US-Bes (flux was zero in January, February, March, April, November, and December)

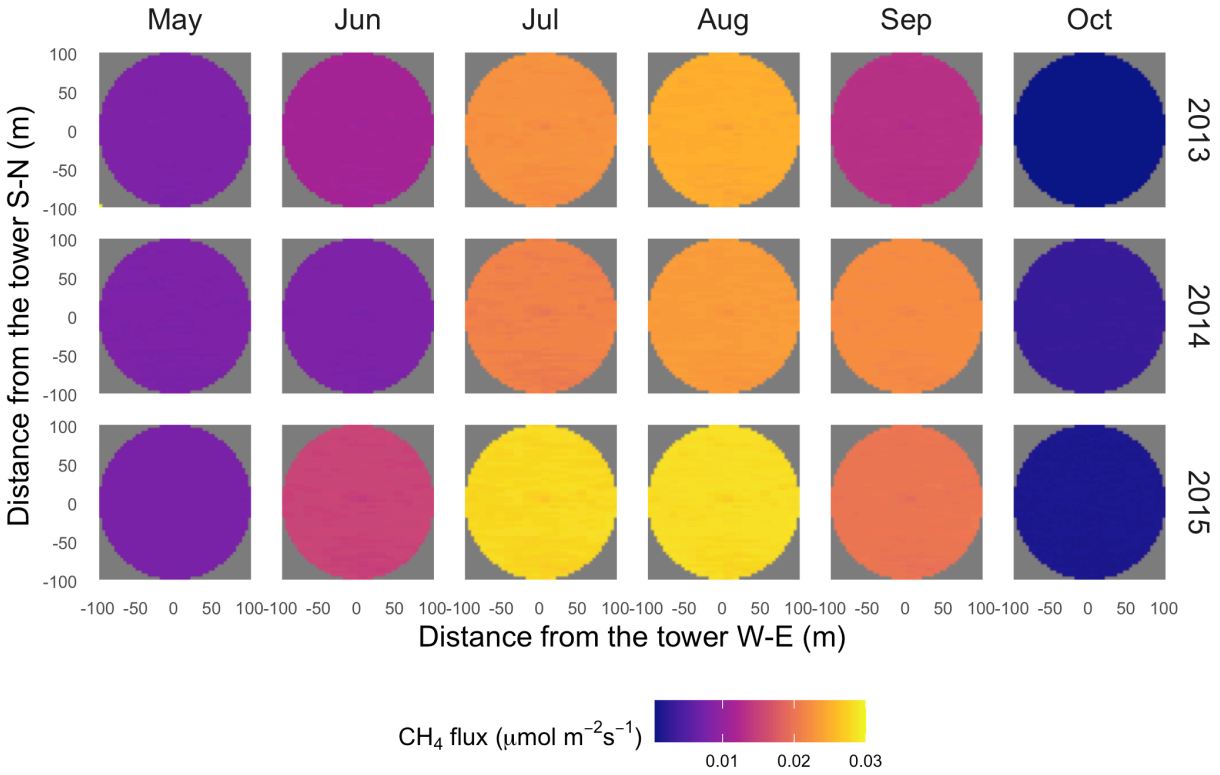

Figure S11. Spatial distribution of upcaled CH_4 flux using the homogeneous footprint (HF) algorithm for each month in 2013-2015 for US-Brw (flux was zero in January, February, March, April, November, and December)

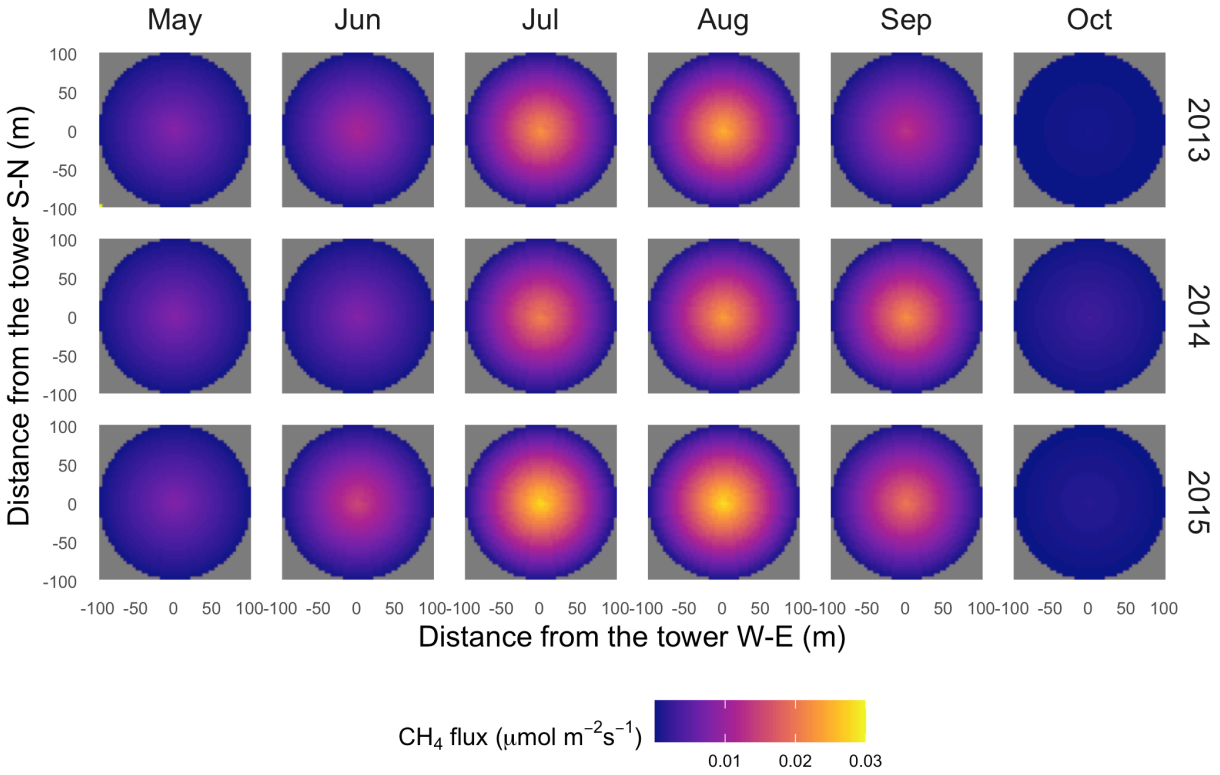

Figure S12. Spatial distribution of upscaled CH_4 flux using the gradient footprint (GF) algorithm for each month in 2013-2015 for US-Brw (fluxes were zero in January, February, March, April, November, and December)

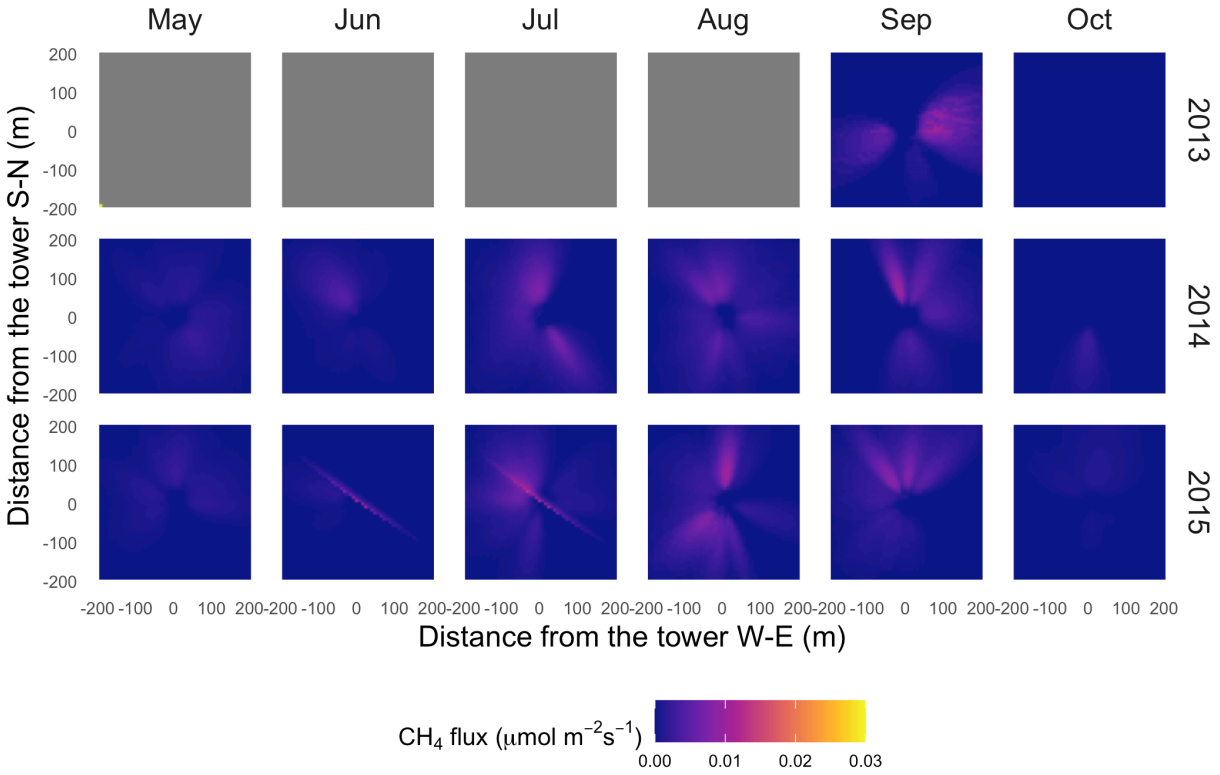

Figure S13. Spatial distribution of upscaled CH_4 flux using the dynamic footprint (DF) algorithm for each month in 2013-2015 for US-Brw (flux was zero in January, February, March, April, November, and December)

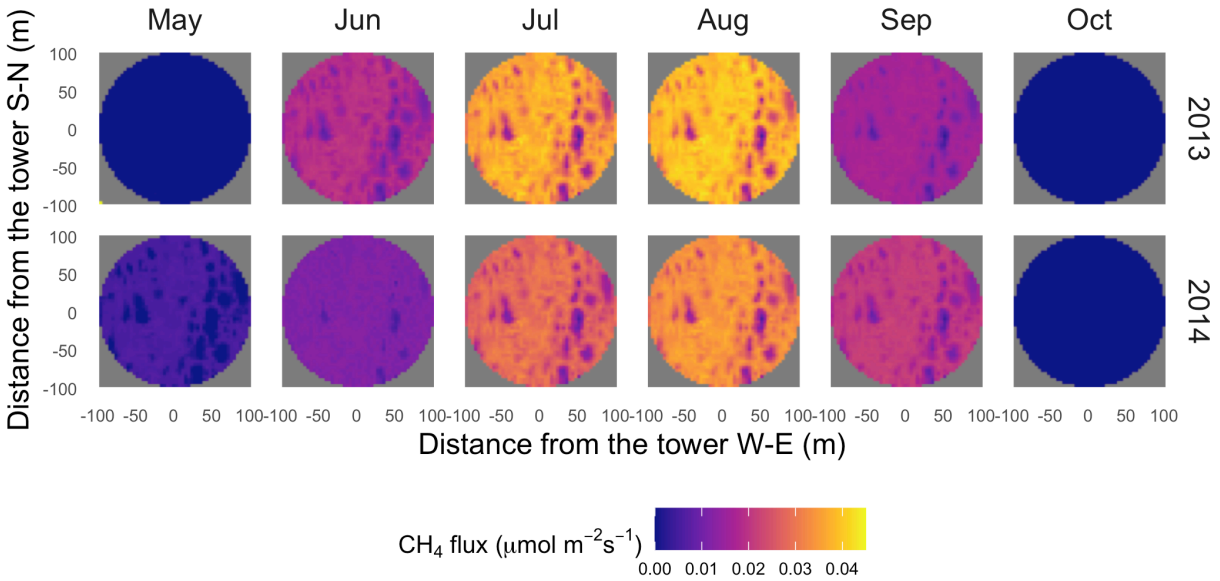

Figure S14. Spatial distribution of upscaled CH_4 flux using the homogeneous footprint (HF) algorithm for each month in 2013-2014 for US-Atq (flux was zero in January, February, March, April, November, and December)

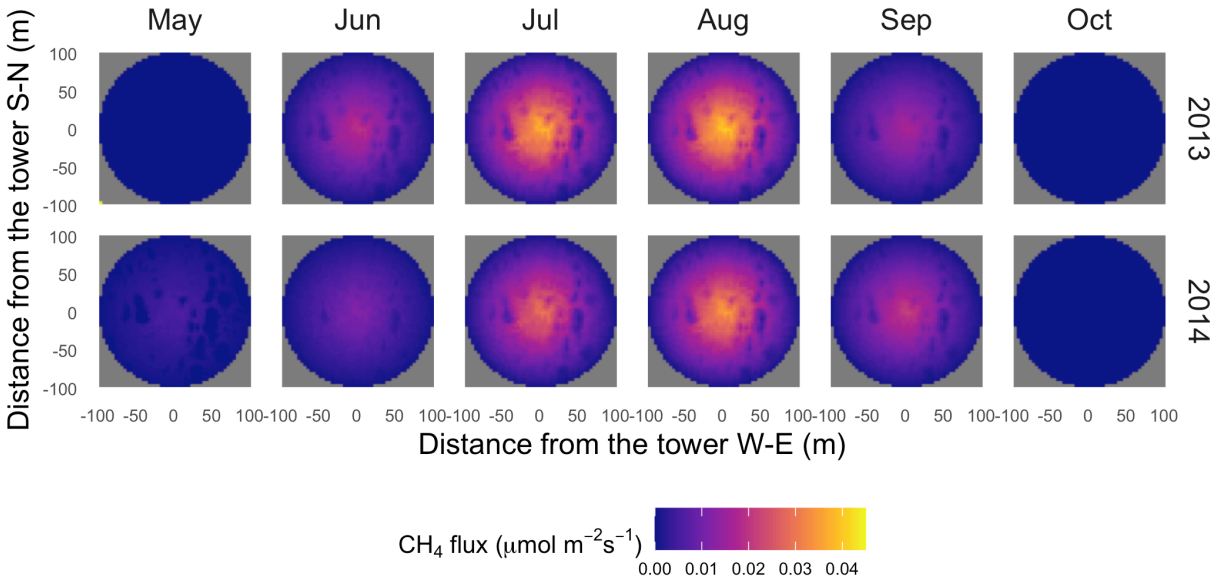

Figure S15. Spatial distribution of upscaled CH_4 flux using the gradient footprint (GF) algorithm for each month in 2013-2014 for US-Atq (flux was zero in January, February, March, April, November, and December)

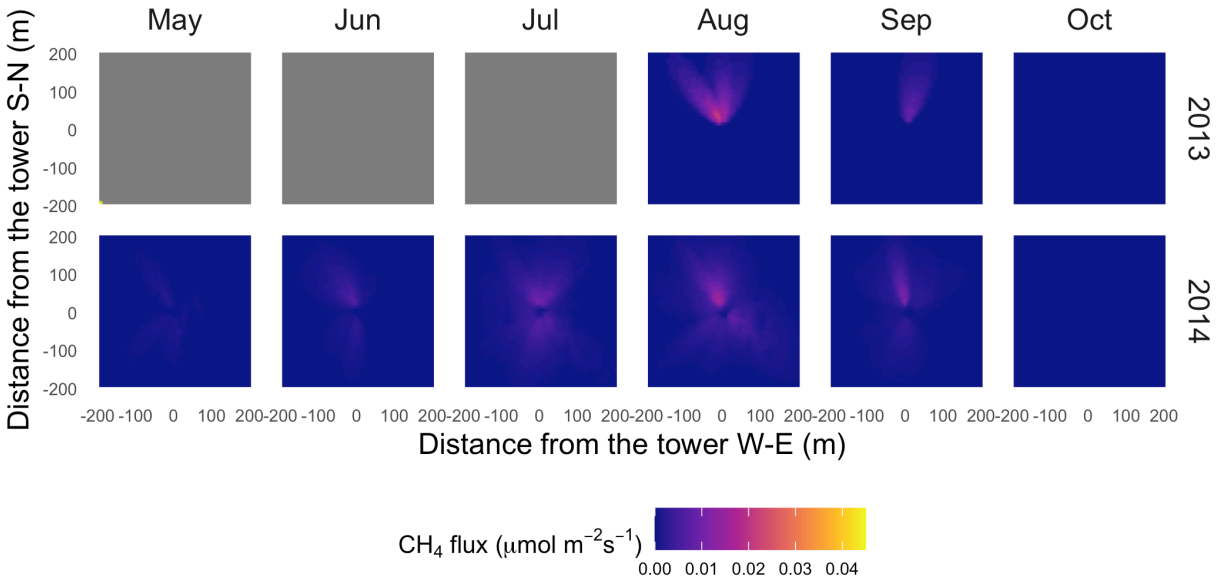

Figure S16. Spatial distribution of upscaled CH_4 flux using the dynamic footprint (DF) algorithm for each month in 2013-2014 for US-Atq (flux was zero in January, February, March, April, November, and December)

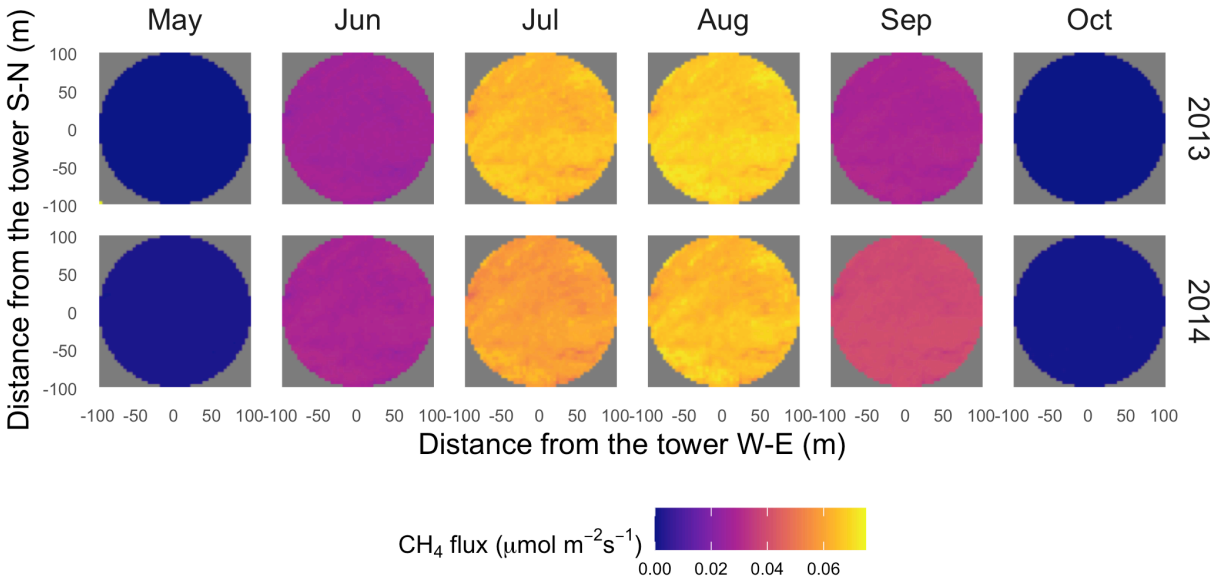

Figure S17. Spatial distribution of upscaled CH_4 flux using the homogeneous footprint (HF) algorithm for each month in 2013-2014 for US-Ivo (flux was zero in January, February, March, April, November, and December)

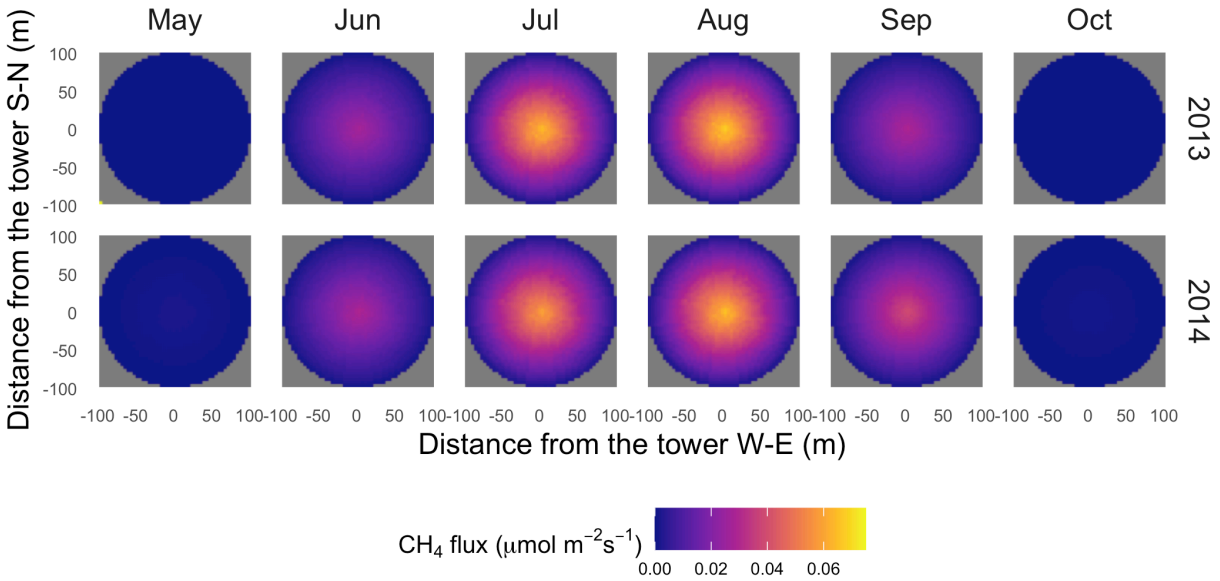

Figure S18. Spatial distribution of upscaled CH_4 flux using the gradient footprint (GF) algorithm for each month in 2013-2014 for US-Ivo (flux was zero in January, February, March, April, November, and December)

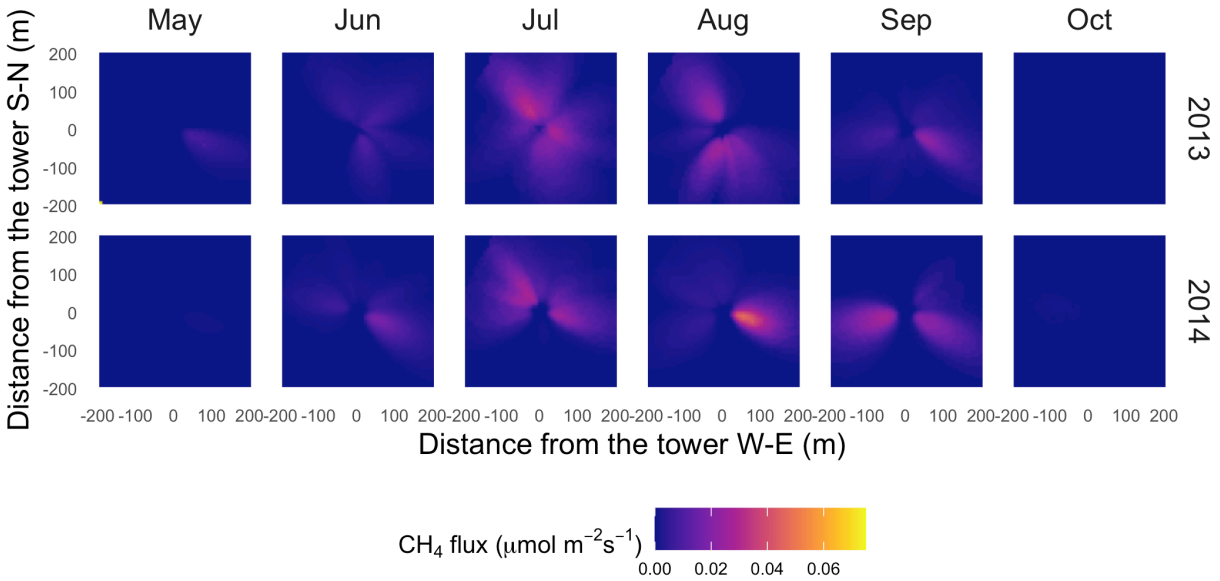

Figure S19. Spatial distribution of upscaled CH_4 flux using the dynamic footprint (DF) algorithm for each month in 2013-2014 for US-Ivo (flux was zero in January, February, March, April, November, and December)

Table S1. Coefficients for calculating SOC concentrations at five study sites

Sites	Coefficients	
	a	β
US-Beo	44.35	0.008
US-Bes	44.35	0.008
US-Brw	44.35	0.008
US-Atq	51.678	-0.002
US-Ivo	51.761	-0.007

Table S2 Annual averages and variations (mean±sd) of upscaled CH_4 flux using the homogeneous footprint algorithm (HF), gradient footprint algorithm (GF) and dynamic footprint algorithm (DF) for all study sites in 2013-2015 (Unit: μmol $\cdot m^{-2} \cdot s^{-1}$, n.a.: not available)

Footprint	Site	2013	2014	2015
HF	US-Beo	0.014±0.008	0.014±0.007	0.017±0.009
	US-Bes	0.015±0.009	0.016±0.007	0.018±0.009
	US-Brw	0.015±0.009	0.016±0.008	0.019±0.010
	US-Atq	0.020±0.016	0.018±0.012	n.a.
	US-Ivo	0.036±0.030	0.037±0.025	n.a.
GF	US-Beo	0.013±0.008	0.014±0.006	0.017±0.008
	US-Bes	0.015±0.009	0.016±0.007	0.019±0.010
	US-Brw	0.015±0.009	0.016±0.008	0.019±0.010
	US-Atq	0.020±0.016	0.018±0.012	n.a.
	US-Ivo	0.036±0.030	0.037±0.025	n.a.
DF	US-Beo	0.017±0.006	0.014±0.006	0.017±0.008
	US-Bes	n.a.	n.a.	0.020±0.009
	US-Brw	0.005±0.006	0.016±0.008	0.020±0.009
	US-Atq	0.020±0.014	0.019±0.012	n.a.
	US-Ivo	0.051±0.024	0.040±0.021	n.a.

Table S3 Coefficients for upscaled CH_4 flux using the homogeneous footprint algorithm (HF), gradient footprint algorithm (GF) and dynamic footprint algorithm (DF) compared with observed fluxes for all study sites (RMSE: root mean square error and NNSE: the Normalized Nash-Sutcliffe Efficiency)

Coefficient	Site	HF	GF	DF
R^2	US-Beo	0.511	0.512	0.526
	US-Bes	0.633	0.631	0.629
	US-Brw	0.427	0.427	0.427
	US-Atq	0.607	0.605	0.610
	US-Ivo	0.209	0.209	0.210
RMSE	US-Beo	0.011	0.011	0.010
	US-Bes	0.009	0.009	0.009
	US-Brw	0.008	0.008	0.008
	US-Atq	0.010	0.010	0.011
	US-Ivo	0.023	0.023	0.023
NNSE	US-Beo	0.621	0.623	0.631
	US-Bes	0.693	0.690	0.688
	US-Brw	0.397	0.397	0.397
	US-Atq	0.237	0.232	0.214
	US-Ivo	0.241	0.242	0.244

Table S4 Spatial averages and spatial variations (mean±sd) of upscaled CH_4 flux using the homogeneous footprint algorithm (HF), gradient footprint algorithm (GF) and dynamic footprint algorithm (DF) for all study sites in 2013-2015 (Unit: μmol $\cdot m^{-2} \cdot s^{-1}$, n.a.: not available)

Footprint	Site	2013	2014	2015
HF	US-Beo	0.0051±0.0027	0.0054±0.0028	0.0064±0.0033
	US-Bes	0.0047±0.0025	0.0050±0.0026	0.0059±0.0030
	US-Brw	0.0053±0.0028	0.0057±0.0029	0.0067±0.0034
	US-Atq	0.0069±0.0037	0.0062±0.0034	n.a.
	US-Ivo	0.0125±0.0065	0.0129±0.0067	n.a.
GF	US-Beo	0.0018±0.0017	0.0019±0.0018	0.0023±0.0021
	US-Bes	0.0016±0.0015	0.0017±0.0016	0.0020±0.0018
	US-Brw	0.0019±0.0017	0.0020±0.0018	0.0024±0.0021
	US-Atq	0.0025±0.0023	0.0022±0.0021	n.a.
	US-Ivo	0.0044±0.0040	0.0046±0.0042	n.a.
DF	US-Beo	0.0005±0.0006	0.0005±0.0006	0.0005±0.0006
	US-Bes	0.0004±0.0005	0.0003±0.0004	0.0004±0.0006
	US-Brw	0.0001±0.0001	0.0005±0.0004	0.0004±0.0004
	US-Atq	0.0002±0.0006	0.0004±0.0006	n.a.
	US-Ivo	0.0017±0.0017	0.0012±0.0016	n.a.

Table S5. Pearson's correlation coefficients (r_p) for relationships of vegetation composition, soil temperature, soil water content (top 2 cm), elevation with up-scaled CH_4 flux using the homogeneous footprint algorithm (HF), gradient footprint algorithm (GF) and dynamic footprint algorithm (DF) for all study sites (Bold indicates $| r_p | > 0.2$ and P <0.05, *: <0.05, and **: < 0.01)

Footprint	Site	Bare soil (%)	Arctic C3 grass (%)	Soil temperature (K)	Soil water content (m^3 m^{-3})	Elevation (m)
HF	US-Beo	**-0.387****	**0.385****	0.055**	0.054**	0.172**
	US-Bes	**-0.488****	**0.488****	**0.265****	**0.249****	**0.263****
	US-Brw	-0.073**	0.068**	0.009	0.009	-0.007
	US-Atq	**-0.718****	**0.718****	-0.060**	-0.058**	0.166**
	US-Ivo	**-0.290****	**0.305****	-0.053**	0.052**	0.030
GF	US-Beo	**-0.276****	**0.284****	**0.232****	**0.229****	0.116**
	US-Bes	0.175**	-0.171**	**-0.242****	**-0.210****	**-0.367****
	US-Brw	-0.009	0.051**	0.025	0.037*	0.134**
	US-Atq	**-0.305****	**0.305****	0.120**	0.100**	-0.010
	US-Ivo	-0.031	0.028**	0.035*	-0.083**	0.072**
DF	US-Beo	**-0.270****	**0.265****	0.070**	0.064**	0.093**
	US-Bes	0.182**	-0.180**	**-0.229****	**-0.200****	**-0.301****
	US-Brw	-0.062**	0.064**	0.107**	0.105**	0.177**
	US-Atq	**-0.280****	**0.280****	0.049	0.029	**-0.369****
	US-Ivo	0.039	0.192**	0.101**	0.048*	0.022

Chapter 3

Projecting methane emissions in Arctic tundra ecosystems under different climate scenarios

Yihui Wang, Liyuan He, Jianzhao Liu, Kyle A. Arndt, Jorge L.Mazza Rodrigues, Donatella Zona, David A. Lipson, Walter C. Oechel, Daniel M. Ricciuto, Stan D. Wullschleger, and Xiaofeng Xu

Abstract

Methane (CH_4) emissions from the Arctic tundra are known to increase with climate warming. However, interactions among temperature, soil moisture status, and vegetation complicate a full understanding of emission rates and their magnitude in a changing climate. In this study, we applied the CLM-Microbe model to project CH_4 emissions under three Shared Socioeconomic Pathways (SSP) scenarios using climate data from three climate models from 2016 to 2100. Five sites (200 m × 200 m) in the Alaska North Slope were chosen; three of them are in Utqiaġvik (US-Beo, US-Bes, and US-Brw), one in Atqasuk (US-Atq), and one in Ivotuk (US-Ivo). Simulated CH_4 emissions substantially increased by a factor of 5.3-7.5 under SSP5-8.5 scenario compared to the SSP1-2.6 and SSP2-4.5 scenarios. The projected CH_4 emissions were comparable to historical emissions during 2006-2015 across the five sites. CH_4 emission exhibited a stronger response to rising temperature under the SSP5-8.5 scenario than under SPP1-2.6 and SSP2-4.5 scenarios, likely supported by a simultaneous enhanced precipitation-induced expansion of anoxic conditions for methanogenesis. The CH_4 transport via ebullition and plant-mediated transport is projected to increase under all three SSP scenarios, and ebullition dominated CH_4 transport by 2100 across five sites. Projected CH_4 emission varies in temperature sensitivity, with a Q_{10} range of 2.7-60.9 under SSP1-2.6, 3.8-17.6 under SSP2-4.5, and 5.7-17.2 under SSP5-8.5. Compared with the other three sites, US-Atq and US-Ivo were estimated to have greater increases in CH_4

emissions due to higher temperature and precipitation. The CLM-Microbe model is a practical tool for projecting landscape-scale CH_4 emissions and investigating the mechanisms of CH_4 cycling under different climate scenarios in the Arctic. The nonlinear warming impacts on CH_4 emission in the Arctic indicate strong positive CH_4-climate feedback that has been overlooked in previous model simulations.

Introduction

Methane (CH_4) is one of the most potent greenhouse gases in the atmosphere (Tan and Zhuang, 2015). CH_4 concentrations in the atmosphere have been rising since 2007 and approached an annual average concentration of 1860 ppb in 2018 (National Oceanic and Atmospheric Administration, NOAA/ESRL, www.esrl.noaa.gov/gmd/ccgg/trends_ch4/) (Clarke et al., 2007; Fujino et al., 2006; Ganesan et al., 2019; Nisbet et al., 2019; van Vuuren et al., 2007; Rubino et al., 2019). Arctic soils are considered as a substantial net emission source of CH_4 to the atmosphere, as methanogenesis is positively correlated with temperature (Oh et al., 2020; Tan and Zhuang, 2015a, b). Arctic CH_4 emissions were estimated to be 15 – 50 Tg CH_4 yr^{-1}, accounting for 20 – 25% of global natural CH_4 emissions (Kirschke et al., 2013). In addition, process-based biochemistry models predicted that Arctic CH_4 emissions will be two to three times greater by 2100 due to warming (Schuur et al., 2013; Koven et al., 2011; Lawrence et al., 2015). Oh et al. (2020) reported a 70 and 100% increase in wetland CH_4 emissions by 2100 under the Representative Concentration Pathways (RCP) of 8.5 $W \cdot m^{-2}$. This undoubtedly emphasizes the importance of CH_4 projections in the Arctic for the next few decades.

Arctic regions have been warming two to four times faster than the global average in recent decades (Hansen et al 2007; Miner et al., 2022). Air temperature in the Arctic has increased at a

rate of 0.755 °C/decade during 1998–2012 (Chen et al., 2020) and could continue to increase by more than 10°C by 2100 relative to present-day, corresponding to about 30% more than the best estimate of warming (IPCC, 2021). Field experiments with manipulated temperature in the Arctic found that warming increased CH_4 fluxes by 15 – 550% or had no effect due to changes in water table and vegetation (Granberg et al., 2001; Turetsky et al., 2008; Updegraff et al., 2001; Verville et al., 1998). For example, the data-constrained projections showed a 400% increase in CH_4 emission under 9°C warming at the Spruce and Peatland Responses Under Changing Environments experimental (SPRUCE) site (Ma et al., 2017). However, large uncertainties still exist in predicting responses of Arctic CH_4 fluxes to future climate change due to changing thaw dynamics and vegetation shifts (Miner et al., 2022), even though CH_4 production and emission processes have been extensively explored (Ma et al., 2017; Oh et al., 2020).

The CLM-Microbe model takes advantages of involving a new microbial-functional-group based CH_4 module (Wang et al., 2019, 2022; Xu et al., 2015, 2016) and a new framework for microbial controls on carbon (C) mineralization (He et al., 2021a,b; Xu et al., 2014) in the default decomposition subroutines in CLM4.5 (Koven et al., 2013; Thornton and Rosenbloom, 2005; Thornton and Zimmermann, 2007). It allows for a better understanding of the mechanisms and dynamics of CH_4 production, oxidation, and transport pathways under climate changes. Our previous studies have validated this module with incubation fluxes and closed-chamber fluxes (Wang et al., 2019; Xu et al., 2015). In addition, CH_4 fluxes have been upscaled from the plot level to landscape scales using different footprint algorithms, which were consistent with Eddy Covariance (EC) fluxes in Alaskan tundra ecosystems (Wang et al., 2019, 2022). CH_4 emissions responding to spatial heterogeneities in vegetation, soil hydrology, and topography can be well studied based on the CLM-Microbe model (Wang et al., 2019; 2022). Therefore, the CLM-

Microbe model could help us to understand the mechanisms of future CH_4 dynamics through each CH_4 process at the landscape scales in the Arctic tundra.

This study continued our research on simulating CH_4 fluxes in the Arctic and further estimated how future Arctic CH_4 fluxes change under climate changes. In this study, we applied the CLM-Microbe model to project CH_4 fluxes from 2016 to 2100 under SSP1-2.6, SSP2-4.5, and SSP5-8.5 scenarios derived from three climate models for five Alaskan tundra ecosystems. We aim to 1) project how Arctic CH_4 emissions change under different SSP scenarios by 2100, 2) understand the mechanisms behind future CH_4 dynamics under different SSP scenarios, and further 3) investigate the differences of projected future CH_4 fluxes across different Alaskan tundra ecosystems.

Methodology

Site Information

We performed model experiments at five sites in the northern Alaskan tundra; detailed site information on the sites is available in Arndt et al. (2019, 2020). Three of these sites are located in Utqiaġvik, including US-Beo (71.2810°N, 156.6124°W), US-Bes (71.2809°N, 156.5965°W), and US-Brw (71.3225°N, 156.6093°W) (referred as Utqiaġvik sites) (Zona et al., 2016). US-Beo is a polygonal coastal tundra site on the Barrow Environmental Observatory; and US-Bes is an inundated wet coastal tundra site at the southern end of the previous Biocomplexity Experiment, usually with a water table above the surface of the soil due to its low elevation (Zona et al., 2009). US-Brw is a well-drained, moist coastal tundra site, and its vegetation is dominated by graminoids (Kwon et al., 2006). The US-Atq site (70.4696°N, 157.4089°W) in Atqasuk, AK is located about 100 km south of Utqiaġvik; and the US-Ivo site (68.4805°N, 155.7569°W) in Ivotuk, AK is located

approximately 300 km south of Utqiaġvik in the northern foothills of the Brooks Range (Davidson et al., 2016). US-Atq is characterized by polygonized tussock tundra and sandy soils (Walker et al., 1989), and US-Ivo, the most inland site, is the warmest and lies on gently sloping tussock tundra (Davidson et al., 2016). These study sites have a polar maritime climate, with the majority of precipitation falling during the summer months (June-August). Detailed meteorological and vegetation information for these sites is posted in the Oak Ridge National Laboratory Distributed Active Archive Center (ORNL DAAC) (https://doi.org/10.3334/ORNLDAAC/1562 and https://doi.org/10.3334/ORNLDAAC/1546).

Climate Models

The Coupled Model Intercomparison Project Phase 6 (CMIP6) includes future warming projections for the 21st century climate with different Shared Socioeconomic Pathways (SSP) scenarios. In comparison to the RCPs, the five main SSPs (SSP1-1.9, SSP1-2.6, SSP2-4.5, SSP3-7.0, and SSP5-8.5) are more evenly spaced and extend to lower 2100 radiative forcing and temperatures (Meinshausen et al., 2020). In this study, we chose SSP1-2.6, SSP2-4.5, and SSP5-8.5 for CMIP6, which allowed us to explore the impact of different magnitudes of anthropogenic forcing and the response of the climate system simulated with varying representations of the model (Nazarenko et al., 2015). In addition, three climate models in CMIP6 were selected to retrieve data for SSP1-2.6, SSP2-4.5, and SSP5-8.5 from 2016 to 2100. 1) The BCC-CSM2-MR is a medium-resolution version of the BBC-CSM (T106 in the atmosphere and 1˚ latitude × 1˚ longitude in the ocean) which is the baseline for BCC participation in CMIP6 (https://esgf-node.llnl.gov/search/cmip6/). 2) The CESM Version 2 (CESM2) is the latest generation of the coupled climate/Earth system model. The output fields from previous CESM2 simulations have been posted on the Earth System Grid Federation (ESGF; https://esgf-node.llnl.gov/search/cmip6).

3) EC-Earth3 is the latest version of EC-Earth in CMIP6 that utilizes the original idea of a climate model system based on the seasonal prediction system of the European Centre for Medium-Range Weather Forecasts (ECMWF). Development started in 2012 by re-designing the software infrastructure and updating the atmosphere model to IFS 36r4, corresponding to the ECMWF seasonal prediction system 4. Since then, various updates, improvements and forcings have been implemented and the model has been tuned for several intermediate versions and finally for the CMIP6 version, EC-Earth3 (Döscher et al., 2022) (https://esgf-node.llnl.gov/search/cmip6/). The required meteorological variables for model simulations are total incident solar radiation, incident longwave radiation, total precipitation, surface air pressure, specific humidity, air temperature and wind speed. Detailed information for meteorological variables of each climate model corresponding to variables of CRUNCEP are shown in Table S1-S3.

Calibration of Future Climate Data

Two major steps for calibration of forcing data were 1) to simulate the trend of meteorological variables during future period and 2) to estimate the offset of variables between historical and future periods. In the first step, we performed a two-dimensional polynomial regression concerning the nonlinear increases of meteorological variables and the increasing computing demand of multi-dimensional polynomial fit. Two-dimensional polynomial regression of these variables during future periods was conducted using "lspoly" function provided in the US National Center for Atmospheric Research (NCAR) command language. In the second step, the offsets of meteorological variables between historical and future periods were estimated by comparing the arithmetic means of 2007-2016 from historical dataset and means of 2015-2024 from future dataset. Following completion of these two steps, calibrated future data were the combination of future trends of variables simulated by two-dimensional polynomial regressions

and the offsets between historical and original future datasets. The climate data (e.g., air temperature, air pressure, and precipitation) after calibration are shown in Figure S1.

Model Description

The CLM-Microbe model branches from the framework of default CLM 4.5 developed in 2013. Therefore, the CLM-Microbe has default decomposition subroutines in CLM4.5 (Koven et al., 2013; Thornton and Rosenbloom, 2005; Thornton and Zimmermann, 2007). The improvements in the CLM-Microbe model include a new microbial-functional-group based CH_4 module (Xu et al., 2015; Wang et al., 2019), and a new framework for microbial controls on C mineralization (He et al., 2021a,b; Xu et al., 2014). Detailed mathematical expressions for CH_4 production, consumption and transport processes were obtained from Wang et al. (2019) and Xu et al. (2015). The code for the CLM-Microbe model is archived at https://github.com/email-clm/clm-microbe. The model version used in this study was obtained from GitHub on 27 May 2020.

Additional forcing data included spatial distribution of vegetation and a digital elevation model with a resolution of 4 m covering the tower domain at each site, and soil organic carbon (SOC) concentration at ten soil layers defined in CLM4.5 (Koven et al., 2013; Thornton et al., 2007; Thornton and Rosenbloom, 2005). Vegetation distribution for Utqiaġvik sites was determined using a random forest algorithm using the plant functional type from Langford et al. (2019) as training data. For the US-Atq and US-Ivo sites, an unsupervised linear spectral unmixing was performed in ENVI V5.2 (L3Harris Geospatial) using the vegetation classes from a previous publication (Davidson et al., 2016), with an additional open water category. Four plant species across five areas were classified into model defined PFTs, including Arctic C3 grass, bare soil, broadleaf evergreen shrub, and broadleaf deciduous boreal shrub. Averages of plant cover at US-

Beo, US-Bes, US-Brw, US-Atq, and US-Ivo sites were 88%, 82%, 91%, 73%, and 78%, respectively; US-Ivo had larger proportions of shrubs than other sites. A vegetation distribution map of the five study sites was available in Wang et al. (2022). A 0.5 m (vertical resolution) digital elevation model (DEM) was used for elevation data at Utqiaġvik sites (Wilson, 2012). Elevation maps for US-Atq and US-Ivo were download from ArcticDEM (v3.0 Pan-Arctic) with a resolution of 2 m based on the geographic information of these two sites, and further processed to maps with a resolution of 4 m using MATLAB software (R2018a, the MatWorks). SOC concentrations at 0-10, 10-20, 20-30 and 30-40 cm at US-Bes, US-Atq, and US-Ivo were derived from the Northern Circumpolar Soil Carbon Database (Hugelius et al., 2013). Due to the lack of SOC data, we assumed that US-Beo and US-Brw had the same SOC distribution with US-Bes since these sites are adjacent, which might affect the accuracy of CH_4 projections for these two sites. Detailed calculation processes can be found in Wang et al. (2022).

Shared Socioeconomic Pathways (SSP) Experiments

Model implementation for historical simulation was carried out in three stages, similar to the default CLM4.5 protocols (Oleson et al., 2013). The first phase is accelerated model spin-up that was set up for 2,000 years to allow the system to an accumulate C and reach steady-state. We set the accelerated model spin-up for 2000 years to allow more C accumulation as Arctic tundra has a low rate and long period of C sequestration. Then a final spin-up was set up to 50 years to allow the modeled system to reach a relative steady-state. After the final spin-up, the transient simulation was set to cover the period of 1850–2015 for all five sites. Detailed information for historical simulation is available in Wang et al. (2022).

From 2016 to 2100, we reset the transient simulation to accomplish CH_4 projections with three climate datasets for each of SSP1-2.6, SSP2-4.5 and SSP5-8.5 started from the year 2015.

The SSP1-2.6 "2˚C scenario" of the "sustainability" SSP1 socio-economic family, whose nameplate 2100 radiative forcing level is 2.6 $W \cdot m^{-2}$. This SSP1-2.6 scenario approximately corresponds to the previous scenario generation Representative Concentration Pathway (RCP) 2.6 (Meinshausen et al., 2020). The SSP2-4.5 of the "middle of the road" socio-economic family SSP2 with a nominal 4.5 $W \cdot m^{-2}$ radiative forcing level by 2100 – approximately corresponding to the RCP-4.5 scenario (Meinshausen et al., 2020). The SSP5-8.5 marks the upper edge of the SSP scenario spectrum with a high reference scenario in a high fossil fuel development world throughout the 21st century (Meinshausen et al., 2020). We conducted nine model runs for each site at the annual scale with a spatial resolution of 4 m. For CH_4 projections, all parameter values were kept consistent with previous studies (Wang et al., 2019, 2022; Xu et al., 2015), and the same model parameters and settings were applied to all five sites under different SSP scenarios.

Temperature Sensitivity of CH_4 Fluxes

To analyze the sensitivity of CH_4 fluxes to temperature, we calculated the Q_{10} coefficient as the measures of the change rate of CH_4 fluxes as a consequence of the temperature increment of 10 °C or K. We used a linear regression to estimate the Q_{10} coefficient with all data points of CH_4 fluxes for each SSP scenario and each climate model. The formula for estimating the Q_{10} was as follows:

$$log_{10}\left(\frac{R}{R_0}\right) = a \times log_{10}\left(\frac{T-T_0}{10}\right) + b \quad (1),$$

where R is the CH_4 flux ($gC \cdot m^{-2} \cdot year^{-1}$) at temperature T and R_0 is the CH_4 flux ($gC \cdot m^{-2} \cdot year^{-1}$) at temperature T_0 (K) in 2016. The Q_{10} is estimated as ten to the power of the coefficient *a* and the coefficient *b* is the estimated intercept.

Statistical Analysis

Dynamics of annual CH_4 fluxes, air temperature, precipitation, soil temperature, soil moisture, and net primary production (NPP) were plotted for five sites under different SSP scenarios and the differences among the three climate models were exhibited using the R (version 3.6). Averages of CH_4 fluxes in the periods of 2006-2015, 2016-2015, 2050-2059 (2050s) and 2090-2099 (2090s) were also calculated for comparison over time for different climate models. One-way analysis-of-variance (ANOVA) and the Duncan test were employed to assess the differences in CH_4 fluxes among different time periods for each site and among different sites for each time period. Before this analysis, the data have been tested and followed the assumptions of ANOVA. Changing rates of CH_4 fluxes, each CH_4 process and each environmental factor were calculated based on the general linear regression analysis using all data points and three climate models for each site and each SSP scenario in 2016-2100. Fractions of three CH_4 transport pathways: diffusion, ebullition and plant-mediated transport were displayed in pie charts. Correlations between CH_4 emission and each CH_4 process and environmental factor for each site under each SSP scenario were analyzed using the Pearson's correlation coefficients (r_p). A combined forward/backward multiple linear regression analysis was used to examine the effects of air temperature, precipitation, canopy evapotranspiration (ET) and NPP on CH_4 fluxes. All variables were normalized before the regression analysis, and the 'best' model was chosen based on the lowest Akaike information criterion (AIC) value (Langeveld et al., 2019). All statistical analyses and plots were made using R (version 3.6).

Results

Projected CH_4 Fluxes During 2016-2100 Under Different SSP Scenarios

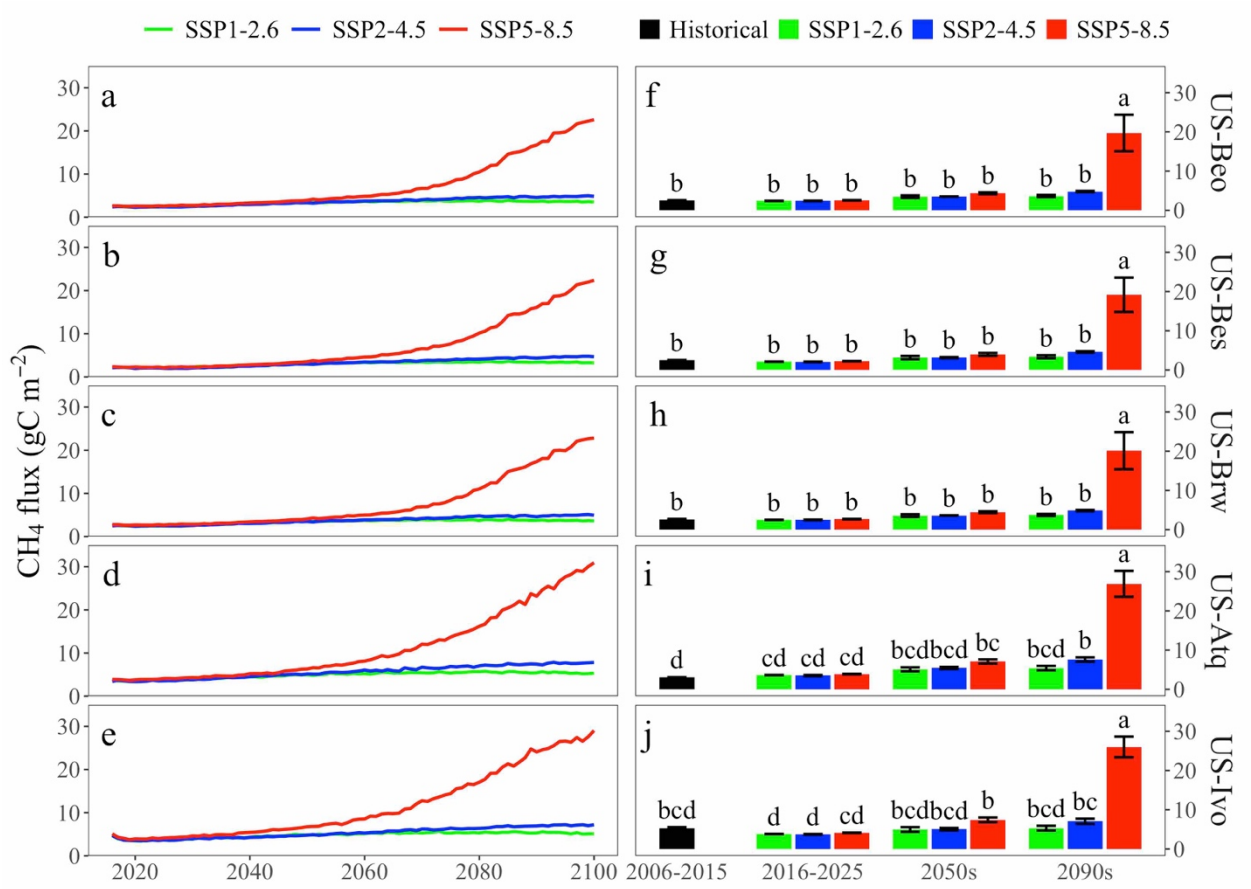

Figure 1. Projections of CH_4 fluxes at a) US-Beo, b) US-Bes, c) US-Brw, d) US-Atq and e) US-Ivo during 2016-2100 under different Shared Socioeconomic Pathways (SSP) scenarios. The bar charts show projected CH_4 fluxes (mean ± SD; n = 10 or 30) for the periods of 2006 - 2015, 2016 - 2025, the 2050s, and 2090s at f) US-Beo, g) US-Bes, h) US-Brw, i) US-Atq and j) US-Ivo under SSP1-2.6, SSP2-4.5, and SSP5-8.5 scenarios. Green indicates SSP1-2.6 scenario, blue indicates SSP2-4.5 scenario, red indicates SSP5-8.5 scenario and black indicate historical fluxes of 2006-2015 simulated by the CLM-Microbe model. Different letters above the rectangular bar mean significantly differences based on the Duncan's multiple range test at the $\alpha = 0.05$; the error bar represents the standard deviation.

Projected CH_4 emissions increased by 2100 under the three SSP scenarios with different change rates among the five study sites (Figure 1 and Figure S2). Especially after 2050, CH_4 fluxes drastically increased under SSP5-8.5 compared with SSP1-2.6 and SSP2-4.5 (Figure 1). Until 2100, projected CH_4 fluxes under SSP5-8.5 were 4 – 7-fold higher than the fluxes under SSP1-2.6 and SSP2-4.5 (Figure 1f - j). There were no significant differences in projected CH_4 fluxes between SSP1-2.6 and SSP2-4.5 (Figure 1f – j), although the fluxes under SSP2-4.5 seemed to be slightly

higher than under SSP1-2.6 over time (Figure 1a-e). In the 2090s, projected CH_4 fluxes increased by 39 – 121% under SSP1-2.6 and SSP2-4.5 but increased by a factor of 5.3 – 7.5 under SSP5-8.5 among the five study sites in Arctic tundra (Figure 1).

Average projected CH_4 fluxes (unit: gC $\cdot m^{-2} \cdot year^{-1}$) during 2016 - 2025 were comparable to that in the 2050s under different SSP scenarios, which were 2.47 ± 0.10 at US-Beo, 2.15 ± 0.09 at US-Bes, 2.56 ± 0.11 at US-Brw, 3.67 ± 0.19 at US-Atq and 3.89 ± 0.20 at US-Ivo (Figure 1f – j). Moreover, they were consistent with the average historical fluxes during 2006 - 2015 as simulated by the CLM-Microbe model (Figure 1f – j) (Wang et al., 2022). Additionally, projected CH_4 fluxes in the warmer study sites of US-Atq and US-Ivo exhibited larger absolute increments than at US-Beo, US-Bes and US-Brw (Figure 1f - j). For example, projected CH_4 fluxes in the 2090s under SSP5-8.5 were around 20 gC $\cdot m^{-2} \cdot year^{-1}$ at US-Beo, US-Bes and US-Brw, whereas fluxes approached 30 gC $\cdot m^{-2} \cdot year^{-1}$ at US-Atq and US-Ivo.

Variations in CH_4 Processes and Climate Factors Under Different SSP Scenarios

Conceptual models of CH_4 processes were built for each study site under different SSP scenarios, which displayed changing rates of each CH_4 process, climate and vegetation factor, including production, oxidation and transport pathways of CH_4, temperature, precipitation and NPP (Figure 2, Table 1). Overall, except for anaerobic oxidation, rates for all CH_4 processes increased by 2100, as well as climate factors (Figure 2, Table 1). Moreover, the magnitude of changes for all CH_4 processes and climate factors was larger under SSP5-8.5 than under SSP1-2.6 and SSP2-4.5 (Figure 2, Table 1). Air temperature increased by 0.020 – 0.130 K$\cdot year^{-1}$ under different SSP scenarios, and the increase of soil temperature was comparable with air temperature (Table 1). The change rates of air temperature and soil temperature under SSP2-4.5 and SSP5-8.5 were approximately 2.6 times and 5.7 times that under SSP1-2.6, except at US-Ivo (Table 1).

Annually, precipitation increased by 0.503 to 0.786 mm under SSP1-2.6 and SSP2-4.5, but increased by 1.861 to 3.084 mm under SSP5-8.5 (Table 1). Soil moisture increased by 0.023 to 0.099 % per year (Table 1). Additionally, the increase of precipitation and soil moisture under SSP2-4.5 were 1.3 – 1.6 times and 1.3 – 2.0 times that under SSP1-2.6, respectively, whereas the increase of precipitation and soil moisture under SSP5-8.5 were 3.1 – 5.6 times and 2.3 – 4.0 times that under SSP1-2.6, respectively (Table 1).

Table 1. Annual changes of air temperature, soil temperature, precipitation and soil moisture at US-Beo, US-Bes, US-Brw, US-Atq and US-Ivo under SSP1-2.6, SSP2-4.5 and SSP5-8.5 scenarios

Variable	Site	SSP1-2.6	SSP2-4.5	SSP5-8.5
Air temperature ($\Delta K \cdot year^{-1}$)	US-Beo	0.023	0.059	0.130
	US-Bes	0.023	0.059	0.130
	US-Brw	0.023	0.059	0.130
	US-Atq	0.021	0.054	0.123
	US-Ivo	0.020	0.042	0.102
Soil temperature ($\Delta K \cdot year^{-1}$)	US-Beo	0.025	0.064	0.133
	US-Bes	0.022	0.059	0.126
	US-Brw	0.025	0.064	0.133
	US-Atq	0.026	0.058	0.123
	US-Ivo	0.016	0.044	0.142
Precipitation ($\Delta mm \cdot year^{-1}$)	US-Beo	0.362	0.440	0.828
	US-Bes	0.362	0.440	0.828
	US-Brw	0.362	0.440	0.828
	US-Atq	0.446	0.606	1.366
	US-Ivo	0.454	0.594	1.861
Soil moisture ($\Delta \% \cdot year^{-1}$)	US-Beo	0.039	0.076	0.092
	US-Bes	0.031	0.055	0.083
	US-Brw	0.039	0.081	0.099
	US-Atq	0.040	0.051	0.094
	US-Ivo	0.023	0.038	0.092

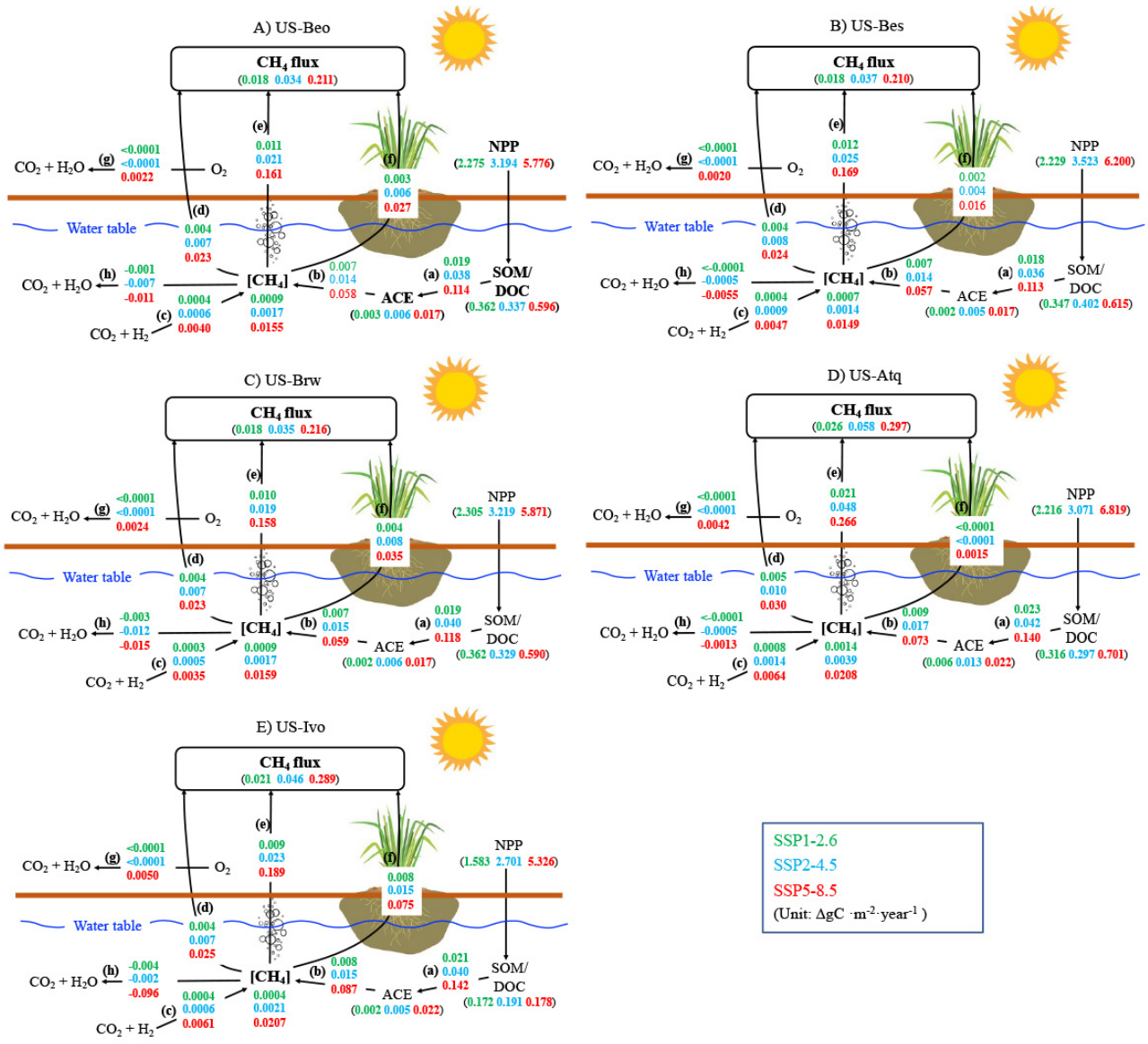

Figure 2. Conceptual model of CH_4 processes at A) US-Beo, B) US-Bes, C) US-Brw, D) US-Atq, and E) US-Ivo under different Shared Socioeconomic Pathways (SSP) scenarios. CH_4 processes (unit: $\Delta gC \cdot m^{-2} \cdot year^{-1}$) include a) fermentation of soil organic matter (SOM)/ dissolved organic carbon (DOC) to acetate, b) acetoclastic methanogenesis, c) hydrogenotrophic methanogenesis, d) diffusion, e) ebullition, f) the plant-mediated transport, g) aerobic oxidation, and h) anaerobic oxidation of CH_4. Vegetation factor is net primary production (NPP, $\Delta gC \cdot m^{-2} \cdot year^{-1}$). The numbers in the conceptual model and table are the changing rates of each process and factor during 2016 - 2100. Green numbers are for SSP1-2.6 scenario, blue numbers are for SSP2-4.5 scenario, and red numbers are for SSP5-8.5 scenario.

Different CH_4 processes showed dissimilar contributions under different SSP scenarios, but mutually strengthened total CH_4 fluxes. Generally, the increase or decrease was larger under SSP5-8.5 than under SSP2-4.5 and SSP1-2.6 (Figure 2). For example, at US-Beo, NPP annually increased by 2.275 gC $\cdot m^{-2}$ under SSP1-2.6, 3.194 gC $\cdot m^{-2}$ under SSP2-4.5 and 5.776 gC $\cdot m^{-2}$ under SSP5-8.5. However, SOM/DOC were only enhanced by approximately 10% that of the increased NPP value (Figure 2A). The production rate of acetate from SOM/DOC was accelerated and the rate under SSP2-4.5 was twice the rate under SSP1-2.6, while the rate under SSP5-8.5 was three times the rate under SSP2-4.5 (Figure 2A). The increase of acetate was about 1% of the increase in SOM/DOC, and the production rate of CH_4 from acetate also speeded up with a higher increase than the increase of acetate concentration under different SSP scenarios (Figure 2A). Annually, the increase in the production rate of CH_4 from $CO_2 + H_2$ was 0.0004 gC $\cdot m^{-2}$ under SSP1-2.6, 0.0009 gC $\cdot m^{-2}$ under SSP2-4.5 and 0.0047 gC $\cdot m^{-2}$ under SSP5-8.5, which were lower than that from acetate (Figure 2A). Moreover, the difference in change rates between these two processes narrowed under SSP5-8.5 compared with SSP1-2.6 and SSP2-4.5. All transport pathways were accelerated and the ebullition rate changed substantially compared with diffusion and plant-mediated transport under each SSP scenario (Figure 2A). Ebullition annually increased by 0.011, 0.021 and 0.161 gC $\cdot m^{-2}$ under SSP1-2.6, SSP2-4.5 and SSP5-8.5, respectively; which were about 3 – 7 times higher than other transport pathways (Figure 2A). CH_4 oxidation changed little compared with production and transport of CH_4 and changes of aerobic oxidation can be ignored under SSP1-2.6 and 2-4.5 (Figure 2A). Anaerobic oxidation annually reduced by 0.001, 0.007 and 0.011 gC $\cdot m^{-2}$ under SSP1-2.6, SSP2-4.5 and SSP5-8.5, respectively (Figure 2A). In total, CH_4 fluxes annually increased by 0.018 gC $\cdot m^{-2}$ under SSP1-2.6, 0.034 gC $\cdot m^{-2}$ under SSP2-4.5 and 0.211 gC $\cdot m^{-2}$ under SSP5-8.5 (Figure 2A).

Changes in CH_4 Processes and Climate Factors Among the Five Study Sites

Utqiaġvik sites had very similar changes in air temperature, soil temperature and precipitation, distinct with US-Atq and US-Ivo, especially for precipitation (Table 1). Under the similar climate conditions, the increase of CH_4 fluxes were comparable, which were about 0.018 gC $\cdot m^{-2}$, 0.035 gC $\cdot m^{-2}$, 0.212 gC $\cdot m^{-2}$ under SSP1-2.6, SSP2-4.5 and SSP5-8.5, respectively (Figure 2A-C). Among these three sites, there were no significant differences in the production of CH_4 from acetate; however, the increase in NPP at US-Bes was larger under SSP2-4.5 and SSP5-8.5 than at US-Bes and US-Brw sites (Figure 2A-C). Changes in the production of CH_4 from CO_2 + H_2 showed little difference among these sites, especially under SSP2-4.5 and SSP5-8.5 (Figure 2A-C). US-Bes showed a greater increase in this production process, but changes were still smaller than the acetate production pathway. Additionally, there were no significant differences in aerobic oxidation of CH_4 among these sites (Figure 2A-C). Anaerobic oxidation at US-Bes had the smallest changes under different scenarios across sites (Figure 2B); whereas the US-Brw site displayed the largest annual decrease of -0.003 gC $\cdot m^{-2}$, -0.012 gC $\cdot m^{-2}$ and -0.015 gC $\cdot m^{-2}$ under SSP1-2.6, SSP2-4.5 and SSP5-8.5, respectively (Figure 2C). Ebullition dominated the transport of CH_4 among these three sites, and changes in each transport mechanism were different among sites (Figure 2A-C). Diffusion changes were comparable; however, US-Bes had a greater increase in ebullition and smaller change in plant-mediated transport, whereas US-Brw had a smaller increase in ebullition, but larger increase in plant-mediated transport (Figure 2A-C).

With higher precipitation, US-Atq had greatest CH_4 fluxes across all five sites with 0.026 gC $\cdot m^{-2}$, 0.058 gC $\cdot m^{-2}$, 0.297 gC $\cdot m^{-2}$ under SSP1-2.6, SSP2-4.5 and SSP5-8.5, respectively (Figure 2D, Table 1). Compared with US-Beo, the increases of NPP and SOM/DOC at US-Atq were smaller under SSP1-2.6 and SSP2-4.5, but production rates, concentrations of acetate and

production rates of CH_4 from acetate increased under all SSP scenarios (Figure 2A-D). The production of CH_4 from CO_2 + H_2 also increased, but the changes were small compared with production from acetate. Changes in CH_4 oxidation could be ignored under SSP1-2.6 and SSP2-4.5; although the aerobic oxidation under SSP5-8.5 was increased by 0.0042 gC $\cdot m^{-2}$ per year, but was still small compared with the production processes. In addition, plant-mediated transport at US-Atq showed little change, although NPP increased the most under SSP5-8.5 among all five sites (Figure 2). Both diffusion and ebullition accelerated, but ebullition showed the largest increase among all five sites with annual values of 0.021 gC $\cdot m^{-2}$, 0.048 gC $\cdot m^{-2}$, and 0.266 gC $\cdot m^{-2}$ under SSP1-2.6, SSP2-4.5 and SSP5-8.5, respectively (Figure 2D).

The US-Ivo had a higher increase in precipitation, but relatively smaller increase in air temperature among the five sites for all SSP scenarios (Table 1). Under SSP1-2.6 and SSP2-4.5, the increases of precipitation at US-Ivo were higher than at US-Beo, US-Bes and US-Brw and were comparable that at US-Atq, but the increases of soil moisture were much lower than the other four sites (Table 1). CH_4 flux at US-Ivo under SSP1-2.6 and SSP2-4.5 increased by 0.021 and 0.058 gC $\cdot m^{-2}$, which were lower than that at US-Atq but higher than that among Utiagtik three sites (Figure 2). At US-Ivo, NPP and SOM/DOC displayed much smaller increases than at the other sites under all SSP scenarios. Aerobic oxidation of CH_4 showed little change under SSP1-2.6 and SSP2-4.5, but increased by 0.005 gC$\cdot m^{-2}\cdot year^{-1}$ under SSP5-8.5 (Figure 2E). Anaerobic oxidation annually decreased by 0.004 gC$\cdot m^{-2}$, 0.002 gC$\cdot m^{-2}$ and 0.096 gC$\cdot m^{-2}$ under SSP1-2.6, SSP2-4.5 and SSP5-8.5, respectively (Figure 2E). Diffusion and ebullition of CH_4 showed comparable increases with US-Beo, US-Bes and US-Brw, and plant-mediated transport had the largest increases among the five sites (Figure 2).

Changes in CH_4 Transport Pathways Under Different SSP Scenarios

Of all CH_4 processes, three transport pathways regulated the increasing CH_4 fluxes among the five sites, even with contrasting changes in CH_4 production and oxidation processes under different SSP scenarios. Overall, the contribution rates of the three transport pathways were similar during 2016 – 2025 and 2050s among different SSP scenarios but differed in the 2090s (Figure 3 and 4, Figure S8). Both the contributions of plant-mediated transport and ebullition to CH4 transport increased, whereas the contribution of diffusion decreased over time across five sites under different SSP scenarios. Until 2100, ebullition dominated CH_4 transport across all sites under all SSP scenarios (Figure 4).

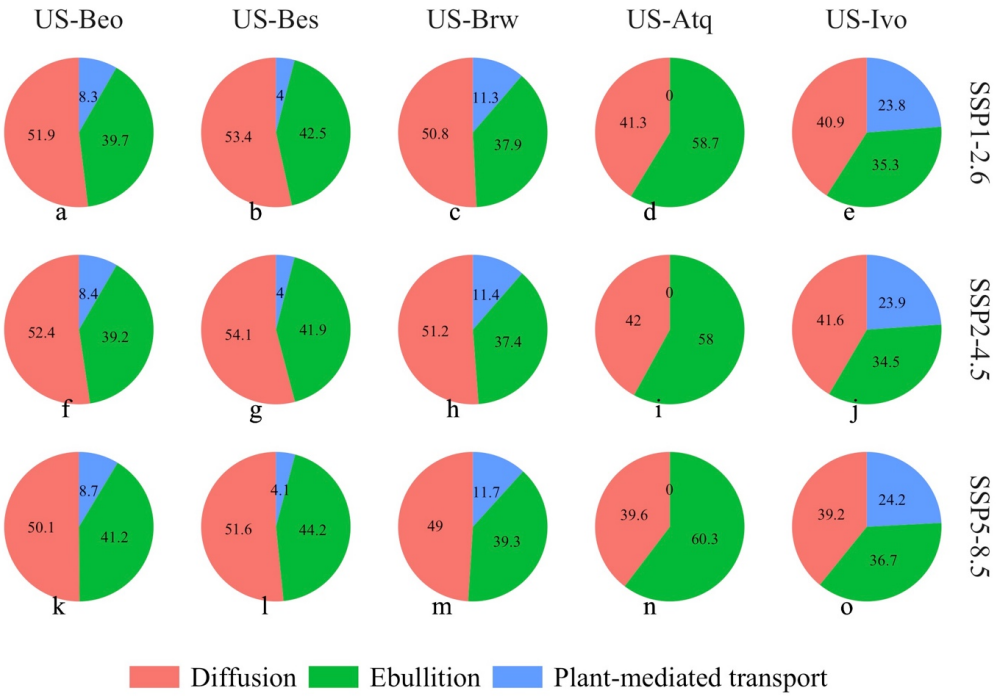

Figure 3. Contribution of three transport pathways to total CH_4 fluxes during 2016 - 2025 at US-Beo, US-Bes, US-Brw, US-Atq, and US-Ivo under a-e) SSP1-2.6, f-j) SSP2-4.5 and k-o) SSP5-8.5 scenarios. Red indicates diffusion, green indicates ebullition, and blue indicates plant-mediated transport

During 2016 – 2025, diffusion dominated CH_4 transport at US-Beo, US-Bes and US-Brw, contributing approximately half of total CH_4 fluxes for all SSP scenarios (Figure 3). Ebullition

contributed about 40% of CH_4 fluxes across the three sites, whereas plant-mediated transport contributed about 8.5% at US-Beo, 4% at US-Bes, and 11.5% at US-Brw (Figure 3). At US-Atq, ebullition contributed about 59% of total CH_4 fluxes whereas the contribution of plant-mediated transport can be ignored under all SSP scenarios (Figure 3d, 3i and 3n). Diffusion also dominated CH_4 transport at US-Ivo, but all three transport pathways contributed more comparable CH_4 fluxes, ~41% from diffusion, ~35% from ebullition, and ~24% via plants (Figure 3e, 3j, and 3o).

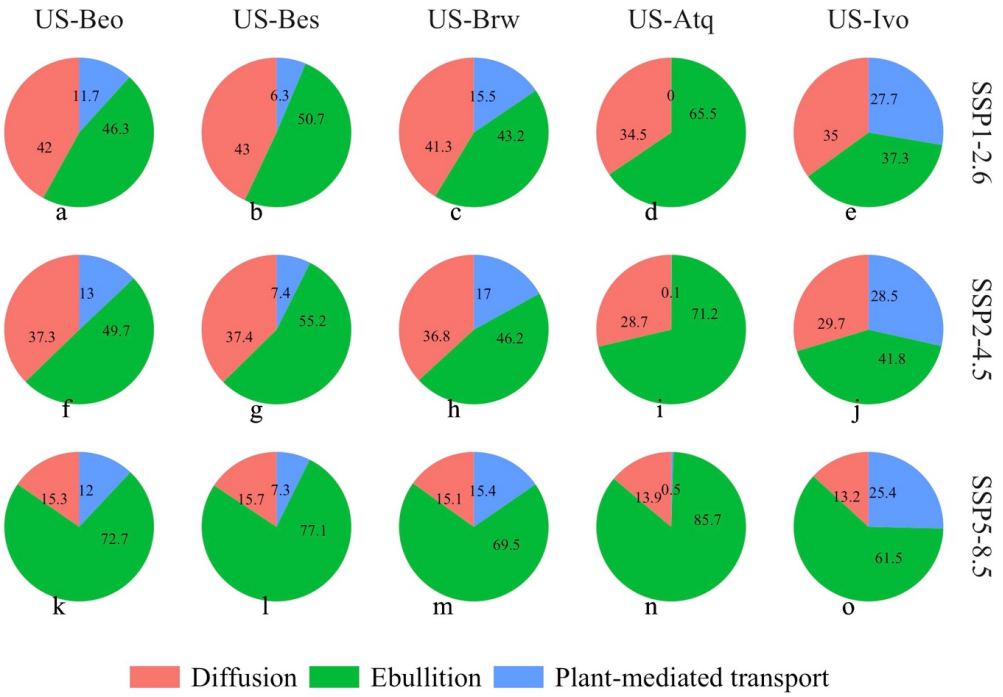

Figure 4. Contribution of three transport pathways to total CH_4 fluxes in the 2090s at US-Beo, US-Bes, US-Brw, US-Atq, and US-Ivo under a-e) SSP1-2.6, f-j) SSP2-4.5 and k-o) SSP5-8.5 scenarios. Red indicates diffusion, green indicates ebullition, and blue indicates plant-mediated transport

In the 2050s, CH_4 transport decreased via diffusion, whereas it increased via plant-mediated transport and ebullition across the five sites and under all SSP scenarios (Figure S8). In the 2090s, both plant-mediated transport and ebullition continued to increase under all SSP scenarios, but their contribution ratios were somewhat changed compared to the 2050s for SSP1-

2.6 and SSP2-4.5 (Figure 4). However, under SSP5-8.5, ebullition increased to 72.7% at US-Beo, 77.1% at US-Bes, 69.5% at US-Brw, 85.7% at US-Atq and 61.5% at US-Ivo (Figure 4k-o). At US-Beo, US-Bes and US-Brw, diffusion contributed about 42% of total CH_4 fluxes under SSP1-2.6 and about 37% under SSP2-4.5 (Figure 4). Plant-mediated transport could be ignored at US-Atq as it contributed less than 0.5% for all SSP scenarios (Figure 4d, 4i, and 4n). US-Ivo had the largest contribution rates from plant-mediated transport across the five sites, with approximately 27% under all SSP scenarios (Figure 4e, 4j, and 4o).

Temperature Sensitivity of CH_4 Fluxes Under Different SSP Scenarios

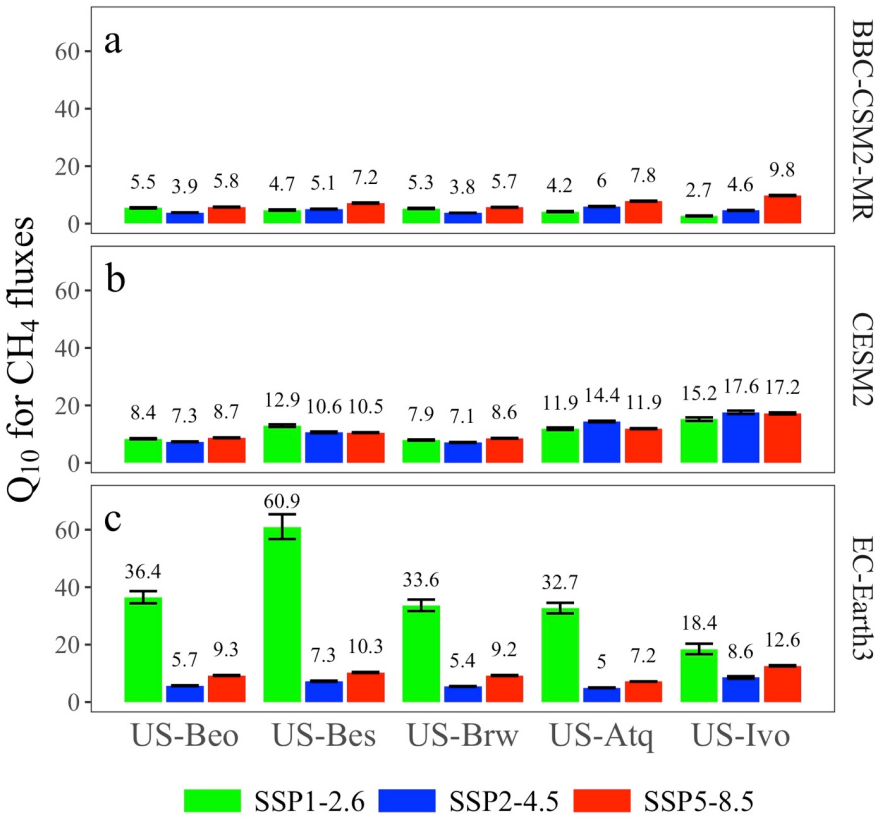

Figure 5. Temperature sensitivity (Q_{10}) of CH_4 fluxes (mean ± SD; n = 83) at US-Beo, US-Bes, US-Brw, US-Atq, and US-Ivo under SSP scenarios derived from a) BBC-CSM2-MR, b) CESM2, and c) EC-Earth3 models. Green indicates SSP1-2.6 scenario, blue indicates SSP2-4.5 scenario, and red indicates SSP5-8.5 scenario. Numbers above the rectangular bar are values of Q_{10}; the error bar represents the standard deviation.

The Q_{10} values for CH_4 fluxes differed among different SSP scenarios being lower with BBC-CSM2-MR and relatively higher with CESM2 and EC-Earth3 (Figure 5). The Q_{10} range was 2.7 – 9.8 using BBC-CSM2-MR, 7.1 – 17.6 with CESM2 and 5 – 60.9 with EC-Earth3 (Figure 5). Using EC-Earth3, Q_{10} had extremely high values under SSP1-2.6, ranging from 18.4 at US-Ivo to 60.9 at US-Bes; however, Q_{10} was lower under SSP2-4.5 than under SSP5-8.5 (Figure 5). Q_{10} increased along the gradient of SSP1-2.6, SSP2-4.5 and SSP5-8.5 at US-Bes, US-Atq and US-Ivo using BBC-CSM2-MR, whereas there were no obvious trends for Q_{10} along such scenario gradient using the other climate models across all five sites (Figure 5). US-Beo and US-Brw had comparable Q_{10} values for the different SSP scenarios with each climate model.

Discussion

Mechanisms of Future CH_4 Emission Under Different SSP Scenarios

Future CH_4 emission has been projected to gradually increase under different SSP scenarios. Our results showed that air temperatures were increased by 1 – 2 °C under SSP1-2.6, 3 – 5 °C under SSP2-4.5, and 7 – 12 °C under SSP5-8.5, leading to an increase of 39 – 60%, 89-121%, and 531 – 751% in CH_4 emissions under SSP1-2.6, SSP2-4.5, and SSP5-8.5, respectively (Figure S2 and S4). This confirmed that warmer temperatures (r_p = 0.832, p < 0.05; Figure S9) and more precipitation (r_p = 0.696, p < 0.05; Figure S9) could enhance CH_4 emissions, which was consistent with previous studies (Shindell et al., 2004; Ma et al., 2017). In addition, previous studies reported that a 3 – 5 °C warming more than doubled boreal emissions (Frolking, 1991), and a ~5 °C warming tripled northern Alaskan emissions in the mid-summer (Livingston and Morrissey, 1991). Ma et al. (2017) showed that modeled CH_4 emissions increased by 30%, 100%, 275%, and 400% under 2.25, 4.5, 6.75, and 9 °C warming at SPRUCE sites. Compared with

previous studies, our projected CH_4 emission under SSP1-2.6 and SSP2-4.5 had comparable increases, but showed much stronger response under SSP5-8.5. It can be explained by changes of other climate factors that strengthened CH_4 emissions. Unchanged soil water levels or increased precipitation along with warming could cause greater increases in CH_4 emissions (Shindell et al., 2004; Ma et al., 2017). Shindell et al. (2004) found that annual-average CH_4 emission doubled in the case with a fixed wetland distribution due to around 0.4 – 0.8 $mm \cdot day^{-1}$ (annually 146 – 292 mm) increases of precipitation for doubled CO_2 over northern Eurasia. In this study, precipitation was annually increased by 41 – 48 mm (24 – 30%), 58 – 66 mm (33 – 45%) and 143 – 241 mm (83 – 116%) under SSP1-2.6, SSP2-4.5 and SSP5-8.5, respectively (Figure S5). Thus, under the SSP scenarios with the simultaneous increases in temperature and precipitation, CH_4 emission could enhance or double its response to only warming.

In this study, air temperature (43%) and precipitation (48%) acted as the main factors to explain variations in CH_4 emission (Table S5). Compared with Utqiaġvik sites, US-Ivo had smaller increases in temperature but larger increases in precipitation, and its CH_4 emission exhibited a 17-38% greater increase (Figure 2). Additionally, air temperature at US-Ivo were lower than at Utqiaġvik sites (Figure S4). Thus, enhanced precipitation could result in this stronger CH_4 response; however, the strength of precipitation effects was hard to evaluate because of their interactions with warming and other climate factors on CH_4 emission. Furthermore, more precipitation did not necessarily increase soil moisture and the depth of waterlogged soils that further to facilitate CH_4 production. Among all five sites, soil moisture was projected to increase under different SSP scenarios; however, the soil water table was deepened probably due to enhanced ET under warming (Figure S1), which might cause a shrinkage of inundated (i.e., anaerobic) soil volume. Stronger ET was related to the reduce in CH_4 emissions and it can explain

about 23% of variations of CH_4 emissions (Table S5). Our previous study found that the soil water table level was reduced under warming due to hydrological feedbacks, therefore mitigated the stimulating effects of warming on CH_4 emission (Yuan et al., 2021). Hydrological feedbacks under warming could exacerbate the challenges for projecting future CH_4 emissions. Therefore, precipitation impacts were significantly more uncertain than the temperature in predicting CH_4 emission in Arctic regions.

Both CH_4 production and oxidation are microbiological processes affected by soil C input, soil temperature, and aerobic vs anaerobic conditions (Segers et al., 1998). Therefore, under different SSP scenarios, CH_4 emissions are also affected by vegetation and microbial activities (Miner et al., 2022; Oh et al., 2020). Our results showed that about 20% of variations in CH_4 emission can be explained by NPP (Table S5). NPP can influence the amount of soil C inputs and SOM/DOC concentrations further to regulate CH_4 production and emission, but its strength was limited because the availability of soil C for methanogenesis depended on microbial decomposition rates. More NPP did not necessarily lead to a higher increase in SOM/DOC concentrations; in contrast, sometimes NPP could increase while SOM/DOC concentrations decreased because the microbial decomposition of SOM/DOC to acetate were stronger than their production from NPP. CH_4 production by methanogens profoundly strengthened under SSP5-8.5 compared with SSP1-2.6 and SSP2-4.5. Additionally, increases in the rate of acetoclastic methanogenesis were more than 10 times greater than the rate of hydrogenotrophic methanogenesis under different SSP scenarios. Therefore, acetoclastic methanogenesis, the main pathway of CH_4 production, displayed a stronger response to future climate change than hydrogenotrophic methanogenesis. Moreover, increases in the rate of aerobic CH_4 oxidation was much smaller relative to CH_4 production and its effects could be ignored in CH_4 emission. Change

rates of anaerobic oxidation were negative, indicating that more CH_4 was freed by methanotrophs and preserved in soils. Furthermore, three CH_4 transport pathways were also accelerated under SSP scenarios, but their increases were less than the increases in the input of soil CH_4 concentrations from enhanced production and reduced oxidation. As a result, soil CH_4 concentrations gradually grew by 2100 under different SSP scenarios with more concentrations under stronger warming scenarios. Of the three CH_4 transport pathways, ebullition increased faster than plant-mediated transport and diffusion and finally dominated the CH_4 transport under SSP scenarios. In the CLM-Microbe model, diffusion was determined by CH_4 concentrations in the atmosphere and soils, which were slightly affected by temperature and precipitation. The plant-mediated transport and ebullition can be largely influenced by warming and enhanced precipitation. Plant-mediated transport was controlled by soil CH_4 concentrations, NPP, and root factions, whereas ebullition was affected by soil CH_4 concentrations and plant cover. Goodrich et al. (2011) reported that higher ebullition rates in the summer were likely related to both higher rates of CH_4 production and the reduced solubility of CH_4 at higher temperatures. In our projection, changes in plant cover and composition cannot be simulated in current version of the CLM-Microbe model; therefore, the substantial increase of ebullition was caused by the accumulation of soil CH_4 concentrations. In addition, the accelerated plant-mediated transport was in response to increased NPP.

Differences in Future CH_4 Emission Among the Five Study Sites

Projected CH_4 emissions gradually grew under three SSP scenarios across all five sites; and by 2100, the emissions were largest at US-Atq and lower at US-Beo and US-Bes (Table S4). The initial conditions of climate and environmental factors could affect the magnitude of increases in CH_4 emissions. Warmer and wetter conditions at US-Atq corresponded with greater initial CH_4

emissions than other sites; moreover, projected CH_4 emissions at US-Atq showed a stronger response to climate warming. It indicated that more attention should be paid to the areas with large CH_4 emissions because they can be affected by climate change to a greater extent. Plant cover also affected the responses of CH_4 emissions to climate change, despite that its effects were limited. For example, US-Atq had 73% of plant cover which was the smallest among five sites, leading to litter increases and ignorable contributions of plant-mediated transport to total CH_4 emissions over time (Figure 2B, 3, 4 and S8). Similarly, Utqiaġvik sites had more than 80% of plant cover, corresponding to greater increases in plant-mediated transport and larger contributions to emissions among five sites. Besides, although US-Ivo had lower plant cover (i.e., 78%) than Utqiaġvik sites, plant-mediated transport increased most and contributed most to CH_4 emissions among five sites. This may be related to larger below-ground NPP and greater root fractions at US-Ivo than other sites.

Differences in Future CH_4 Emissions Using Different Climate Models

Projected CH_4 emissions differed among five sites under the three SSP scenarios derived from BBC-CSM2-MR, CESM2, and EC-Earth3. Moreover, CH_4 emissions from Arctic regions tend to increase with temperature, and therefore the Q_{10} of CH_4 emission is an essential parameter for estimating CH_4 emission and CH_4-climate feedbacks under warming (Chadburn et al., 2020; Ma et al., 2021). Our study reported various temperature sensitivities of projected CH_4 emissions using BBC-CSM2-MR, CESM2, and EC-Earth3. Under SSP1-2.6, projected CH_4 emissions were CESM2 > EC-Earth3 > BBC-CSM2-MR (Figure S2), with temperature sensitivities of EC-Earth3 > CESM2 > BBC-CSM2-MR (Figure 5). Under SSP2-4.5, the emissions were comparable among three climate models (Figure S2), with temperature sensitivities of CESM2 > EC-Earth3 > BBC-CSM2-MR (Figure 5). Furthermore, under SSP5-8.5, CH_4 emissions were EC-Earth3 > CESM2 >

BBC-CSM2-MR at Utqiaġvik sites, whereas were CESM2 > EC-Earth3 > BBC-CSM2-MR at US-Atq and US-Ivo (Figure S2). Temperature sensitivities of CH_4 emissions were lower using BBC-CSM2-MR and higher using CESM2 and EC-Earth3 (Figure 5). Gill et al. (2017) estimated the mean CH_4 flux Q_{10} to be 5.63 (2.92 – 10.52 with a 95% confidence interval) using a linearized Q_{10} function (Humphreys et al., 2005) at the SPRUCE site during the 2015 growing season. Ma et al. (2017) also reported a constrained Q_{10} range of 2.34 – 6.33 with a 95% confidence interval for CH_4 emissions. The Q_{10} for CH_4 production was reported in peatlands, ranging from 1.9 to 3.5 and 2.4 to 5.8 for sedge and Sphagnum mire sites (Lupascu et al., 2012). Here, we quantified a longer-term temperature sensitivity using a linearized Q_{10} function that showed a much stronger response of CH_4 emission to warming. Across the five sites, the ranges of Q_{10} for CH_4 emission were 2.7 – 9.8 based on BBC-CSM2-MR and 7.1 – 17.6 based on CESM2 (Figure 5). This indicated that CH_4 emission increased by 2.7 – 9.8 and 7.1 – 17.6 times in response to a 10-degree increase in temperature. The Q_{10} for CH_4 emission in our study were generally fell in the Q_{10} ranges for emissions but higher than CH_4 production reported in previous studies. Based on EC-Earth3, the Q_{10} of CH_4 emission was 5 – 12.6 under SSP2-4.5 and SSP5-8.5, which were comparable to the ranges from the other two climate models, but it was extremely high under SSP1-2.6 with a range of 18.4 – 60.9. These extreme values could be explained by comparing changes in CH_4 fluxes with air temperature. We found that changes of air temperature were the lowest by 2100 among the three climate models, but changes of CH_4 fluxes were larger than BBC-CSM2-MR. It indicated that even a small temperature change could result in a substantial increase in CH_4 fluxes. In addition to mitigate the uncertainties in CH_4 emissions under SSP scenarios, we should involve multiple climate models for future CH_4 projections.

Implications

This study demonstrated three major implications for CH_4 emission projections of SSP scenarios in Arctic ecosystems. First, the CLM-Microbe model projected Arctic CH_4 emission from 2016 to 2100 at the landscape scale under SSP1-2.6, SSP2-4.5, and SSP5-8.5 with different climate datasets derived from BBC-CSM2-MR, CESM2, and EC-Earth3. CH_4 emissions were projected to have no significant increases by 2100 under SSP1-2.6 and SSP2-4.5, whereas they were estimated to grow by a factor of 5.3 – 7.5 under SSP5-8.5 across the five Arctic sites. Second, this study demonstrated the mechanisms of future CH_4 dynamics with detailed information on CH_4 processes and environmental variables for the five study sites under different SSP scenarios. Our projected CH_4 emissions had a stronger response to rising temperatures than previous studies (Ma et al., 2017; Shindell et al., 2004), primarily due to the precipitation-induced expansion of anaerobic environments facilitating methanogenesis. Ebullition was the main pathway for CH_4 transport across the five sites with climate impacts under SSP scenarios. Third, this study emphasized the importance of including different climate datasets for CH_4 projections, which can help to mitigate the uncertainties of CH_4 flux estimates and budgets. Model simulations had different responses to the multiple climate datasets (BBC-CSM2-MR, CESM2, and EC-Earth3); even a slight difference in temperature or precipitation induced changes in CH_4 processes and their factors, leading to a significant change in CH_4 emission.

Future work

Previous and current studies have validated the CLM-Microbe model in simulating contemporary and future CH_4 emissions at the landscape scale in the Arctic tundra by incorporating different upscaling techniques (Wang et al., 2019, 2022). Here we identify several tasks required to further advance the projection of CH_4 emissions and budgets in the Arctic. First,

vegetation shifts in shrub growth and abundance have been observed and modeled in the Arctic tundra (Cornelissen et al., 2001; Sistla et al 2013; Tape et al., 2006; Tremblay et al., 2012; Wahren et al., 2005; Zhang et al., 2013). This shrub expansion may affect tundra C balances by enhancing ecosystem C uptake and altering ecosystem respiration, and through complex feedback mechanisms that affect snowpack dynamics, permafrost degradation, surface energy balance, and litter inputs (Mekonnen et al., 2021). However, our projection did not involve the effects of shrub expansion, which could underestimate CH_4 emission. Shrub expansion induced a deeper snowpack that may deepen the active layer (Nowinski et al., 2010). It also increased soil wetness and anaerobic condition that enhanced CH_4 production (Blanc-Betes et al., 2016). Hence, the accuracy of CH_4 projections can be improved with consideration of shifts in shrub cover under rapid Arctic warming. Second, permafrost underlies ~25% of the Northern Hemisphere land surface and stores an estimated ~1,700 Pg (1,700 Gt) of C in frozen ground (Lindgren et al., 2018; Olefeldt et al., 2016). Permafrost thaws due to warming-induced expansion creating anoxic conditions that tend to increase CH_4 emissions (Anisimov, 2007; Christensen et al., 2004; Miner et al., 2022). Substantial permafrost degradation was projected under RCP8.5 involving widespread landscape collapse, while thawing was moderated by stabilizing feedbacks under RCP4.5 (Nitzbon et al., 2020). Our projected CH_4 emission could be underestimated without considering permafrost thaw, especially under strong warming scenarios. Thus, adding a module for permafrost thaw and permafrost C-climate feedbacks in the CLM-Microbe model could improve future CH_4 estimation for different SSP scenarios. Third, this study explored future CH_4 dynamics and the influence of various CH_4 processes on emissions that benefited from the CLM-Microbe model, including different microbial functional groups (methanogens vs. methanotrophs). In addition, incorporating various climate models can reduce the uncertainties of future CH_4 emissions. Based on the current

study, integrated modeling efforts provide a reasonable approach to project CH_4 dynamics and budgets for the Arctic and globe for different climate trajectories and further ascertain the mechanisms of future CH_4 emissions.

Conclusions

This study applied the CLM-Microbe model to project future CH_4 emissions across five sites in the Arctic tundra under SSP1-2.6, SSP2-4.5, and SSP5-8.5 scenarios using different climate datasets derived from BBC-CSM2-MR, CESM2, and EC-Earth3 models. Projected CH_4 emissions increased by a factor of 5.3-7.5 under SSP5-8.5 across the five sites, whereas they remained relatively consistent with current emissions under SSP1-2.6 and SSP2-4.5. Our CH_4 projections showed a more robust response to rising temperature, mainly due to a simultaneous increase in precipitation-induced expansion of anoxic conditions favoring methanogenesis. CH_4 production from acetate and $CO_2 + H_2$ was more strongly accelerated under SSP5-8.5 than SSP1-2.6 and SSP2-4.5, generating substantial soil CH_4 concentrations. Ebullition rates increased and were identified as the dominant CH_4 transport pathway under the different SSP scenarios. This study developed the conceptual models for understanding the mechanisms of future CH_4 emissions responding to different SSP scenarios regarding each CH_4 process that can be applied to future CH_4 projections.

Reference

Anisimov, O. A. (2007). Potential feedback of thawing permafrost to the global climate system through methane emission. *Environmental Research Letters*, 2(4), 045016. Doi: 10.1088/1748-9326/2/4/045016

Arndt, K. A., Lipson, D. A., Hashemi, J., Oechel, W. C., and Zona, D. (2020). Snow Melt Stimulates Ecosystem Respiration in Arctic Ecosystems. *Global Change Biology.* 26 (9), 5042–5051. doi:10.1111/gcb.15193

Arndt, K. A., Oechel, W. C., Goodrich, J. P., Bailey, B. A., Kalhori, A., Hashemi, J., et al. (2019). Sensitivity of Methane Emissions to Later Soil Freezing in Arctic Tundra Ecosystems. *Journal of Geophysical Research: Biogeosciences*. 124 (8), 2595–2609. doi:10.1029/2019jg005242

Blanc-Betes, E., Welker, J. M., Sturchio, N. C., Chanton, J. P., & Gonzalez-Meler, M. A. (2016). Winter precipitation and snow accumulation drive the methane sink or source strength of Arctic tussock tundra. *Global Change Biology*, 22(8), 2818-2833. doi.org/10.1111/gcb.13242

Chadburn, S. E., Aalto, T., Aurela, M., Baldocchi, D., Biasi, C., Boike, J., ... & Westermann, S. (2020). Modeled microbial dynamics explain the apparent temperature sensitivity of wetland methane emissions. *Global Biogeochemical Cycles*, 34(11), e2020GB006678. doi: 10.1029/2020GB006678

Chen, Y., Liu, A., Zhang, Z., Hope, C., & Crabbe, M. J. C. (2019). Economic losses of carbon emissions from circum-Arctic permafrost regions under RCP-SSP scenarios. *Science of The Total Environment*, 658, 1064-1068. doi:10.1016/j.scitotenv.2018.12.299

Chen, Y., Liu, A., & Moore, J. C. (2020). Mitigation of Arctic permafrost carbon loss through stratospheric aerosol geoengineering. *Nature Communications*, 11(1), 1-10. doi:10.1016/j.scitotenv.2018.12.299

Christensen, T. R., Johansson, T., Åkerman, H. J., Mastepanov, M., Malmer, N., Friborg, T., ... & Svensson, B. H. (2004). Thawing sub-arctic permafrost: Effects on vegetation and methane emissions. *Geophysical Research Letters*, 31(4). doi:10.1029/ 2003gl018680

Clarke, L. E. (2007). *Scenarios of Greenhouse Gas Emissions and Atmospheric Concentrations. Sub-report 2.1A of Synthesis and Assessment Product 2.1 by the US Climate Change Science Program and the Subcommittee on Global Change Research* (Washington, DC: Department of Energy, Office of Biological & Environmental Research) p154. https://digitalcommons.unl.edu/usdoepub/6

Cornelissen, J. H. C., Callaghan, T. V., Alatalo, J. M., Michelsen, A., Graglia, E., Hartley, A. E., ... & Aerts, R. (2001). Global change and arctic ecosystems: is lichen decline a function of increases in vascular plant biomass? *Journal of Ecology*, 89(6), 984-994. doi: 10.1111/j.1365-2745.2001.00625.x

Davidson, S. J., Sloan, V. L., Phoenix, G. K., Wagner, R., Fisher, J. P., Oechel, W. C., & Zona, D. (2016). Vegetation type dominates the spatial variability in CH_4 emissions across multiple Arctic tundra landscapes. *Ecosystems*, *19*(6), 1116–1132. https://doi.org/10.1007/ s10021-016-9991-0

Döscher, R., Acosta, M., Alessandri, A., Anthoni, P., Arsouze, T., Bergman, T., ... & Zhang, Q. (2022). The EC-Earth3 Earth system model for the Coupled Model Intercomparison Project 6. *Geoscientific Model Development*. doi:10.5194/gmd-15-2973-2022

Frolking, S. (1991). Methane from northern peatlands and climate change. *Carbon Cycling in Boreal Forest and Sub-arctic Ecosystems: Biospheric Responses and Feedbacks to Global Climate Change*. United States Environmental Protection Agency Publication 600R–93/084. Corvallis, OR, 109-124.

Fujino, J., Nair, R., Kainuma, M., Masui, T., & Matsuoka, Y. (2006). Multi-gas mitigation analysis on stabilization scenarios using AIM global model. *The Energy Journal*, (Special Issue# 3). doi: 10.5547/ISSN0195-6574-EJ-VolSI2006-NoSI3-17

Hansen, J., Sato, M., Ruedy, R., Kharecha, P., Lacis, A., Miller, R., ... & Zhang, S. (2007). Dangerous human-made interference with climate: a GISS modelE study. *Atmospheric Chemistry and Physics*, 7(9), 2287-2312. doi: 10.5194/acp-7-2287-2007

IPCC, 2021: Climate Change 2021: The Physical Science Basis. *Contribution of Working Group I to the Sixth Assessment Report of the Intergovernmental Panel on Climate Change* [Masson-Delmotte, V., P. Zhai, A. Pirani, S.L.Connors, C. Péan, S. Berger, N. Caud, Y. Chen, L. Goldfarb, M.I. Gomis, M. Huang, K. Leitzell, E. Lonnoy, J.B.R.Matthews, T.K. Maycock, T. Waterfield, O. Yelekçi, R. Yu, and B. Zhou (eds.)]. Cambridge University Press,Cambridge, United Kingdom and New York, NY, USA, In press, doi:10.1017/9781009157896.

Ganesan, A. L., Schwietzke, S., Poulter, B., Arnold, T., Lan, X., Rigby, M., ... & Manning, M. R. (2019). Advancing scientific understanding of the global methane budget in support of the Paris Agreement. *Global Biogeochemical Cycles*, 33(12), 1475-1512. doi:10.1029/2018GB006065

Goodrich, J. P., Varner, R. K., Frolking, S., Duncan, B. N., & Crill, P. M. (2011). High-frequency measurements of methane ebullition over a growing season at a temperate peatland site. *Geophysical Research Letters*, 38(7). doi: 10.1029/2011GL046915

Granberg, G., Sundh, I., Svensson, B. H., & Nilsson, M. (2001). Effects of temperature, and nitrogen and sulfur deposition, on methane emission from a boreal mire. *Ecology*, 82(7), 1982-1998. doi:10.1890/0012-9658(2001)082[1982:EOTANA]2.0.CO;2

Gill, A. L., Giasson, M. A., Yu, R., & Finzi, A. C. (2017). Deep peat warming increases surface methane and carbon dioxide emissions in a black spruce-dominated ombrotrophic bog. *Global Change Biology*, 23(12), 5398-5411. doi:10.1111/gcb.13806

He, L., Lai, C. T., Mayes, M. A., Murayama, S., & Xu, X. (2021a). Microbial seasonality promotes soil respiratory carbon emission in natural ecosystems: A modeling study. *Global Change Biology*, 27(13), 3035-3051. doi:10.1111/gcb.15627

He, L., Lipson, D. A., Mazza Rodrigues, J. L., Mayes, M., Björk, R. G., Glaser, B., ... & Xu, X. (2021b). Dynamics of fungal and bacterial biomass carbon in natural ecosystems: Site-level applications of the CLM-microbe model. *Journal of Advances in Modeling Earth Systems*, 13(2), e2020MS002283. doi:10.1029/2020MS002283

Humphreys, E. R., Andrew Black, T., Morgenstern, K. A. I., Li, Z., & Nesic, Z. (2005). Net ecosystem production of a Douglas-fir stand for 3 years following clearcut harvesting. *Global Change Biology*, 11(3), 450-464. doi:/10.1111/j.1365-2486.2005.00914.x

Kirschke, S., Bousquet, P., Ciais, P., Saunois, M., Canadell, J. G., Dlugokencky, E. J., ... & Zeng, G. (2013). Three decades of global methane sources and sinks. *Nature Geoscience*, 6(10), 813-823. doi:10.1038/ngeo1955

Koven, C. D., Ringeval, B., Friedlingstein, P., Ciais, P., Cadule, P., Khvorostyanov, D., ... & Tarnocai, C. (2011). Permafrost carbon-climate feedbacks accelerate global warming.

Proceedings of the National Academy of Sciences, 108(36), 14769-14774. doi:10.1073/pnas.110391010

Koven, C. D., Riley, W. J., Subin, Z. M., Tang, J. Y., Torn, M. S., Collins, W. D., ... & Swenson, S. C. (2013). The effect of vertically resolved soil biogeochemistry and alternate soil C and N models on C dynamics of CLM4. *Biogeosciences*, 10(11), 7109-7131. doi:10.5194/bg-10-7109-2013

Langeveld, J., Bouwman, A. F., van Hoek, W. J., Vilmin, L., Beusen, A. H., Mogollón, J. M., & Middelburg, J. J. (2019). Global database and model on dissolved carbon in soil solution. *Biogeosciences Discussions*, 1-35. doi: 10.5194/bg-2019-238

Langford, Z. L., Kumar, J., Hoffman, F. M., Breen, A. L., & Iversen, C. M. (2019). Arctic vegetation mapping using unsupervised training datasets and convolutional neural networks. *Remote Sensing*, 11(1), 69. doi: 10.3390/rs11010069

Lawrence, D. M., Koven, C. D., Swenson, S. C., Riley, W. J., & Slater, A. G. (2015). Permafrost thaw and resulting soil moisture changes regulate projected high-latitude CO_2 and CH_4 emissions. *Environmental Research Letters*, 10(9), 094011. doi:10.1088/1748-9326/10/9/094011

Lindgren, A., Hugelius, G., & Kuhry, P. (2018). Extensive loss of past permafrost carbon but a net accumulation into present-day soils. *Nature*, 560(7717), 219-222. doi:10.1038/s41586-018-0371-0

Livingston, G. P., & Morrissey, L. A. (1992). Methane emissions from Alaska arctic tundra in response to climatic change (No. AD-P-007311/4/XAB). National Aeronautics and Space Administration, Moffett Field, CA (United States). Ames Research Center.

Lupascu, M., Wadham, J. L., Hornibrook, E. R., & Pancost, R. D. (2012). Temperature sensitivity of methane production in the permafrost active layer at Stordalen, Sweden: A comparison with non-permafrost northern wetlands. *Arctic, Antarctic, and Alpine Research*, 44(4), 469-482. doi:10.1657/1938-4246-44.4.469

Ma, S., Jiang, J., Huang, Y., Shi, Z., Wilson, R. M., Ricciuto, D., ... & Luo, Y. (2017). Data-constrained projections of methane fluxes in a northern Minnesota peatland in response to elevated CO_2 and warming. *Journal of Geophysical Research: Biogeosciences*, 122(11), 2841-2861. doi:10.1002/2017JG003932

Ma, S., Worden, J. R., Bloom, A. A., Zhang, Y., Poulter, B., Cusworth, D. H., ... & Jacob, D. J. (2021). Satellite constraints on the latitudinal distribution and temperature sensitivity of wetland methane emissions. *AGU Advances*, 2(3), e2021AV000408. doi:10.1029/2021AV000408

Meinshausen, M., Nicholls, Z. R., Lewis, J., Gidden, M. J., Vogel, E., Freund, M., ... & Wang, R. H. (2020). The shared socio-economic pathway (SSP) greenhouse gas concentrations and their extensions to 2500. *Geoscientific Model Development*, 13(8), 3571-3605. doi:10.5194/gmd-13-3571-2020

Mekonnen, Z. A., Riley, W. J., Berner, L. T., Bouskill, N. J., Torn, M. S., Iwahana, G., ... & Grant, R. F. (2021). Arctic tundra shrubification: a review of mechanisms and impacts on ecosystem carbon balance. *Environmental Research Letters*, 16(5), 053001. doi:10.1088/1748-9326/abf28b

Mekonnen, Z. A., Riley, W. J., & Grant, R. F. (2018). 21st century tundra shrubification could enhance net carbon uptake of North America Arctic tundra under an RCP8. 5 climate trajectory. *Environmental Research Letters*, 13(5), 054029. doi:10.1088/1748-9326/aabf28

Miner, K. R., Turetsky, M. R., Malina, E., Bartsch, A., Tamminen, J., McGuire, A. D., ... & Miller, C. E. (2022). Permafrost carbon emissions in a changing Arctic. *Nature Reviews Earth & Environment*, 3(1), 55-67. doi:10.1038/s43017-021-00230-3

Nazarenko, L., Schmidt, G. A., Miller, R. L., Tausnev, N., Kelley, M., Ruedy, R., ... & Zhang, J. (2015). Future climate change under RCP emission scenarios with GISS ModelE2. *Journal of Advances in Modeling Earth Systems*, 7(1), 244-267. doi:10.1002/2014MS000403

Nisbet, E. G., Manning, M. R., Dlugokencky, E. J., Fisher, R. E., Lowry, D., Michel, S. E., et al. (2019). Very strong atmospheric methane growth in the 4 years 2014–2017: Implications for the Paris Agreement. *Global Biogeochemical Cycles*, 33, 318–342. doi:10.1029/2018GB006009

Nitzbon, J., Westermann, S., Langer, M., Martin, L. C., Strauss, J., Laboor, S., & Boike, J. (2020). Fast response of cold ice-rich permafrost in northeast Siberia to a warming climate. *Nature Communications*, 11(1), 1-11. doi:10.1038/s41467-020-15725-8

Nowinski, N. S., Taneva, L., Trumbore, S. E., & Welker, J. M. (2010). Decomposition of old organic matter as a result of deeper active layers in a snow depth manipulation experiment. *Oecologia*, 163(3), 785-792. doi:10.1007/s00442-009-1556-x

Oh, Y., Zhuang, Q., Liu, L., Welp, L. R., Lau, M. C., Onstott, T. C., ... & Elberling, B. (2020). Reduced net methane emissions due to microbial methane oxidation in a warmer Arctic. *Nature Climate Change*, 10(4), 317-321. doi:10.1038/s41558-020-0734-z

Olefeldt, D., Goswami, S., Grosse, G., Hayes, D., Hugelius, G., Kuhry, P., ... & Turetsky, M. R. (2016). Circumpolar distribution and carbon storage of thermokarst landscapes. *Nature Communications*, 7(1), 1-11. doi:10.1038/ncomms13043

Oleson, K., Lawrence, D., Bonan, G. B., Drewniak, B. A., Huang, M., Koven, C. D., et al. (2013). *Technical Description of Version 4.5 of the Community Land Model (CLM)*. Bounder, Colorado: National Center for Atmospheric Research.

Riahi, K., Grübler, A., & Nakicenovic, N. (2007). Scenarios of long-term socio-economic and environmental development under climate stabilization. *Technological Forecasting and Social Change,* 74(7), 887-935. doi:10.1016/j.techfore.2006.05.026

Rubino, M., Etheridge, D. M., Thornton, D. P., Howden, R., Allison, C. E., Francey, R. J., et al. (2019). Revised records of atmospheric trace gases CO_2, CH_4, N_2O, and $\delta 13C$-CO_2 over the last 2000 years from Law Dome, *Antarctica. Earth System Science Data*, 11(2), 473–492. doi:10.5194/essd-11-473-2019

Saunois, M., Bousquet, P., Poulter, B., Peregon, A., Ciais, P., Canadell, J. G., ... & Zhu, Q. (2016a). The global methane budget 2000–2012. *Earth System Science Data*, 8(2), 697-751. doi:10.5194/essd-8-697-2016

Saunois, M., Jackson, R. B., Bousquet, P., Poulter, B., & Canadell, J. G. (2016b). The growing role of methane in anthropogenic climate change. *Environmental Research Letters*, 11(12), 120207. doi:10.1088/1748-9326/11/12/120207

Schuur, E. A., Abbott, B. W., Bowden, W. B., Brovkin, V., Camill, P., Canadell, J. G., ... & Zimov, S. A. (2013). Expert assessment of vulnerability of permafrost carbon to climate change. *Climatic Change*, 119(2), 359-374. doi:10.1007/s10584-013-0730-7

Segers, R. (1998). Methane production and methane consumption: a review of processes underlying wetland methane fluxes. *Biogeochemistry*, 41(1), 23-51. doi:10.1023/A:1005929032764

Shindell, D. T., Walter, B. P., & Faluvegi, G. (2004). Impacts of climate change on methane emissions from wetlands. *Geophysical Research Letters*, 31(21). doi:10.1029/2004GL021009

Sierra, C. A., Trumbore, S. E., Davidson, E. A., Vicca, S., & Janssens, I. (2015). Sensitivity of decomposition rates of soil organic matter with respect to simultaneous changes in temperature and moisture. *Journal of Advances in Modeling Earth Systems*, 7(1), 335-356. doi:10.1002/2014MS000358

Sistla, S. A., Moore, J. C., Simpson, R. T., Gough, L., Shaver, G. R., & Schimel, J. P. (2013). Long-term warming restructures Arctic tundra without changing net soil carbon storage. *Nature*, 497(7451), 615-618. doi:10.1038/nature12129

Tan, Z., & Zhuang, Q. (2015a). Arctic lakes are continuous methane sources to the atmosphere under warming conditions. *Environmental Research Letters*, 10(5), 054016. doi:10.1088/1748-9326/10/5/054016

Tan, Z., & Zhuang, Q. (2015b). Methane emissions from Pan-Arctic lakes during the 21st century: An analysis with process-based models of lake evolution and biogeochemistry. *Journal of Geophysical Research: Biogeosciences*, 120(12), 2641-2653. doi:10.1002/2015JG003184

Tape, K. E. N., Sturm, M., & Racine, C. (2006). The evidence for shrub expansion in Northern Alaska and the Pan-Arctic. *Global Change Biology*, 12(4), 686-702. doi:10.1111/j.1365-2486.2006.01128.x

Thornton, P. E., Lamarque, J. F., Rosenbloom, N. A., & Mahowald, N. M. (2007). Influence of carbon-nitrogen cycle coupling on land model response to CO_2 fertilization and climate variability. *Global Biogeochemical Cycles*, 21(4). doi:10.1029/2006GB002868

Thornton, P. E., & Rosenbloom, N. A. (2005). Ecosystem model spin-up: Estimating steady state conditions in a coupled terrestrial carbon and nitrogen cycle model. *Ecological Modelling*, 189(1-2), 25-48. doi:10.1016/j.ecolmodel.2005.04.008

Thornton, P.E. and Zimmermann, N.E., 2007. An improved canopy integration scheme for a land surface model with prognostic canopy structure. *Journal of Climate*, 20: 3902-3923. doi:10.1175/jcli4222.1

Tremblay, B., Lévesque, E., & Boudreau, S. (2012). Recent expansion of erect shrubs in the Low Arctic: evidence from Eastern Nunavik. *Environmental Research Letters*, 7(3), 035501. doi:10.1088/1748-9326/7/3/035501

Turetsky, M. R., Treat, C. C., Waldrop, M. P., Waddington, J. M., Harden, J. W., & McGuire, A. D. (2008). Short-term response of methane fluxes and methanogen activity to water table and soil warming manipulations in an Alaskan peatland. *Journal of Geophysical Research: Biogeosciences*, 113(G3). doi:10.1029/2007JG000496

Updegraff, K., Bridgham, S. D., Pastor, J., Weishampel, P., & Harth, C. (2001). Response of CO_2 and CH_4 emissions from peatlands to warming and water table manipulation. *Ecological Applications*, 11(2), 311-326. doi:10.1890/1051-0761(2001)011[0311:ROCACE]2.0.CO;2

Van Vuuren, D. P., Den Elzen, M. G., Lucas, P. L., Eickhout, B., Strengers, B. J., Van Ruijven, B., ... & Van Houdt, R. (2007). Stabilizing greenhouse gas concentrations at low levels: an assessment of reduction strategies and costs. *Climatic Change*, 81(2), 119-159. doi:10.1007/s10584-006-9172-9

Verville, J. H., Hobbie, S. E., Chapin, F. S., & Hooper, D. U. (1998). Response of tundra CH_4 and CO_2 flux to manipulation of temperature and vegetation. *Biogeochemistry*, 41(3), 215-235. doi:10.1023/A:1005984701775

Wahren, C. H., Walker, M. D., & Bret-Harte, M. S. (2005). Vegetation responses in Alaskan arctic tundra after 8 years of a summer warming and winter snow manipulation experiment. *Global Change Biology*, 11(4), 537-552. doi:10.1111/j.1365-2486.2005.00927.x

Wang, Y., Yuan, F., Arndt, K. A., Liu, J., He, L., Zuo, Y., ... & Xu, X. (2022). Upscaling Methane Flux From Plot Level to Eddy Covariance Tower Domains in Five Alaskan Tundra Ecosystems. *Frontiers in Environmental Science*, 822. doi:10.3389/fenvs.2022.939238

Wang, Y., Yuan, F., Yuan, F., Gu, B., Hahn, M. S., Torn, M. S., ... & Xu, X. (2019). Mechanistic modeling of microtopographic impacts on CO_2 and CH_4 fluxes in an Alaskan tundra ecosystem using the CLM-microbe model. *Journal of Advances in Modeling Earth Systems*, 11(12), 4288-4304. doi:10.1029/2019MS001771

Walker, D. A., Binnian, E., Evans, B. M., Lederer, N. D., Nordstrand, E., & Webber, P. J. (1989). Terrain, vegetation and landscape evolution of the R4D research site, Brooks Range Foothills, Alaska. *Ecography*, 12(3), 238-261. doi:10.1111/j.1600-0587.1989.tb00844.x

Xu, X., F. Yuan, P. J. Hanson, S. D. Wullschleger, P. E. Thornton, W. J. Riley, X. Song, D. E. Graham, C. Song and H. Tian (2016). Review and Synthesis: Four decades of modeling methane cycling within terrestrial ecosystems. *Biogeosciences* 13: 3735-3755. doi:10.5194/bg-13-3735-2016

Xu, X., Elias, D. A., Graham, D. E., Phelps, T. J., Carroll, S. L., Wullschleger, S. D., & Thornton, P. E. (2015). A microbial functional group-based module for simulating methane production and consumption: Application to an incubated permafrost soil. *Journal of Geophysical Research: Biogeosciences*, 120(7), 1315-1333. doi:10.1002/2015JG002935

Xu, X., Schimel, J. P., Thornton, P. E., Song, X., Yuan, F., & Goswami, S. (2014). Substrate and environmental controls on microbial assimilation of soil organic carbon: a framework for Earth system models. *Ecology letters*, 17(5), 547-555. doi:10.1111/ele.12254

Yuan, F., Wang, Y., Ricciuto, D. M., Shi, X., Yuan, F., Brehme, T., ... & Xu, X. (2021). Hydrological feedbacks on peatland CH_4 emission under warming and elevated CO_2: A modeling study. *Journal of Hydrology*, 603, 127137. doi:10.1016/j.jhydrol.2021.127137

Yvon-Durocher, G., Allen, A. P., Bastviken, D., Conrad, R., Gudasz, C., St-Pierre, A., ... & Del Giorgio, P. A. (2014). Methane fluxes show consistent temperature dependence across microbial to ecosystem scales. *Nature*, 507(7493), 488-491. doi:10.1038/nature13164

Zhang, W., Miller, P. A., Smith, B., Wania, R., Koenigk, T., & Döscher, R. (2013). Tundra shrubification and tree-line advance amplify arctic climate warming: results from an individual-based dynamic vegetation model. *Environmental Research Letters*, 8(3), 034023. doi:10.1088/1748-9326/8/3/034023

Zona, D., Gioli, B., Commane, R., Lindaas, J., Wofsy, S. C., Miller, C. E., ... & Oechel, W. C. (2016). Cold season emissions dominate the Arctic tundra methane budget. *Proceedings of the National Academy of Sciences*, 113(1), 40-45. doi:10.1073/pnas.1516017113

Zona, D., Oechel, W. C., Kochendorfer, J. U. K. T. P., Paw U, K. T., Salyuk, A. N., Olivas, P. C., ... & Lipson, D. A. (2009). Methane fluxes during the initiation of a large-scale water

table manipulation experiment in the Alaskan Arctic tundra. *Global Biogeochemical Cycles*, 23(2). doi:10.1029/2009GB003487

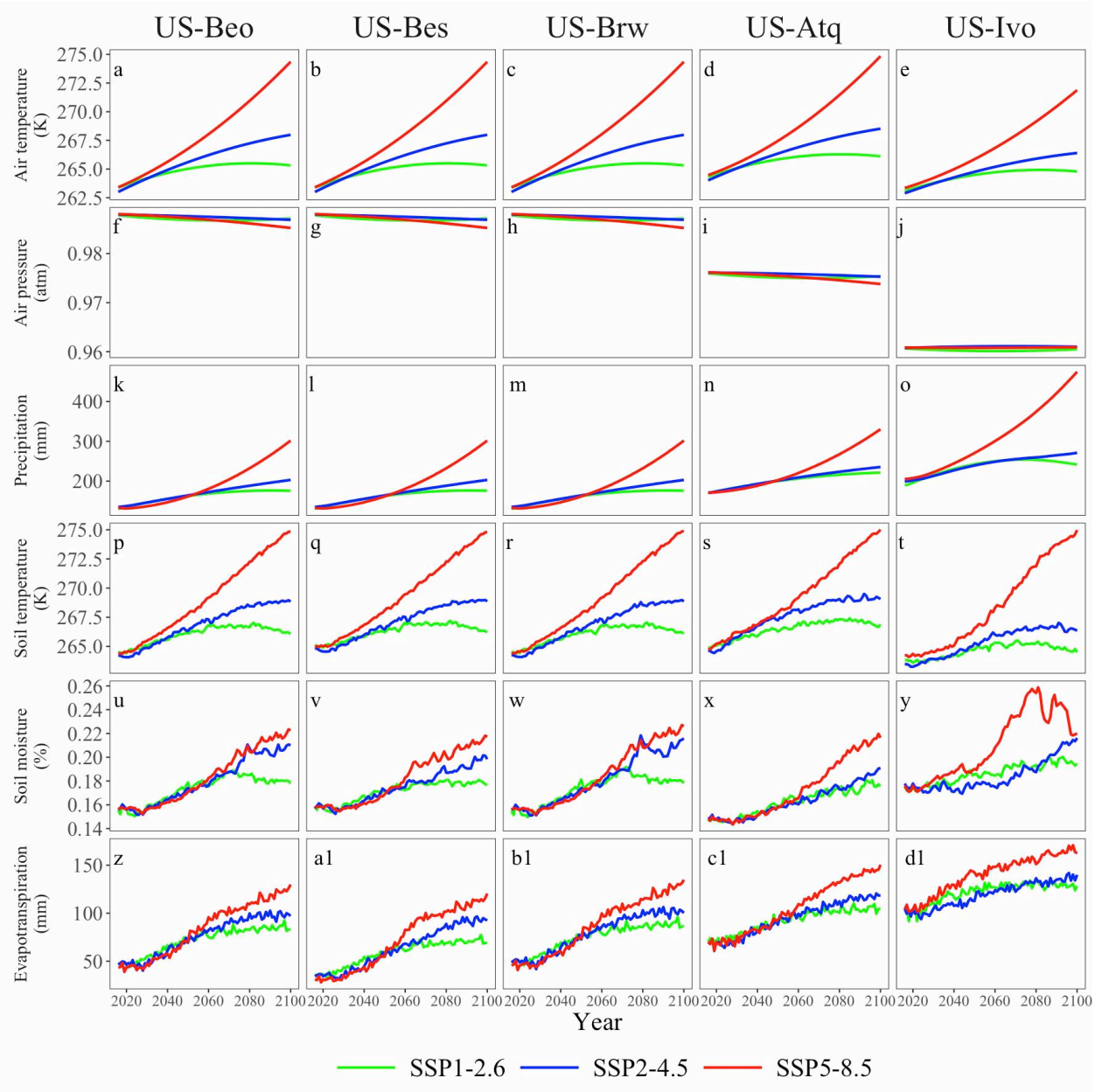

Figure S1. Projected dynamics of air temperature (K), air pressure (atm), precipitation (mm), soil temperature (K), soil moisture (%), and evapotranspiration (mm) during 2016-2100 at a, f, k, p, u, z) US-Beo, b, g, l, q, v, a1) US-Bes, c, h, m, r, w, b1) US-Brw, d, I, n, s, x, c1) US-Atq and e, j, o, t, y, d1) US-Ivo under SSP1-2.6, SSP2-4.5 and SSP5-8.5 scenarios

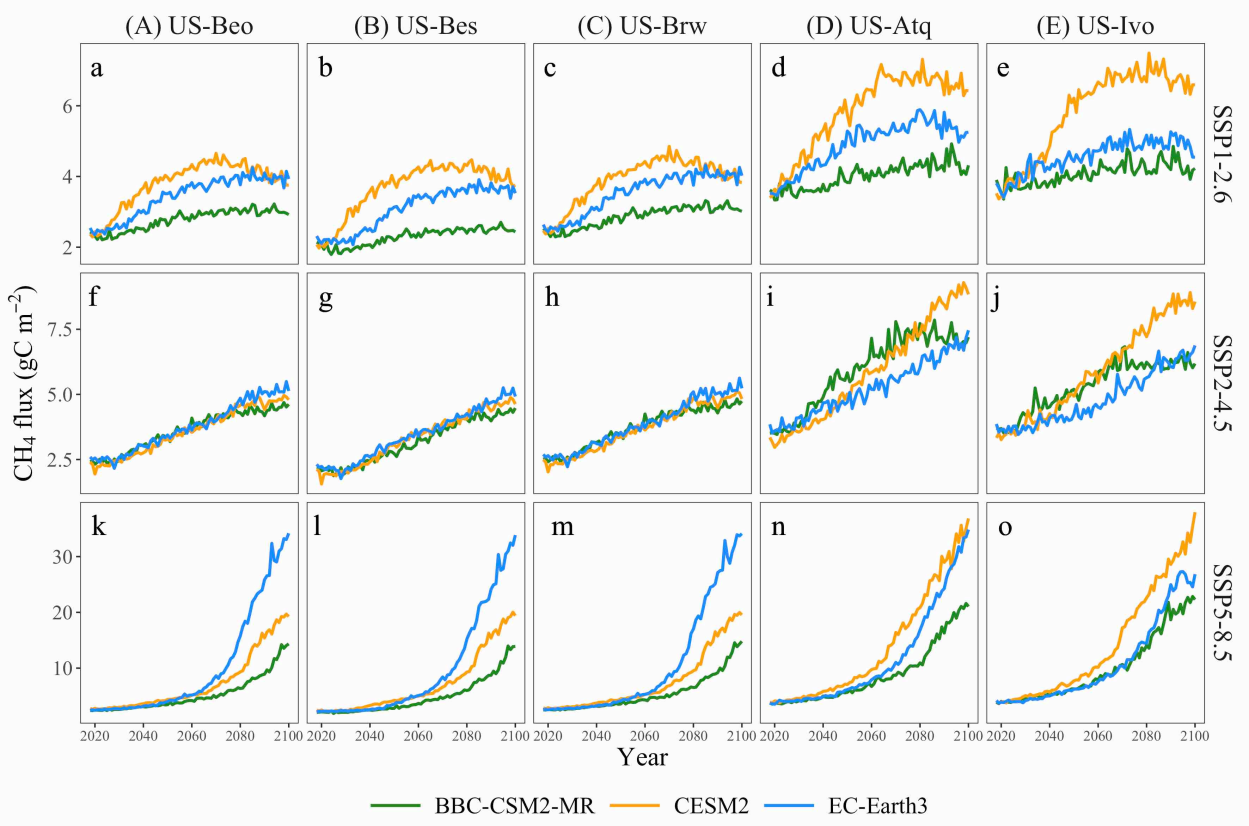

Figure S2. Projected dynamics of CH_4 fluxes ($gC \cdot m^{-2}$) during 2016-2100 at a, f, k) US-Beo, b, g, l) US-Bes, c, h, m) US-Brw, d, I, n) US-Atq and e, j, o) US-Ivo under SSP1-2.6, SSP2-4.5 and SSP5-8.5 scenarios using climate data from BBC-CSM2-MR, CESM2 and EC-Earth3 models in CMIP6

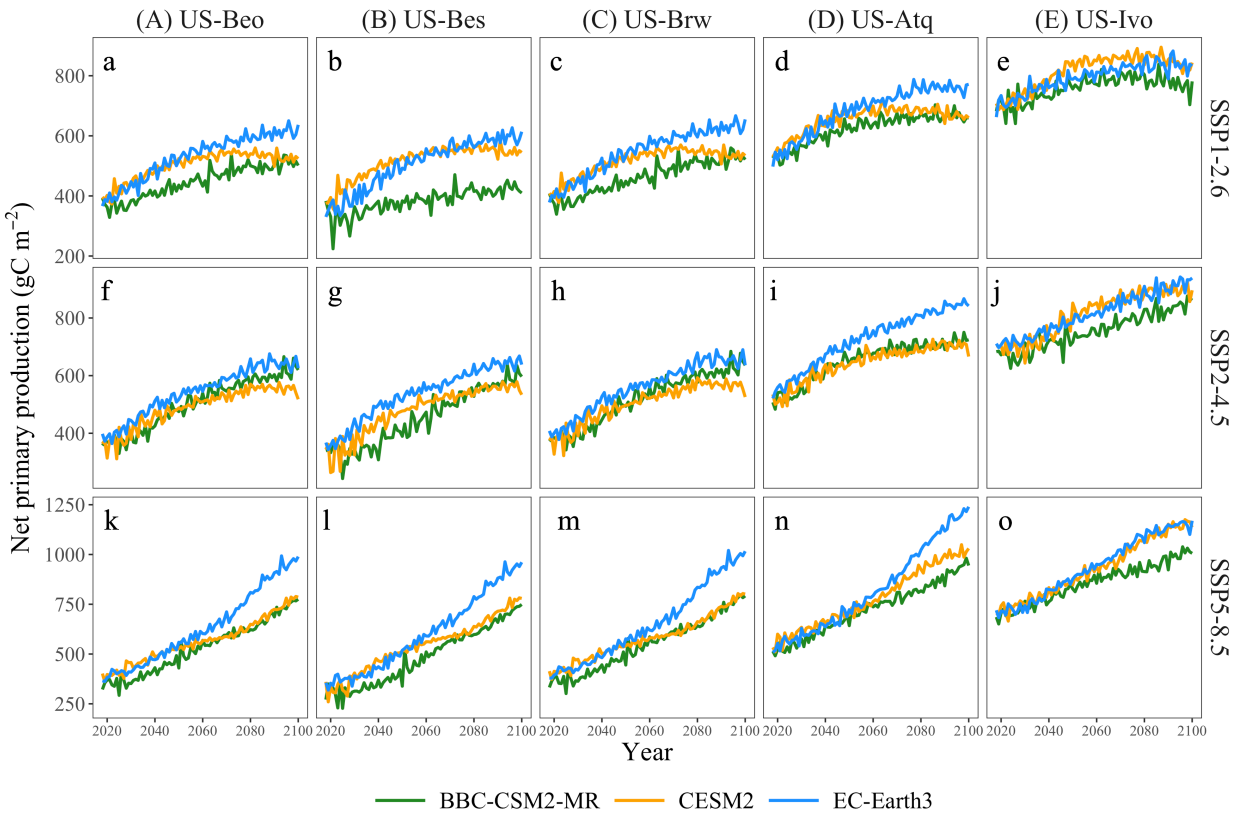

Figure S3. Projected dynamics of net primary production (NPP) ($gC \cdot m^{-2}$) during 2016-2100 at a, f, k) US-Beo, b, g, l) US-Bes, c, h, m) US-Brw, d, I, n) US-Atq and e, j, o) US-Ivo under SSP1-2.6, SSP2-4.5 and SSP5-8.5 scenarios using climate data from BBC-CSM2-MR, CESM2 and EC-Earth3 models in CMIP6

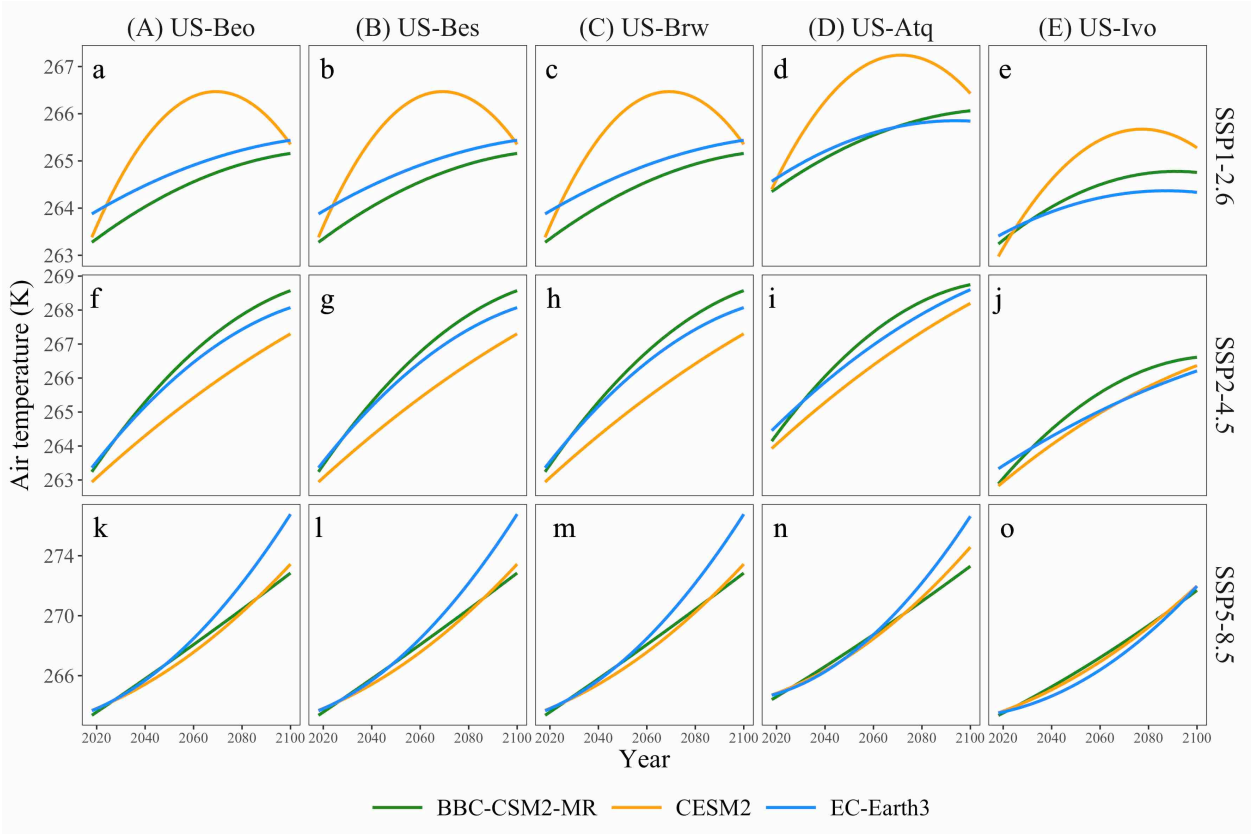

Figure S4. Projected dynamics of air temperature (K) during 2016-2100 at a, f, k) US-Beo, b, g, l) US-Bes, c, h, m) US-Brw, d, I, n) US-Atq and e, j, o) US-Ivo under SSP1-2.6, SSP2-4.5 and SSP5-8.5 scenarios using climate data from BBC-CSM2-MR, CESM2 and EC-Earth3 models in CMIP6

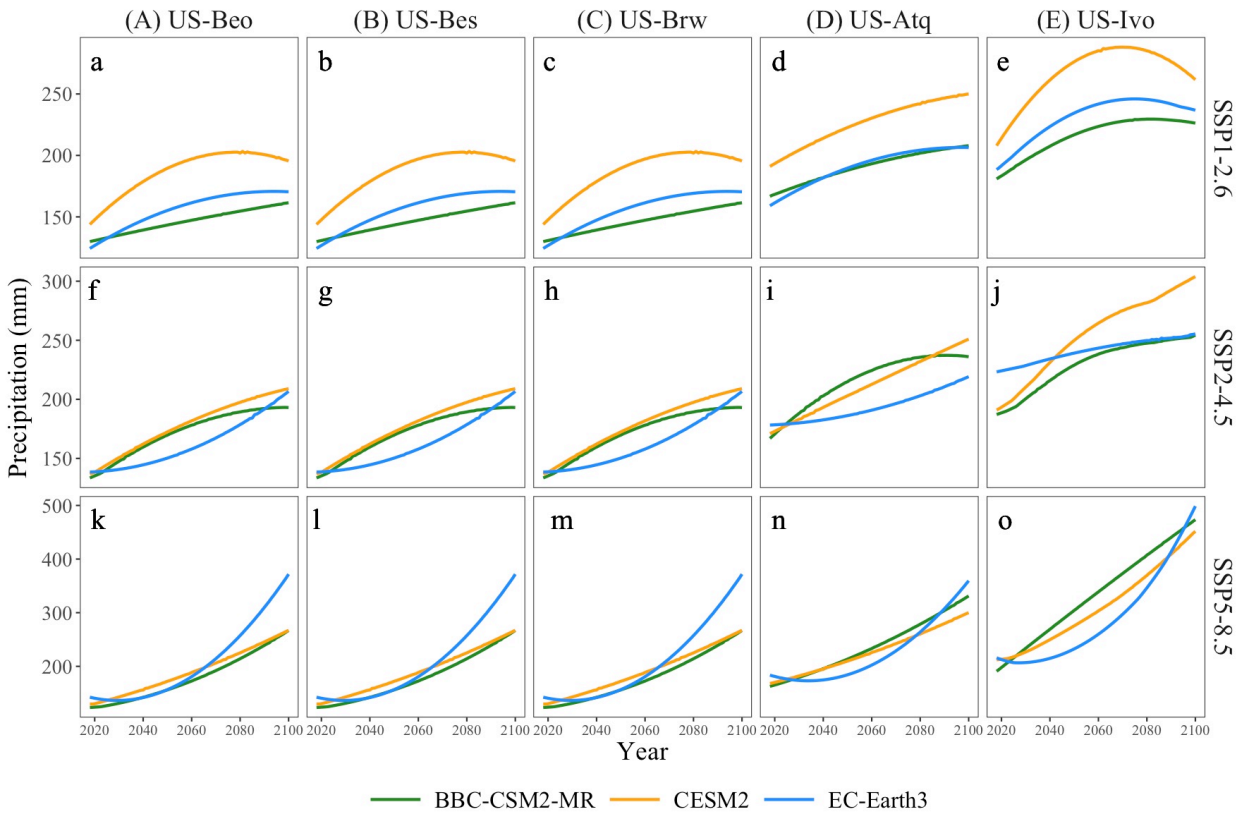

Figure S5. Projected dynamics of precipitation (mm) during 2016-2100 at a, f, k) US-Beo, b, g, l) US-Bes, c, h, m) US-Brw, d, I, n) US-Atq and e, j, o) US-Ivo under SSP1-2.6, SSP2-4.5 and SSP5-8.5 scenarios using climate data from BBC-CSM2-MR, CESM2 and EC-Earth3 models in CMIP6

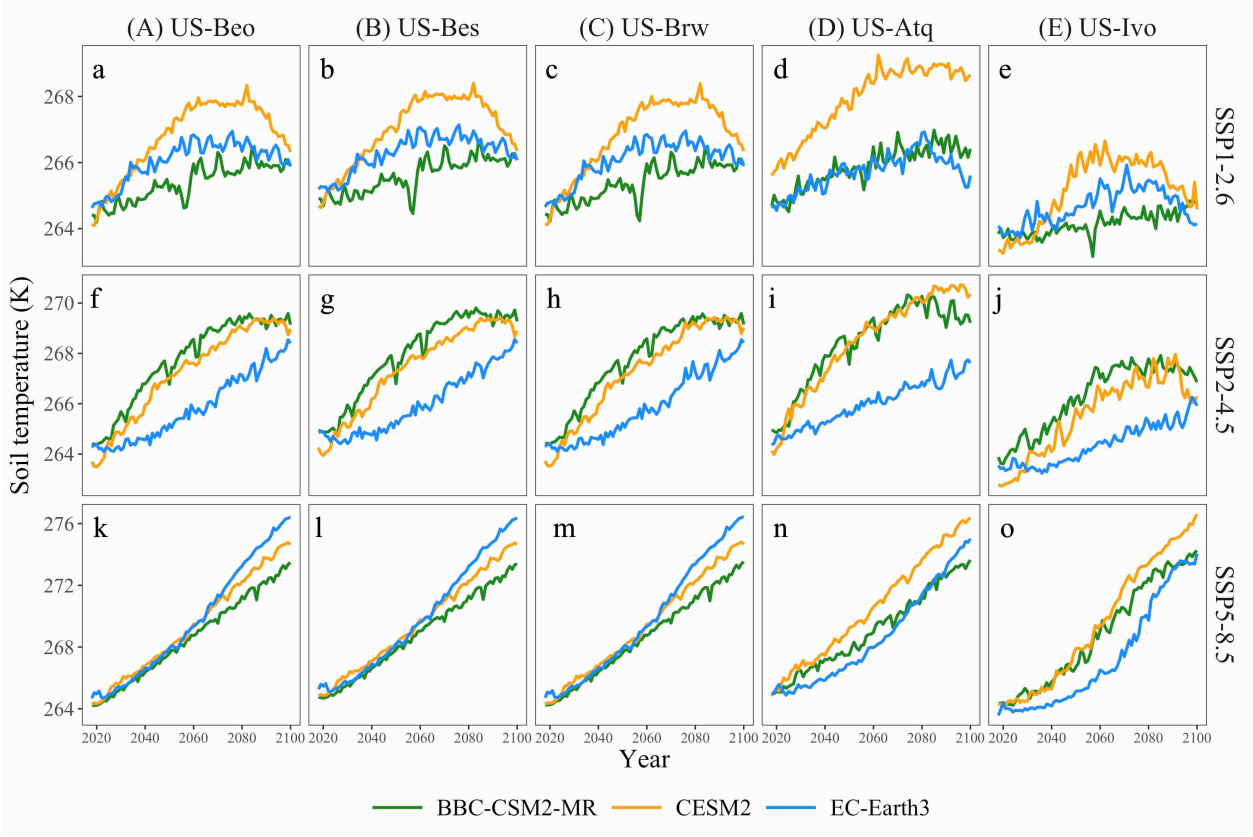

Figure S6. Projected dynamics of soil temperature (K) during 2016-2100 at a, f, k) US-Beo, b, g, l) US-Bes, c, h, m) US-Brw, d, I, n) US-Atq and e, j, o) US-Ivo under SSP1-2.6, SSP2-4.5 and SSP5-8.5 scenarios using climate data from BBC-CSM2-MR, CESM2 and EC-Earth3 models in CMIP6

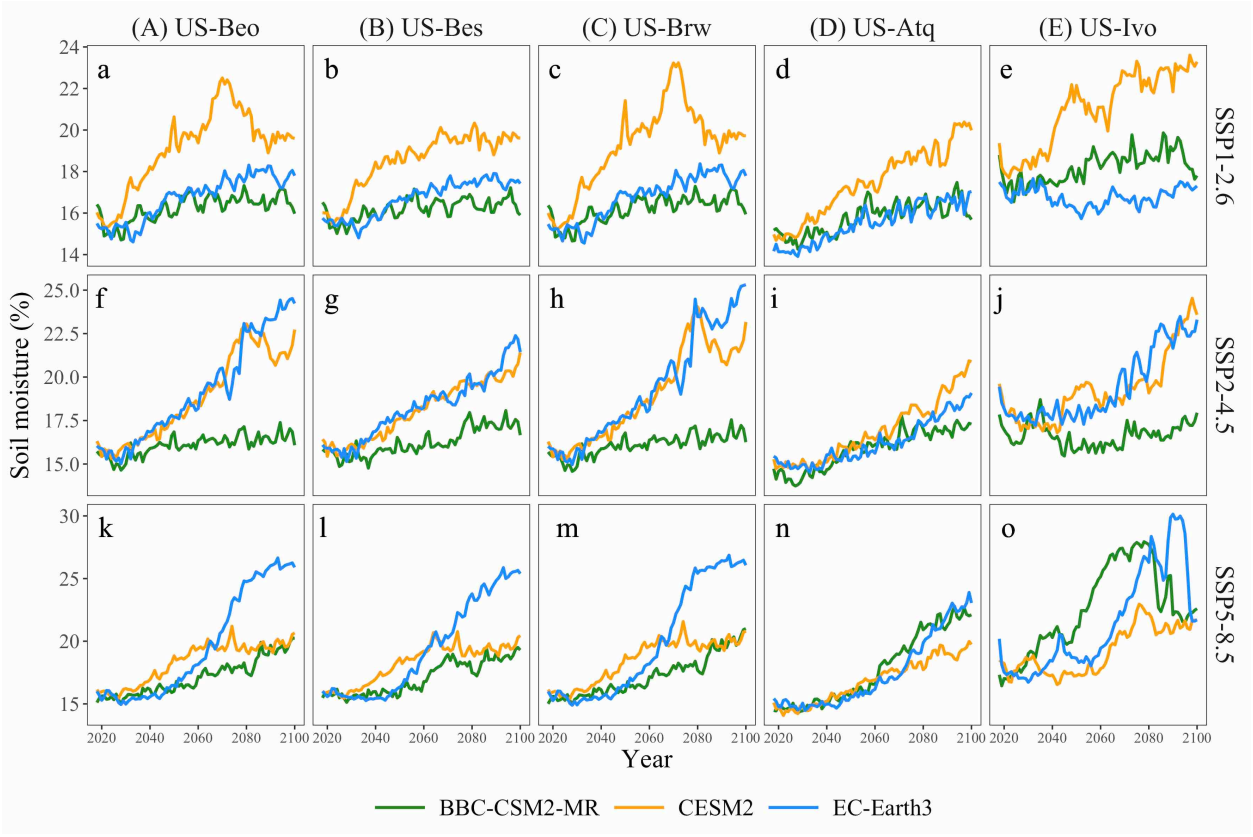

Figure S7. Projected dynamics of soil moisture (%) during 2016-2100 at a, f, k) US-Beo, b, g, l) US-Bes, c, h, m) US-Brw, d, I, n) US-Atq and e, j, o) US-Ivo under SSP1-2.6, SSP2-4.5 and SSP5-8.5 scenarios using climate data from BBC-CSM2-MR, CESM2 and EC-Earth3 models in CMIP6

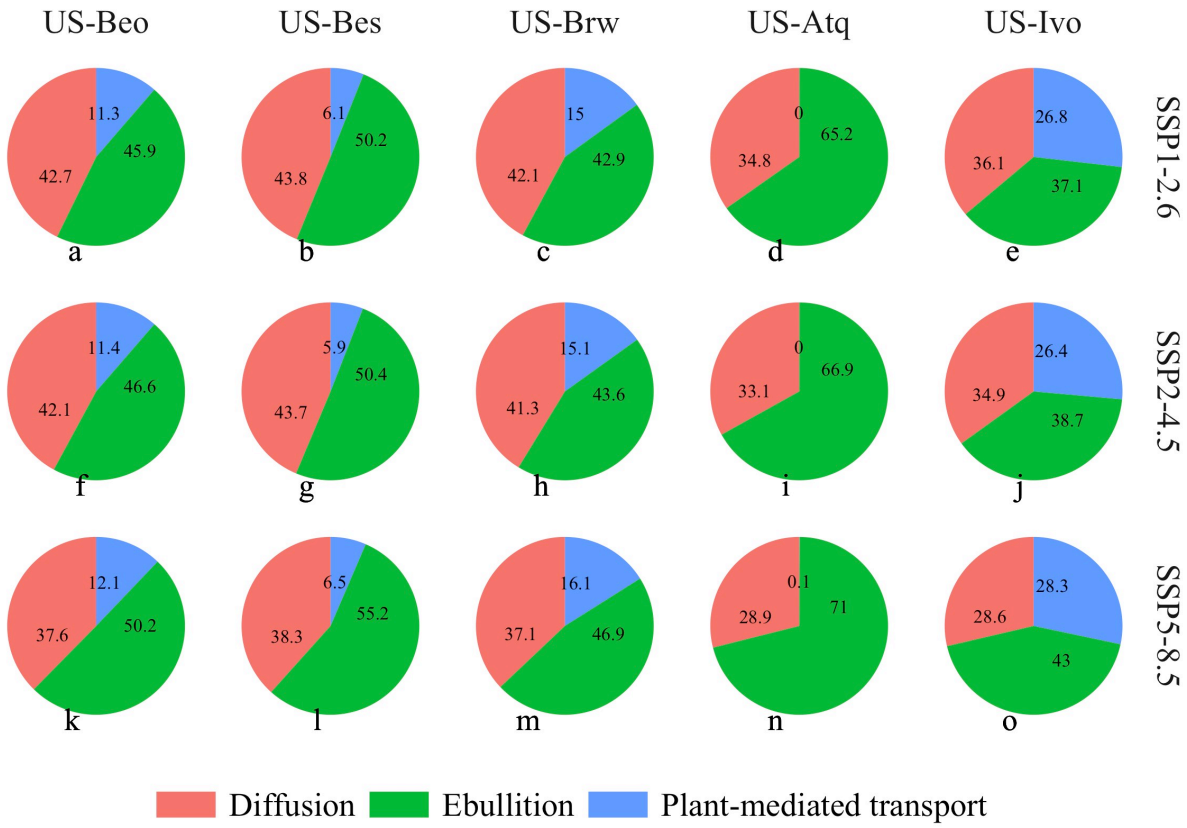

Figure S8. The pie charts represent the contributions of three transport pathways to total CH_4 fluxes in the 2050s at a, f, k) US-Beo, b, g, l) US-Bes, c, h, m) US-Brw, d, I, n) US-Atq and e, j, o) US-Ivo under a-e) SSP1-2.6, f-j) SSP2-4.5 and k-o) SSP5-8.5 scenarios. Red indicates diffusion, green indicates ebullition, and blue indicates plant-mediated transport

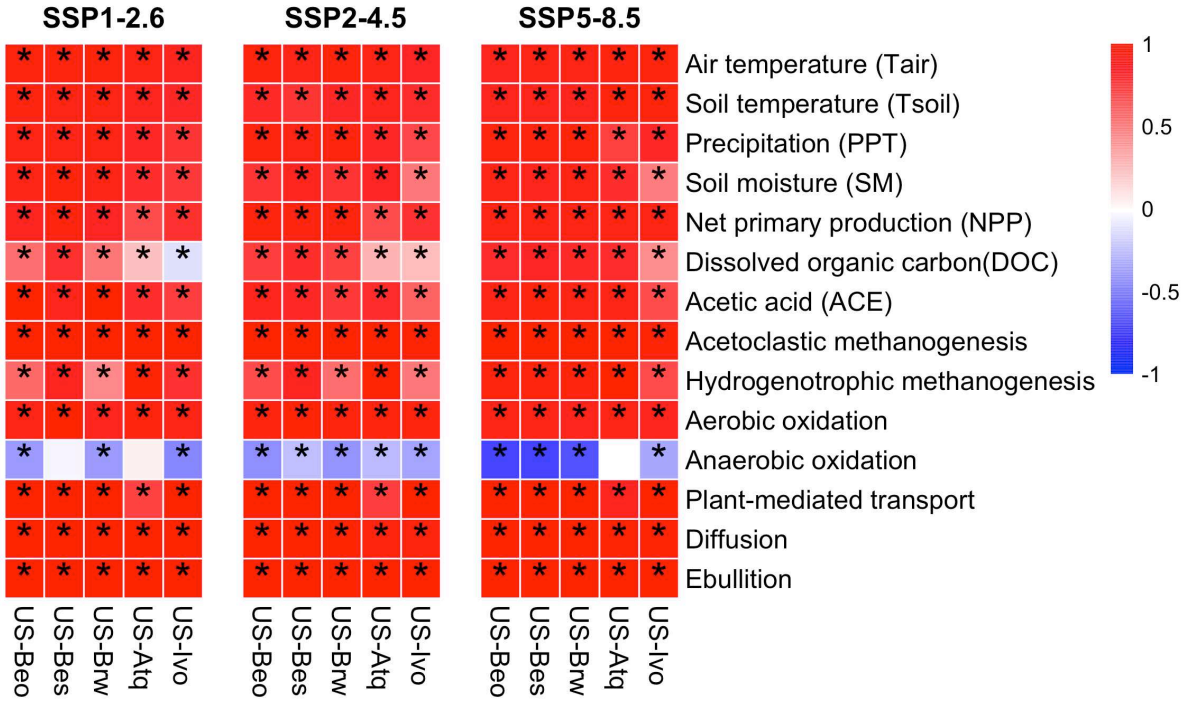

Figure S9. Correlation analysis for projected CH4 fluxes with 14 factors or processes: air temperature (Tair), soil temperature (Tsoil), precipitation (PPT), soil moisture (SM), net primary production (NPP), dissolved organic carbon (DOC) concentration, acetate (ACE) concentration, rates of acetoclastic methanogenesis, rates of hydrogenotrophic methanogenesis, rates of aerobic oxidation, rates of anaerobic oxidation, rates of plant-mediated transport, rates of diffusion, and rates of ebullition, at US-Beo, US-Bes, US-Brw, US-Atq and US-Ivo for three Representative Concentration Pathway (SSP) scenarios. The symbol "*" indicates the significance level at of $\alpha = 0.05$. Darker red and darker blue indicate a stronger positive or negative correlation with CH_4 fluxes.

Table S1. Climate variables of BCC-CSM2-MR in CMIP6 corresponding to required variables of CRUNCEP for CH_4 projections

CRUNCEP		BCC-CSM2-MR in CMIP6		Units
Variable	Description	Variable	Description	
FSDS	Total incident solar radiation	rsds	Surface downwelling shortwave Radiation	$W \cdot m^{-2}$
PRECTmms	Total precipitation	pr	Precipitation	$kg \cdot m^{-2} \cdot s^{-1}$
FLDS	Incident longwave radiation	rlds	Surface downwelling longwave Radiation	$W \cdot m^{-2}$
PSRF	Surface pressure at the lowest atmospheric level	ps	Surface ir pressure	Pa
QBOT	Specific humidity at the lowest atmospheric level	huss	Near-surface specific humidity	$kg \cdot kg^{-1}$
TBOT	Temperature at the lowest atmospheric level	tas	Near-surface air temperature	K
WIND	Wind at the lowest atmospheric level	uas	Eastward near-surface wind speed	$m \cdot s^{-1}$
		vas	Northward near-surface wind speed	$m \cdot s^{-1}$

Table S2. Climate variables of CESM2 in CMIP6 corresponding to required variables of CRUNCEP for CH_4 projections

CRUNCEP		CESM2 in CMIP6		
Variable	Description	Variable	Description	Units
WIND	Wind at the lowest atmospheric level	a2x3h_Sa_u	Zonal wind at the lowest model	$m \cdot s^{-1}$
		a2x3h_Sa_v	Meridional wind at the lowest model level	$m \cdot s^{-1}$
TBOT	Temperature at the lowest atmospheric level	a2x3h_Sa_tbot	Temperature at the lowest model level	K
		a2x3h_Sa_ptem	Potential temperature at the lowest model level	K
QBOT	Specific humidity at the lowest atmospheric level	a2x3h_Sa_shum	Specific humidity at the lowest model level	$kg \cdot kg^{-1}$
		a2x3h_Sa_dens	Density at the lowest model level	$kg \cdot m^{-3}$
PSRF	Surface pressure at the lowest atmospheric level	a2x3h_Sa_pbot	Pressure at the lowest model level	Pa
		a2x3h_Sa_pslv	Sea level pressure	Pa
FLDS	Incident longwave radiation	a2x3h_Faxa_lwdn	Downward longwave heat flux	$W \cdot m^{-2}$
PRECTmms	Total precipitation	a2x3h_Faxa_rainc	Convective precipitation rate	$kg \cdot m^{-2} \cdot s^{-1}$
		a2x3h_Faxa_rainl	Large-scale (stable) precipitation rate	$kg \cdot m^{-2} \cdot s^{-1}$
		a2x3h_Faxa_snowc	Convective snow rate (water equivalent)	$kg \cdot m^{-2} \cdot s^{-1}$
		a2x3h_Faxa_snowl	Large-scale (stable) snow rate (water equivalent)	$kg \cdot m^{-2} \cdot s^{-1}$
FSDS	Total incident solar radiation	a2x3h_Faxa_swndr	Direct near-infrared incident solar radiation	$W \cdot m^{-2}$
		a2x3h_Faxa_swvdr	Direct visible incident solar radiation	$W \cdot m^{-2}$
		a2x3h_Faxa_swndf	Diffuse near-infrared incident solar radiation	$W \cdot m^{-2}$
		a2x3h_Faxa_swvdf	Diffuse visible incident solar radiation	$W \cdot m^{-2}$

Table S3. Climate variables of EC-Earth3 in CMIP6 corresponding to required variables of CRUNCEP for CH_4 projections

CRUNCEP		EC-Earth3 in CMIP6		Units
Variable	Description	Variable	Description	
FSDS	Total incident solar radiation	rsds	Surface Downwelling Shortwave Radiation	$W \cdot m^{-2}$
PRECTmms	Total precipitation	pr	Precipitation	$kg \cdot m^{-2} \cdot s^{-1}$
FLDS	Incident longwave radiation	rlds	Surface Downwelling Longwave Radiation	$W \cdot m^{-2}$
PSRF	Surface pressure at the lowest atmospheric level	ps	Surface Air Pressure	Pa
QBOT	Specific humidity at the lowest atmospheric level	huss	Near-Surface Specific Humidity	$kg \cdot kg^{-1}$
TBOT	Temperature at the lowest atmospheric level	tas	Near-Surface Air Temperature	K
WIND	Wind at the lowest atmospheric level	sfcWind	Near-Surface Wind	$m \cdot s^{-1}$

Table S4. Averages of CH4 fluxes (mean ± sd) in the periods of 2006-2015, 2016-2025, 2050s and 2090s at US-Beo, US-Bes, US-Brw, US-Atq and US-Ivo under SSP1-2.6, SSP2-4.5 and SSP5-8.5 scenarios Different letters mean significantly differences based on the Duncan's multiple range test at the $\alpha = 0.05$.

Period	Scenario	US-Beo	US-Bes	US-Brw	US-Atq	US-Ivo
2006-2015	n.a.	2.52±0.20bc	2.49±0.16c	2.64±0.21bc	3.03±0.14b	5.31±0.50a
2016-2025	SSP1-2.6	2.41±0.11d	2.12±0.13d	2.50±0.11c	3.63±0.18b	3.81±0.37a
	SSP2-4.5	2.41±0.15c	2.09±0.15c	2.50±0.15b	3.52±0.26a	3.74±0.39a
	SSP5-8.5	2.58±0.12d	2.25±0.13d	2.68±0.13c	3.88±0.20b	4.12±0.39a
2050s	SSP1-2.6	3.48±0.54b	3.17±0.69b	3.59±0.56ab	5.11±0.88a	4.97±0.98a
	SSP2-4.5	3.51±0.16b	3.16±0.25b	3.62±0.16b	5.45±0.53a	5.05±0.58a
	SSP5-8.5	4.35±0.49b	3.99±0.69b	4.47±0.49b	7.09±1.03a	7.43±1.16a
2090s	SSP1-2.6	3.65±0.46c	3.38±0.64c	3.73±0.45abc	5.42±0.93a	5.31±1.02ab
	SSP2-4.5	4.78±0.32b	4.61±0.32b	4.87±0.30b	7.61±0.93a	7.07±1.09a
	SSP5-8.5	19.72±8.00b	19.18±7.62b	20.13±8.11ab	26.88±6.00a	26.00±4.67ab

Table S5. Coefficients of the forward/backward multiple linear regression analysis for effects of air temperature (T_{air}), precipitation (PPT), canopy evapotranspiration (ET) and NPP on CH_4 fluxes. Significant level: '***': < 0.0001, '**': < 0.001, '*': < 0.01.

	Estimate	Standard error	t value	Pr(>|t|)
Intercept	-0.0875	0.0029	-30.38	<2e-16 ***
T_{air}	0.4312	0.0070	61.50	<2e-16 ***
PPT	0.4843	0.0162	29.98	<2e-16 ***
ET	-0.2306	0.0129	-17.81	<2e-16 ***
NPP	0.2027	0.0158	12.85	<2e-16 ***

CONCLUSION

This dissertation advanced our understandings of the mechanisms of CH_4 cycling at the plot and landscape scales in Arctic tundra, and projected the responses of Arctic CH_4 emission and processes to climate change by 2100. Moreover, the process-based biogeochemical model, the CLM-Microbe model, facilitate my research on simulating, upscaling and projecting CH_4 cycling by involving the detailed information of CH_4 processes and different microbial functional groups. In the first chapter, I applied the CLM-Microbe model to investigate microtopographic impacts on CH_4 processes and emissions from seven landscape types in Arctic tundra near Utqiagvik, AK. Sensitivity analysis and uncertainty analysis were employed to reveal the main factors of CH_4 cycling at daily and hourly time scales. Additionally, combined with the area-average weighted approach, I upscaled the modeled fluxes from seven microtopographic types to EC domains in Arctic tundra. In the second chapter, I upscaled simulated plot-level fluxes to EC domains at high spatial resolution combined with three footprint algorithms and compared the performance of these footprint algorithms at monthly and annual time scales for five Arctic ecosystems in northern Alaska. Spatial heterogeneity in CH_4 emissions and its controls were also analysized at the landscape scale in Arctic tundra. In the third chapter, I continued the modeling work from the second chapter and projected the future CH_4 emissions in respond to different climate change scenarios derived from three climate models. Conceptual models were built for better examining the mechanisms of CH_4 cycling in the changing climate. Moreover, temperature sensitivity of CH_4 fluxes was analyzed for estimating CH_4-climate feedbacks under warming. The key conclusions are listed as below:

1. Modeled fluxes were promising and consistent with the observational gas fluxes from different microtopographic types.

2. Model results showed that low-elevation landscape types (e.g. trough, transitions, and LCP center) have higher CH_4 emission with greater seasonal variations than high-elevation landscape types (e.g. rims and HCP center).

3. Sensitivity analysis indicated that the substrate (e.g. acetate, $CO_2 + H_2$) availability for methanogens was the most important factor in controlling CH_4 emissions in Arctic ecosystems, and plant photosynthesis greatly affected the NEE and ER.

4. The CLM-Microbe model performed more accurately in simulating the daily EC fluxes than hourly fluxes combined with the area-average weighted approach in the heterogeneous Arctic landscape.

5. The CLM-Microbe model captured the temporal dynamics of landscape-scale CH_4 emission using different footprint algorithms for different study sites, even when using the same model settings and parameters.

6. The dynamic footprint (DF) algorithm improved the accuracy of temporal variations in CH_4 flux at the monthly scale rather than the annual scale, compared with the homogeneous footprint (HF) and gradient footprint (GF) algorithms.

7. Air temperature explained 67-74% while precipitation explained 22-36% of temporal variations of CH_4 fluxes at the landscape scale in Arctic tundra.

8. Extrapolating our modeling results to the northern Arctic tundra ecosystems led to an annual CH_4 emission of 7.54 - 20.87 Tg CH_4 per year.

9. Arctic CH_4 emissions were projected to have a stronger response to intense warming and enhanced precipitation; by 2100, increased by 631-851% under SSP5-8.5 but were relatively consistent with current emissions under SSP1-2.6 and SSP2-4.5 across all sites in Arctic tundra.

10. All CH_4 transport pathways increased and ebullition contributed most among three

transport pathway by 2100.

This dissertation provides a powerful tool to simulate CH_4 cycling at multiple spatial and temporal scales with a fine spatial resolution. The improvements in understanding the mechanisms of CH_4 cycling in Alaskan Arctic tundra ecosystems will broaden our knowledge of microbial contributions to CH_4 emission and improve the accuracy of CH_4 estimation in a changing climate.